Aus dem Institut für Experimentelle Pneumologie
der Ludwig-Maximilians-Universität München
Ehemaliger Direktor: Prof. Dr. O. Eickelberg

und der Abteilung „Lung Repair and Regeneration“
Leitung: Prof. Dr. Dr. M. Königshoff

Runt-related transcription factor 2 in pulmonary fibrosis

Dissertation
zum Erwerb des Doktorgrades der Medizin
an der Medizinischen Fakultät der
Ludwig-Maximilians-Universität zu München

vorgelegt von
Carlo Maria Mümmler
aus Fürth

2019

Mit Genehmigung der Medizinischen Fakultät
der Universität München

Berichterstatterin:	Prof. Dr. Dr. Melanie Königshoff
Mitberichterstatter:	Prof. Dr. André Brändli Prof. Dr. Jürgen Behr Prof. Dr. Dr. Jens Neumann
Dekan:	Prof. Dr. Reinhard Hickel

Tag der mündlichen Prüfung: 10.01.2019

meiner Familie

Parts of this work have been published in the following research article:

Mümmler C, Burgy O, Hermann S, Mutze K, Günther A, Königshoff M
Cell-specific expression of runt-related transcription factor 2
contributes to pulmonary fibrosis
FASEB J, 2018, *32*(2): 703-716.

TABLE OF CONTENTS

ABBREVIATIONS

°C	degree Celsius
Δ Ct	delta cycle of threshold

A

A	adenosine
A	ampere
APS	ammonium peroxodisulfate
AEC	alveolar epithelial cell
αSMA	alpha smooth muscle actin
AT I	alveolar epithelial type I
AT II	alveolar epithelial type II
ACTB	β-actin

B

bp	base pairs
BSA	bovine serum albumin
BLEO	bleomycin

C

C	cytosine
CBFB	core binding factor, β subunit
cDNA	complementary DNA

D

d	day
Da	dalton
DAPI	4′,6-diamidino-2-phenylindole
DLCO	diffusing capacity for carbon monoxide
DNA	deoxyribonucleic acid
dNTP	deoxyribonucleoside triphosphate

E

ECL	enhanced chemiluminescence
ECM	extracellular matrix
EMT	epithelial-to-mesenchymal transition

F

FBS	fetal bovine serum
FVC	forced vital capacity
fw	forward

G

g	gram
g	gravitational acceleration
G	guanosine
GEO	gene expression omnibus

H

h	hour
H&E	hematoxylin & eosin
HPRT	hypoxanthine-guanine-phosphoribosyltransferase

HRP	horse radish peroxidase
HRCT	high resolution computed tomography

I

IgG	immunoglobulin G
IIP	idiopathic interstitial pneumonia
ILD	interstitial lung disease
IPF	idiopathic pulmonary fibrosis
IF	immunofluorescence

K

K	kilo

L

L	liter
LTRC	lung tissue research consortium

M

µ	micro
m	milli
M	molar
$MgCl_2$	magnesium chloride
min	minute
MMP	matrix metalloproteinase
mRNA	messenger RNA

N

n	nano
NaCl	sodium chloride
NMTS	nuclear-matrix targeting signal
CBFB	core-binding factor beta, subunit
siRNA	small interfering RNA

O

ON	over night

P

p.a.	*pro analysis*
PBS	phosphate buffered saline
PCR	polymerase chain reaction
PDGF	platelet derived growth factor
PFA	paraformaldehyde
phLF	primary human lung fibroblast
proSPC	pro-surfactant protein C
P/S	penicillin / streptomycin

Q

qPCR	quantitative PCR

R

RIPA	radioimmunoprecipitation buffer
RNA	ribonucleic acid
RT	room temperature

RUNX	RUNT-related (transcription factor)
rv	reverse

S

s	second
scr	scrambled siRNA
siRUNX2	siRNA against RUNX2 mRNA
SDS	sodium dodecyl sulfate
SEM	standard error of the mean
SHH	sonic hedgehog

T

TBS	tris buffered saline
TBST	tris buffered saline with Tween 20
TGF-β	transforming growth factor β
T	thymidine
TRIS	tris(hydroxymethyl)-aminomethane

U

UIP	usual interstitial pneumonia

V

V	volt

W

WB	western blot
WNT	wingless/integrase 1

Nomenclature:

Gene names were written in small, italic letters for murine genes ("*Runx2")* and in capital, italic letters for human genes (*"RUNX2").* For murine and human protein names capital, non-italic letters were used ("RUNX2"). However, to improve readability, all gene and protein names in the discussion section were written in non-italic, capital letters

1. ZUSAMMENFASSUNG

Die Idiopathische Lungenfibrose (IPF) ist eine schwerwiegende Lungenerkrankung mit unklarer Ätiologie und eingeschränkten Therapieoptionen. Pathophysiologische Merkmale sind die (repetitive) Schädigung des Alveolarepithels sowie die Bildung fibroblastischer Foci mit vermehrter Produktion von Extrazellulärmatrix. In seltenen Fällen kann dieser Prozess bis zur pulmonalen Ossifikation führen. Runt-related transcription factor (RUNX) 2 ist ein für Ossifikationsprozesse essentieller Transkriptionsfaktor, dessen Expression über profibrotische Signalwege wie TGF-β und WNT/β-catenin reguliert wird. Ziel dieser Studie war die Bestimmung des zellspezifischen Expressionslevels sowie der pathophysiologischen Rolle von RUNX2 in der IPF.

Die Expression von RUNX2 war sowohl im Bleomycin-induzierten Mausmodell der Lungenfibrose (BLEO) als auch in der humanen IPF erhöht. Die erhöhte Expression von RUNX2 in den Lungen von IPF Patienten korrelierte mit einer verringerten Diffusionskapazität und einer Hochregulation der IPF Biomarker SPP1 und MMP7. Durch Immunfluoreszenzfärbungen konnten wir Alveolarepithel Typ (AT) II Zellen als die wesentliche Quelle von erhöhten RUNX2-Spiegeln in der IPF identifizieren. Wir beobachteten die Expansion einer proSPC-positiven/RUNX2-positiven Zellpopulation in BLEO und IPF, während die Vergrößerung der αSMA-positiven Myofibroblasten-Population hauptsächlich durch RUNX2-negative Zellen verursacht wurde. Weiterhin konnten wir zeigen, dass aus IPF-Lungen isolierte Fibroblasten verringerte RUNX2-Spiegel exprimierten. Der siRNA-vermittelte Knockdown von RUNX2 führte in ATII Zellen zu einer reduzierten Expression von CCND1 und S100A4 und beeinträchtigte die Zellmigration in A549 Zellen. Im Gegensatz dazu führte eine Herunterregulation von RUNX2 in Lungenfibroblasten zu einer deutlich verstärkten Expression der mesenchymalen Marker ACTA2, TNC und COL1A1, während CCND und S100A4 reduziert waren.

Zusammengefasst weisen die Ergebnisse der vorliegenden Arbeit auf einen signifikanten Beitrag des Proteins RUNX2 zur Lungenfibrose hin. Unsere Daten erlauben ein Modell, in dem die erhöhte Expression von RUNX2 in ATII Zellen die Zellproliferation und Zellmigration stimuliert, während die Herunterregulation von RUNX2 in Lungenfibroblasten zur verstärkten Ablagerung von Extrazellulärmatrix beiträgt. Die zell-spezifische, medikamentöse Regulation von RUNX2 könnte eine neuartige Behandlungsstrategie für die idiopathische Lungenfibrose darstellen.

2. SUMMARY

Idiopathic pulmonary fibrosis (IPF) is a fatal lung disease with unknown etiology and limited therapeutic options. IPF is characterized by epithelial cell injury, impaired cellular crosstalk between epithelial cells and fibroblasts, and the formation of fibroblast foci with increased extracellular matrix (ECM) deposition. In rare cases, this can even lead to pulmonary ossification. We investigated the cell-specific expression and pathophysiologic role of runt-related transcription factor (RUNX) 2, a master regulator of bone development linked to profibrotic signaling.

RUNX2 expression was upregulated in experimental bleomycin-induced lung fibrosis (BLEO) as well as in lung homogenates from IPF patients. RUNX2 levels correlated with disease severity as measured by decreased diffusing capacity of the lung for carbon monoxide (DLCO) or increased levels of the IPF biomarkers MMP7 and SPP1. We observed nuclear RUNX2 expression in proSPC-positive hyperplastic epithelial cells in IPF, demonstrated an increase of a proSPC-positive/RUNX2-positive epithelial cell population in IPF and BLEO and showed that RUNX2 expression was increased in alveolar epithelial type (AT) II cells isolated from bleomycin-treated mice. Interestingly, the increase in αSMA-positive myofibroblasts in pulmonary fibrosis was mainly due to an increase in a RUNX2-negative cell population. Further evidence demonstrated that primary human lung fibroblasts (phLF) isolated from IPF tissue displayed reduced levels of RUNX2. Functionally, siRNA-mediated RUNX2 knockdown decreased expression of S100A4 and CCND1 in murine ATII cells and impaired the migration of A549 cells. In phLF, RUNX2 knockdown led to an induction of mesenchymal markers ACTA2, TNC and COL1A1 while CCND1 and S100A4 were decreased.

In summary, this study suggests that regulation of RUNX2 expression contributes to fibrotic processes in the lung. In alveolar epithelial cells, upregulation of RUNX2 induced cell proliferation and migration whereas the downregulation of RUNX2 in fibroblasts contributed to the increased ECM deposition. We conclude, that cell-specific targeting of RUNX2 may represent a novel therapeutic approach for IPF.

3. INTRODUCTION

3.1 Idiopathic pulmonary fibrosis

Idiopathic pulmonary fibrosis (IPF) is a chronic, irreversible lung disease and the most frequent entity in the family of idiopathic interstitial pneumonias (IIP). The term IIP comprises six major entities, idiopathic pulmonary fibrosis (IPF), nonspecific interstitial pneumonia (NSIP), cryptogenic organizing pneumonia (COP), acute interstitial pneumonia (AIP), respiratory bronchiololitis-interstitial lung disease (RB-ILD) and desquamative interstitial pneumonia (DIP) (1, 2). The annual incidence of IPF is 2.8 - 9.3 cases per 100.000, with an increasing trend (3). Usually older people are affected, the median age of IPF diagnosis is 66 years (4). IPF predominantly affects men and is more prevalent in people with a history of smoking or exposure to organic and anorganic dust. Patients typically present with chronic dyspnea, dry cough and finger clubbing. Basally pronounced inspiratory crackles can sometimes be heard on auscultation (1). Diagnosis of IPF requires high-resolution CT (HRCT) with a typical usual interstitial pneumonia (UIP) pattern (Figure 1), the exclusion of other known causes of interstitial lung disease (ILD) and in case of an unclear HRCT a surgical lung biopsy showing characteristic histopathologic changes. The HRCT pattern consists of reticular opacities and honeycombing (clustered, cystic airspaces) that are found pronounced in peripheral and basal areas of the lung (1).

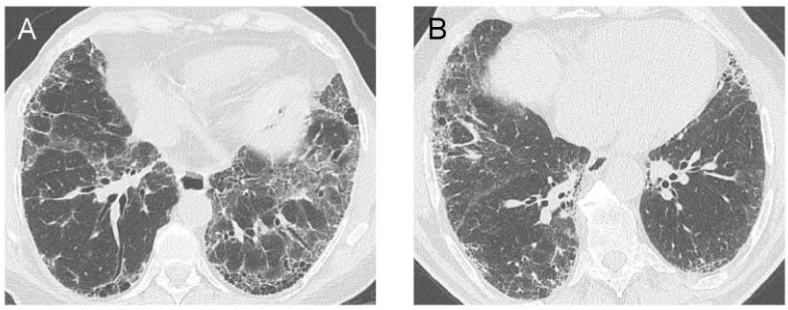

Figure 1: CT patterns of definite UIP and possible UIP.
High-resolution computed tomography (HRCT) images showing (A) subpleural basal honeycombing with traction bronchiectasis, reticular and ground glass opacities or (B) patchy, peripheral reticular opacities without obvious honeycombing (images modified from Sverzellati et al. (5) with permission from Springer Nature).

Histological slides of surgical lung biopsies of IPF patients show a heterogeneous distribution of areas of dense fibrosis, areas of epithelial hyperplasia and normal airways. Interstitial inflammation can be seen but usually plays a minor role (6).

The median survival of IPF patients is 2 to 3 years (1). However, the clinical course of IPF can be variable. Most of the patients exhibit a slow and gradual decline of lung function, whereas a minority decreases rapidly. Rapid worsening can be triggered by acute exacerbations (4). Several comorbidities, e.g. lung cancer, pulmonary hypertension, gastro-oesophageal reflux and obstructive sleep apnoea are often associated with IPF, although it is unclear if a causal relation exists (7). Recently, two molecules have shown efficacy in modifying the disease course of IPF. Nintedanib, a multi-tyrosine kinase inhibitor, reduced lung function decline and the incidence of acute exacerbations in IPF patients in the INPULSIS-trials (8, 9). The mechanism of action of the second approved drug, pirfenidone, has not been clearly identified yet. In animal models of pulmonary fibrosis, it has been demonstrated to exert pleiotropic antifibrotic effects by downregulating TGF-β levels and reducing collagen synthesis (10-13). In the ASCEND-trial, administration of pirfenidone reduced lung function decline, increased 6-minute walk distance and increased the time of progression-free survival (14). Of note, neither pirfenidone nor nintedanib had a significant effect on mortality (9, 14). According to the recent national and international guidelines, all symptomatic patients should be started on one of these drugs at the time of diagnosis (15). Ongoing trials investigate potential combination therapies. Further recommendations for IPF therapy are the use of supplemental oxygen therapy in patients with hypoxemia and finally lung transplantation (1).

Although major advances have been made in the past years, IPF remains an incurable and devastating disease. Better understanding of IPF pathophysiology is urgently needed to design more effective treatments.

3.1.1 IPF pathophysiology

For a long time, IPF has been considered a mostly inflammation-driven disease. However the failure of anti-inflammatory drugs like azathioprine, prednisone or cyclosporine led to a paradigm-change (1, 16). Current pathophysiologic theories suggest that perpetuated microinjuries to the alveolar epithelium aberrantly activate repair mechanisms (17, 18).

Epithelial cell apoptosis leads to a hallmark of IPF, the re-epithelialization of injury sites with hyperplastic alveolar epithelial type II (ATII) cells (Figure 2), often overlying spots of activated myofibroblasts (18). These activated myofibroblasts form so-called myofibroblast foci with increased deposition of extracellular matrix (ECM) (Figure 2) (17). It has been suggested that disturbed epithelial-mesenchymal crosstalk is driven through the epithelial secretion of different growth factors, e.g. TGF-β, PDGF (19) and the reactivation of developmental pathways like WNT, SHH or Notch (20).

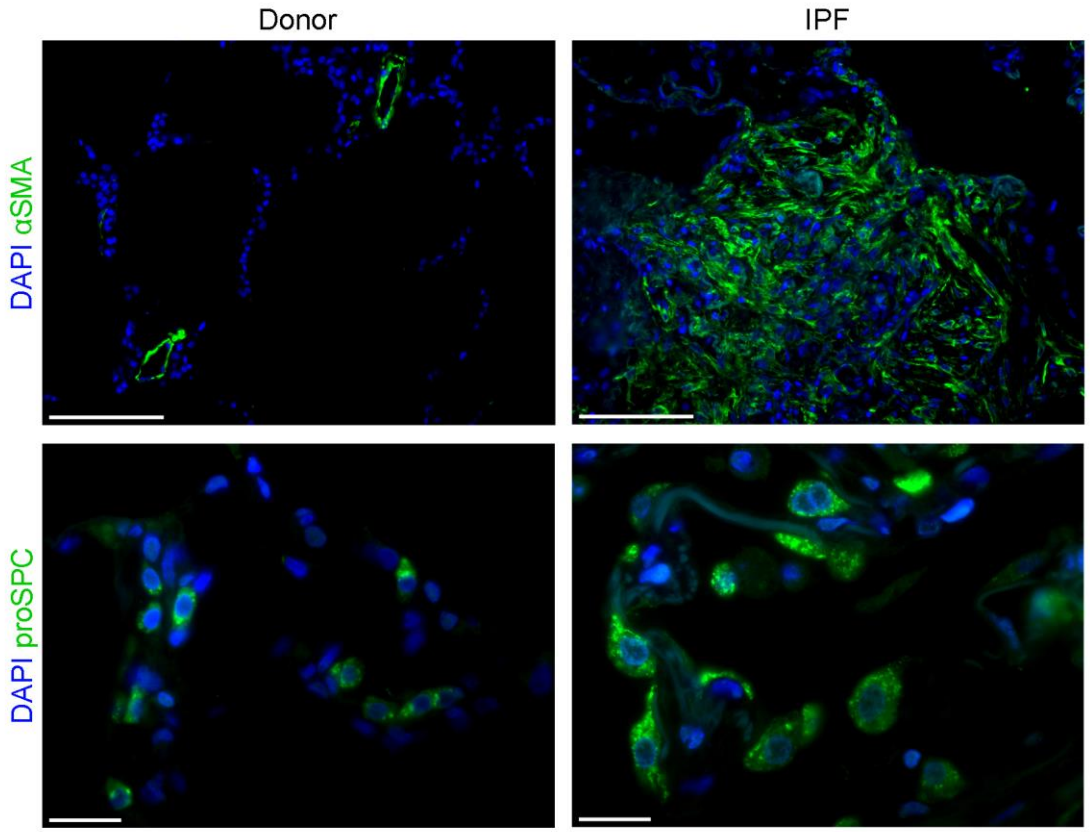

Figure 2: Myofibroblast foci and hyperplastic alveolar epithelial type II cells are hallmarks of IPF. Immunoflourescence stainings were performed on paraffine sections of IPF and donor lungs. Staining with the myofibroblast and smooth muscle cell marker alpha smooth muscle actin (αSMA) and the alveolar epithelial type II cell marker pro-surfactant protein C (proSPC), is shown in green. 4′,6-Diamidin-2-phenylindol (DAPI) was used to visualize cell nuclei and is shown in blue. Scale bars represent 100 µm for αSMA stainings and 20 µm for proSPC stainings.

3.2 Bleomycin model of pulmonary fibrosis

Bleomycin is an anticancer drug that is currently used for the treatment of a variety of cancer types, such as germ-cell tumors, squamous cell carcinomas and lymphomas (21). However, the use of bleomycin in clinical practice is limited by its severe pulmonary side effects which can lead to interstitial lung disease (ILD) (22). In this work, intratracheal instillation of bleomycin was used to study pulmonary fibrosis in mice. The bleomycin-model is one of the most commonly used models for the induction of pulmonary fibrosis (23). It reflects several pathophysiologic features of IPF, like the release of pro-fibrotic cytokines, myofibroblast activation and direct alveolar epithelial cell (AEC) injury leading to epithelial cell hyperplasia (23-25). Bleomycin causes an inflammatory response with activation of macrophages and neutrophils in the first week after instillation. Subsequently, murine fibrosis develops from day 10 and is most prominent at day 14 to day 28. After the fibrotic phase, Bleomycin-induced fibrosis gradually resolves, which is in contrast to the continuous and irreversible progression of human pulmonary fibrosis (24).

3.3 RUNT-related transcription factors

The RUNT-related transcription factors (RUNX) comprise a family of genes which are essential for regular organ development and which have been implicated in a variety of diseases.

3.3.1 Structure and function of RUNX genes

The three RUNX genes share several conserved features. Firstly, the highly homologous RUNT-domain, which is crucial for DNA binding and the interaction with the coactivator, core-binding factor, β-subunit (CBFB) (26, 27). Secondly, all RUNX factors possess a nuclear-matrix-targeting signal (NMTS), inducing nuclear translocation. Thirdly, the carboxyl terminus of RUNT proteins is formed by the VWRPY-domain, an interaction scaffold for Groucho proteins (Figure 3). Two different promotors encode slightly different RUNX proteins. The distal promoter (P1) generates a RUNT protein with an amino terminus of the amino acids MASXS, whereas the proximal one (P2), generates a RUNT protein with the ending MRIPV (28, 29).

Figure 3: Structure of RUNX genes.
Scheme of the RUNX gene structure depicting the RUNT DNA-binding domain (RUNT), the activation domain (AD), the inhibitory domain (ID), the VWRPY domain and a region of tandem repeats of glutamine and alanine amino acids (QA, unique to RUNX2) (image modified from Ito et al. (30) with permission from Springer Nature).

Whether RUNX proteins act as transcriptional activators or repressors depends on the binding of coregulatory proteins like SMADs, YAP1, p300 and HDACs (31) (Figure 4). Post-translational modifications, namely acetylation and phosphorylation influence RUNX protein activity and stability and probably also play a role in shifting from a gene repressing to a gene activating function and vice versa.

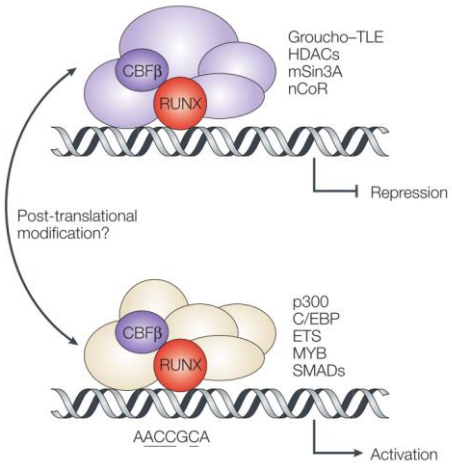

Figure 4: Function of RUNX genes.
RUNX factors can act as both transcriptional activators and repressors, depending on binding of co-regulatory proteins and post-translational modifications (image modified from Blyth et al. (28) with permission from Springer Nature).

3.3.2 Role of RUNX genes in development

The striking phenotypes of RUNX knockout mice underline their importance in development: RUNX1-null mice exhibit defects in hematopoiesis and are embryonically lethal (32). RUNX3-null mice die soon after birth of respiratory failure as a result of impaired alveolar epithelial cell differentiation (33). Knockout mice for RUNX2 do not develop calcified bone and die of respiratory failure as well (Figure 5) (34). This is assumed to be due to restricted respiration caused by lacking ribs, however, it has never been

investigated if RUNX2 also plays a role in alveolar epithelium. CBFB-null mice exhibit a phenotype that resembles combined RUNX1- and RUNX2-deficiency.

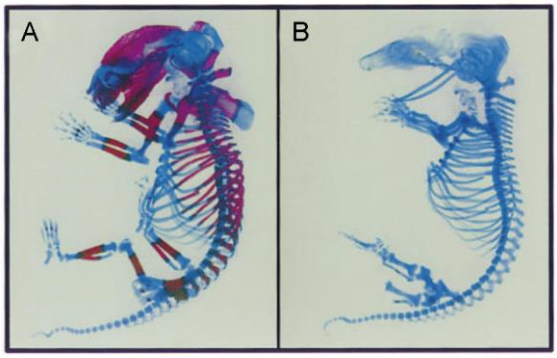

Figure 5: RUNX2 knockout mice fail to develop calcified bone.
Wild-type (A) and RUNX2 mutant (B) mice embryos were stained with Alcian blue (blue, stains cartilage tissue) and Alcian red (red, stains bone tissue) (image modified from Otto et al. (34) with permission from Elsevier).

3.3.3 Role of RUNX genes in disease

RUNX genes play important roles in tumor formation and progression through the regulation of basic cellular processes such as cell differentiation, proliferation and migration. Besides, they can act as both tumor suppressor genes or dominant oncogenes, depending on the cellular context (28).

RUNX1 has been shown to exert a tumor suppressive role and is often mutated in patients with acute myeloid leukemia (AML) (35). Expression of RUNX1 is increased in breast cancer and led to higher invasive potential of mammary epithelial cells (36). Furthermore, higher RUNX1 expression was found to correlate with lower survival of hormone-receptor negative breast cancer patients (37). Besides, a recent study demonstrated that RUNX1 enhances the proliferative capacity of mesenchymal stem cells and that a subsequent loss of RUNX1 leads to differentiation towards a myofibroblast phenotype (38).

Due to the remarkable defects of RUNX2-knockout mice, RUNX2 was extensively studied in the context of bone physiology and disease. Recently, novel roles of RUNX2 in cancer were illuminated. Increased RUNX2 levels were demonstrated in breast, prostate, thyroid and pancreatic cancer as well as in malignant melanoma. RUNX2 function in these cancer types has been linked to increased cell migration, epithelial-to-mesenchymal transition (EMT) and sustained proliferation (39-44). Lung and breast cancer patients with higher RUNX2 expression demonstrated reduced survival (45, 46). In a model of ureteral-obstruction induced kidney fibrosis, RUNX2 heterozygous knockout mice exhibited accelerated disease

progression, increased collagen deposition and upregulated αSMA expression, suggesting an antifibrotic role of RUNX2 (47). Interestingly, RUNX2 staining has been found in epithelium and fibroblastic stroma of a patient with pulmonary ossification (Figure 6), a rare condition in which actual bone is formed in the lung parenchyma. Pulmonary ossification is frequently associated with fibrotic lung diseases like idiopathic pulmonary fibrosis or pulmonary sarcoidosis (48-50). Although not proven, it is regarded as a metaplastic reaction to chronic lung injury with pulmonary fibroblasts differentiating into osteoblasts (48, 51).

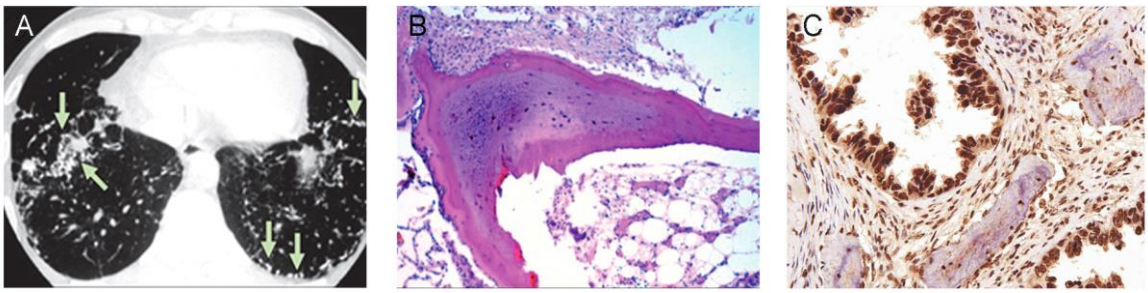

Figure 6: RUNX2 protein is expressed in pulmonary ossification.
(A) CT image showing calcified lines and micronodules. (B) Hematoxylin and eosin staining of human lung showing bone tissue, partially containing bone marrow cells. (C) Immunohistochemical RUNX2 staining within an area of ossification (images A and B modified from Martinez et al. (52) with permission from Elsevier, image C modified from Kim et al. (53) with permission of The Korean Academy of Medical Science).

RUNX3 is a tumor suppressor gene and has been shown to be frequently inactivated by epigenetic mechanisms in a variety of cancer types. Hypermethylation of RUNX3 has been found in gastric, colon, bladder and lung cancer (54-58). Interestingly, RUNX3 knockout-mice showed impaired alveolar epithelial cell differentiation and spontaneously developed lung adenomas (33).

3.3.4 RUNX2 and signaling pathways

Several groups have found crosstalk of RUNX transcription factors with TGF-β, BMP and WNT-signaling (28, 59). These signaling pathways are crucial for normal embryologic development and often deregulated in cancer and other diseases, including IPF (20, 60). It has been demonstrated that canonical WNT signaling activates the RUNX2 promoter and induces RUNX2 gene expression (61). TGF-β signaling induced expression of RUNX2 in C2C12 mesenchymal stem cells (62), but inhibited RUNX2 transcription and activity in primary osteoblasts and the osteosarcoma cell line ROS 17/2.8 (63).

RUNX2 can also interact with TGF-β signaling via modulation of downstream signaling molecules, such as Smad3 or the TGF-β type I receptor (64).

3.4 Aims of the study

Little is known about RUNX genes in fibrotic diseases. Moreover, nobody has investigated the role of RUNX genes and proteins pulmonary fibrosis so far. Fibrosis-associated signaling pathways have been shown to modulate RUNX function and activity. Furthermore, RUNX2 staining has been shown in a patient with pulmonary ossification, a condition that is linked to pulmonary fibrosis. This led to the hypothesis that RUNX genes might be differentially regulated and contribute to disease pathogenesis and cellular dysfunction in pulmonary fibrosis.

Aims of this study were:

- to study the expression of RUNX genes on mRNA and protein level in experimental fibrosis induced by bleomycin
- to study the expression of RUNX genes on mRNA and protein level in human idiopathic pulmonary fibrosis
- to study the localization of RUNX genes in tissue sections in experimental fibrosis as well as in human idiopathic pulmonary fibrosis
- to study the functional role of RUNX genes on gene expression in ATII cells and lung fibroblasts

4. MATERIALS & METHODS

4.1 Materials

4.1.1 Laboratory equipment and software

Table 1: Laboratory equipment

Product	Manufacturer
+4° Fridge, Medline LKV3912	Liebherr; Biberach an der Riß, DE
-20° Freezer, Medline LGEX3410	Liebherr; Biberach an der Riß, DE
-80° Freezer, U570 Premium	New Brunswick; Hamburg, DE
Autoclave DX-45	Systec; Wettenberg, DE
Autoclave VX-120	Systec; Wettenberg, DE
Cell culture bench Herasafe KS180	Thermo Fisher Scientific; Darmstadt, DE
Centrifuge Mikro 200R	Hettich Zentrifugen; Tuttlingen, DE
Centrifuge Rotina 420R	Hettich Zentrifugen; Tuttlingen, DE
CO_2 cell incubator BBD6620	Thermo Fisher Scientific; Darmstadt, DE
Electrophoretic transfer cell, Mini Protean Tetra Cell	Biorad; Hercules, USA
Fluorescence microscope AxioImager M2	Zeiss; Oberkochen, DE
Tissue homogenizer Sartorius Micro Dismembrator S	Thermo Fisher Scientific; Darmstadt, DE
Ice machine ZBE 110-35	Ziegra; Isernhagen, DE
Imaging system Chemidoc XRS+	BioRad; Hercules, USA
Incubator Heraeus B6	Thermo Fisher Scientific; Darmstadt, DE
Liquid nitrogen cell tank BioSafe 420SC	Cryotherm; Kirchen/Sieg, DE
Liquid nitrogen tank Apollo 200	Cryotherm; Kirchen/Sieg, DE
Lung function analysis machine FlexiVent	SciReq; Montreal, CA
Magnetic stirrer KMO 2 basic	IKA,Staufen; DE
Mastercycler nexus	Eppendorf; Hamburg, DE
Medical decloaking chamber	Biocare Medical; Concord, USA
Microscope Axiovert 40C	Zeiss; Oberkochen, DE
Micro-Sprayer Aerosolizer, Model IA-1C	Penn Century; Wyndmoor, USA
Mini Microcentrifuge 230V	Corning LSE; Kaiserslautern, DE
Moticam 1080 BMH camera	Motic; Kowloon Bay, HKG
Multipipette stream	Eppendorf; Hamburg, DE
Nanodrop ND-1000, spectrophotometer	Thermo Fisher Scientific; Darmstadt, DE
PCR platform Lightcycler 480 II	Roche Diagnostics; Mannheim, DE
pH-meter InoLab pH 720	WTW; Weilheim, DE
Pipettes Research Plus	Eppendorf; Hamburg, DE
Platereader Sunrise	Tecan; Männedorf, Switzerland
Platereader TriStar LB941	Berthold Technologies; Bad Wildbad, DE
Powerpac Basic	BioRad; Hercules, USA
Roll mixer	VWR International; Darmstadt, DE
Scale XS4002s deltarange	Mettler Toledo; Greifensee, DE
Thermomixer compact	Eppendorf; Hamburg, DE

Ultrapure water supply MilliQ Advantage A10	Merck Millipore; Darmstadt,DE
Vacuum concentrator plus	Eppendorf; Hamburg, DE
Vacuum pump Ecovac 4	Schuett-Biotec; Göttingen, DE
Vacuum pump Model No 22AN.18	KNF; Freiburg, DE
Vortex mixer 230V	Corning LSE; Kaiserslautern, DE
Water bath Aqua Line AL12	Lauda; Lauda-Königshofen, DE

Table 2: Software

Software	Manufacturer
Adobe CS5 Suite	Adobe Systems; San Jose, USA
Axio Vision	Zeiss; Oberkochen, DE
Endnote X8	Thomson Reuters; Munich, DE
Image Lab 5.0	Biorad; Hercules, USA
Lightcycler 480 Software 1.5	Roche; Mannheim, DE
Magellan Platereader Software	Tecan; Männedorf, CH
Mendeley Desktop	Mendeley Ltd.; London, UK
Microsoft Office 2013	Microsoft Corporation; Redmond, USA
Prism 5	GraphPad Software; La Jolla, USA

4.1.2 Chemicals and reagents

Table 3: Chemicals

Substance	Manufacturer
0.25% Trypsin – EDTA solution	Sigma-Aldrich; Munich, DE
10xPCR Buffer II	Thermo Fisher Scientific; Darmstadt, DE
4′,6-Diamidin-2-phenylindol (DAPI)	Sigma-Aldrich; Munich, DE
Acetone	AppliChem; Darmstadt, DE
Agarose	Sigma Aldrich; St. Louis, USA
Ammoniumperoxodisulfat (APS)	AppliChem; Darmstadt, DE
Antibody diluent	Zytomode Systems; Berlin, DE
BCA Protein Assay Kit	Thermo Fischer Scientific; Darmstadt, DE
Bleomycin sulfate	Almirall; Barcelona, Spain
Bovine serum albumine (BSA)	Sigma-Aldrich; Munich, DE
Bromophenol blue	AppliChem; Darmstadt, DE
CHIR99021	R&D Systems; Wiesbaden-Nordenstadt, DE
complete Mini, EDTA-free	Roche; Mannheim, DE
Dimethylsulfoxide (DMSO)	Carl Roth; Karlsruhe, DE
Dispase	BD Bioscience; Heidelberg, DE
Distilled Water, RNase/DNase-free	Thermo Fisher Scientific; Darmstadt, DE
Dithiothreitol (DTT)	AppliChem; Darmstadt, DE
Dulbecco's PBS (1x)	Thermo Fisher Scientific; Darmstadt, DE
ECL Western Blotting Substrate	Thermo Fisher Scientific; Darmstadt, DE
Ethanol p.a.	AppliChem; Darmstadt, DE
Fluorescence Mounting Medium	Dako; Hamburg, DE

Glycine p.a.	AppliChem; Darmstadt, DE
Isopropanol p.a.	AppliChem; Darmstadt, DE
Lightcycler 480 SYBR Green I Master	Roche; Mannheim, DE
Lipofectamine RNAiMAX Transfection Reagent	Thermo Fisher Scientific; Darmstadt, DE
Methanol p.a.	AppliChem; Darmstadt, DE
$MgCl_2$ solution	Thermo Fisher Scientific; Darmstadt, DE
Milk powder, non-fat, dried	AppliChem; Darmstadt, DE
MuLV Reverse transcriptase	Thermo Fisher Scientific; Darmstadt, DE
PCR Nucleotide Mix	Thermo Fisher Scientific; Darmstadt, DE
peqLab Gold DNase I Digest Kit	VWR International GmbH; Erlangen, DE
peqLab Gold Protein Marker V	VWR International GmbH; Erlangen, DE
peqLab Gold total RNA Kit	VWR International GmbH; Erlangen, DE
PhosStop	Roche; Mannheim, DE
Random Hexamers	Thermo Fisher Scientific; Darmstadt, DE
Restore Plus Western Blot Stripping Puffer	Thermo Fisher Scientific; Darmstadt, DE
RNase Inhibitor	Thermo Fisher Scientific; Darmstadt, DE
Roti-Block	Carl Roth; Karlsruhe, DE
Rotiphorese Gel 30 (37, 5:1)	Carl Roth; Karlsruhe, DE
Roti-Quick-Kit	Carl Roth; Karlsruhe, DE
Sodium Chloride	Thermo Fisher Scientific; Darmstadt, DE
Sodium Dodecyl Sulphate (SDS) Pellets	Carl Roth; Karlsruhe, DE
Tetramethylethylendiamin (TEMED)	Thermo Fisher Scientific; Darmstadt, DE
Tris, buffer grade	AppliChem; Darmstadt, DE
Triton X-100	AppliChem; Darmstadt, DE
Trypan blue	Sigma-Aldrich; Munich, DE
Tween-20	AppliChem; Darmstadt, DE
Western Blot substrate Super Signal West Dura	Thermo Fisher Scientific; Darmstadt, DE
Western Blot substrate Super Signal West Femto	Thermo Fisher Scientific; Darmstadt, DE
Xylene	AppliChem; Darmstadt, DE

Table 4: Recombinant proteins

Recombinant protein	Manufacturer
Recombinant human TGF-β1	R&D Systems; Wiesbaden-Nordenstadt, DE
Recombinant human WNT3a	R&D Systems; Wiesbaden-Nordenstadt, DE

Table 5: Media and media supplements

Media / Media supplement	Manufacturer
DMEM F-12	Thermo Fisher Scientific; Darmstadt, DE
Opti-MEM I Reduced Serum Medium	Thermo Fisher Scientific; Darmstadt, DE
Fetal Bovine Serum (FBS), Sera Plus	PAN Biotech; Aidenbach, DE
Penicillin/Streptomycin (P/S) 10000 U/ml	Thermo Fisher Scientific; Darmstadt, DE
GlutaMAX	Thermo Fisher Scientific; Darmstadt, DE

Table 6: pmATII medium

Ingredient	Amount
DMEM	500 ml
Glucose	1,8 g
GlutaMAX	10 ml

Penicillin/Streptomycin	5 ml
HEPES	5 ml
FBS	50 ml

4.1.3 Consumables

Table 7: Consumables

Consumable	Manufacturer
Cell culture flasks 75 cm^2	Thermo Fisher Scientific; Darmstadt, DE
Cell culture multiwell plates (6-well, 12-well)	TPP; Trasadingen, CH
Cell lifter	Corning Inc.; Corning, USA
Falcon tubes 15 ml	BD Bioscience; Heidelberg, DE
Falcon tubes 50 ml	BD Bioscience; Heidelberg, DE
Filter tips	Biozym Scientific; Hessisch Oldendorf, DE
Glass slides	Duran group; Wertheim, DE
Grinding steel balls	Neolab; Heidelberg, DE
Multipipette tips	Eppendorf; Hamburg, DE
Nitril Gloves	Rösner-Mautby Meditrade; Kiefersfelden, DE
Nylon meshes pore size 100 µm, 20 µm, 10 µm	Sefar; Heiden, CH
Parafilm	Bemis Packaging; Neenah, USA
Pasteur pipettes Cellstar 5 ml, 10 ml, 25 ml, 50 ml	Corning Inc.; Corning, USA
PCR plates and sealing foil	Kisker Biotech; Steinfurt, DE
Reaction tubes 0.5 ml, 1.5 ml, 2.0 ml, 5.0 ml	Greiner Bio-One; Frickenhausen, DE
Western Blot Nitrocellulose membrane	Biozym Scientific; Hessisch Oldendorf, DE
Whatman blotting paper	GE Healthcare; München, DE

4.1.4 Primer

Table 8: Murine primer

Gene	Sequence 5‘ – 3‘	NCBI accession number	Product length (bp)
Acta2	Forward primer: GCTGGTGATGATGCTCCCA Reverse primer: GCCCATTCCAACCATTACTCC	NM_007392.3	81
Cbfb	Forward primer: TAAGTACACGGGCTTCAGGG Reverse primer: AAGTATACGATCTCCGAGCGA	NM_022309.4 NM_001161456.1 NM_001161457.1 NM_001161458.1	93
Ccnd1	Forward primer: ATGCCAGAGGCGGATGAGA Reverse primer: ATGGAGGGTGGGTTGGAAAT	NM_007631.2	104
Cilp	Forward primer: ATGCCCAAGACTAGCCTGAA Reverse primer: ACAATGTATGGGGTCTCTGCC	NM_173385.2	71
Col1a1	Forward primer: CCAAGAAGACATCCCTGAAGTCA Reverse primer: TGCACGTCATCGCACACA	NM_007742.4	129
Fn1	Forward primer: GGTGTAGCACAACTTCCAATTACG Reverse primer: GGAATTTCCGCCTCGAGTCT	NM_010233.2 NM_001276408.1 NM_001276409.1 NM_001276410.1 NM_001276411.1	92

		NM_001276412.1 NM_001276413.1	
Hprt	Forward primer: CCTAAGATGAGCGCAAGTTGAA Reverse primer: CCACAGGACTAGAACACCTGCTAA	NM_013556.2	86
Runx1	Forward primer: CATCGCTTTCAAGGTGGTGG Reverse primer: CGCGGTAGCATTTCTCAGTT	NM_001111021.2 NM_001111022.2 NM_001111023.2 NM_009821.3	109
Runx2	Forward primer: ACGAGGCAAGAGTTTCACCT Reverse primer: TGTCTGTGCCTTCTTGGTTC	NM_001146038.2 NM_001145920.2 NM_009820.5 NM_001271627.1 NM_001271630.1	120
Runx3	Forward primer: TCTGAACCCAACCCCCTGA Reverse primer: TGCTCGGGTCTCGTATGAAG	NM_019732.2	117
S100a4	Forward primer: AGGAGCTACTGACCAGGGAGCT Reverse primer: TCATTGTCCCTGTTGCTGTCC	NM_011311.2	103
Spp1	Forward primer: GTTTGGCATTGCCTCC Reverse primer: GGATCTGGGTGCAGGCTGTA	NM_001204201.1 NM_001204202.1 NM_001204203.1 NM_009263.3 NM_001204233.1	84
Tnc	Forward primer: GGCCCCGGCTTGAAGA Reverse primer: GGGCTTGAACCAGGTGATCA	NM_011607.3	105

Table 9: Human primer

Gene	Sequence 5‘ – 3‘	NCBI accession number	Product length (bp)
ACTA2	Forward primer: GAGATCTCACTGACTACCTCATGA Reverse primer: AGAGCTACATAACACAGTTTCTCCTTG	NM_001141945.2 NM_001613.2 NM_001320855.1	116
CCND1	Forward primer: CCGAGAAGCTGTGCATCTACAC Reverse primer: AGGTTCCACTTGAGCTTGTTCAC	NM_053056.2	94
CILP	Forward primer: CCCAGCTGATTGTCATAGCATC Reverse primer: AGGAGTTGGTGGCATTCTGA	NM_003613.3	105
COL1A1	Forward primer: CAAGAGGAAGGCCAAGTCGAG Reverse primer: TTGTCGCAGACGCAGATCC	NM_000088.3	128
FN1	Forward primer: CCGACCAGAAGTTTGGGTTCT Reverse primer: CAATGCGGTACATGACCCCT	NM_212482.2 NM_002026.3 NM_212478.2 NM_212476.2 NM_212474.2 NM_054034.2 NM_001306129.1 NM_001306130.1 NM_001306131.1 NM_001306132.1	81
HPRT	Forward primer: AAGGACCCCACGAAGTGTTG Reverse primer: GGCTTTGTATTTTGCTTTTCCA	NM_000194.2	157
MMP7	Forward primer: GAACGCTGGACGGATGGTAG Reverse primer: CAGAGGAATGTCCCATACCCA	NM_002423.4	94
RUNX1	Forward primer: TTCACAAACCCACCGCAAGT Reverse primer: TCTGCCGATGTCTTCGAGGTTC	NM_001754.4 NM_001001890.2 NM_001122607.1	88

RUNX2	Forward primer: TATGAGAGTAGGTGTCCCGC Reverse primer: TGCCTGGGGTCTGTAATCTG	NM_001024630.3 NM_001015051.3 NM_001278478.1	102
RUNX3	Forward primer: CTTTGGGGACCTGGAACGG Reverse primer: GAGGTGCCTTGGATTGGGGT	NM_001031680.2 NM_004350.2 NM_001320672.1	120
S100A4	Forward primer: TCTTGGTTTGATCCTGACTGC Reverse primer: AACTTGTCACCCTCTTTGCC	NM_002961.2	105
SPP1	Forward primer: TCGCAGACCTGACATCCAGTACC Reverse primer: CCTTCCCACGGCTGTCCCAA	NM_001040058.1 NM_000582.2 NM_001040060.1 NM_001251829.1 NM_001251830.1	146
TNC	Forward primer: CCATCTATGGGGTGATCCGG Reverse primer: TCGGTAGCCATCCAGGAGAG	NM_002160.3	139

4.1.5 Antibodies and siRNA

Table 10: Primary antibodies for Western Blotting

Antigen	Source	Dilution	Order No.	Manufacturer
ACTB	Mouse	1:50000	A3854	Sigma
αSMA	Mouse	1:1000	A5228	Sigma
CILP	Rabbit	1:1000	ab192881	Abcam
CCND1	Rabbit	1:1000	2978	Cell signaling
COL1	Rabbit	1:1000	600-401-103	Rockland
FN1	Rabbit	1:1000	sc9068	Santacruz
RUNX2	Mouse	1:1000	D130-3	MBL Nagoya
RUNX2	Mouse	1:1000	ab76956	Abcam
TUBB	Rabbit	1:1000	2146	Cell signaling

Table 11: Secondary antibodies for Western Blotting

Antigen	Source	Dilution	Order No.	Manufacturer
Mouse IgG	Sheep	1:4000	NA931V	GE Healthcare
Rabbit IgG	Donkey	1:10000	NA934V	GE Healthcare

Table 12: Primary antibodies for immunofluorescence stainings

Antigen	Source	Dilution	Order No.	Manufacturer
αSMA	Rabbit	1:100	ab5694	Abcam
CK	Rabbit	1:500	Z0622	Dako
GAL3	Rabbit	1:100	sc20157	Santacruz
proSPC	Rabbit	1:100	AB3786	Millipore
RUNX2	Mouse	1:50	ab76956	Abcam

Table 13: Secondary antibodies for immunofluorescence stainings

Antigen	Source	Dilution	Order No.	Manufacturer
Mouse IgG, Alexa-flour 555 conjugate	Goat	1:1000	A21424	Invitrogen
Rabbit IgG, Alexa-flour 488 conjugate	Goat	1:1000	A11008	Invitrogen

Table 14: siRNA

siRNA	Order No.	Manufacturer
Control scrambled siRNA	sc-37007	Santacruz
Human *RUNX2* siRNA	sc-37145	Santacruz
Murine *Runx2* siRNA	sc-37146	Santacruz

4.1.6 Buffers and recipes

Table 15: Buffers and recipes

Solution	Compound	Amount / Concentration
PBS 10x pH=7.4	NaCl	160 g
	HNa_2HPO_4	23 g
	KCl	4 g
	KH_2PO_4	4 g
	H_2O	2000 ml
	pH is adjusted to 7.4	
PBS 1x	PBS 10x	900 ml
	H_2O	100 ml
BSA 0,1% in PBS	PBS 10x	900 ml
	H_2O	100 ml
	BSA	10 ml
Citrate buffer pH=6.0	Citric acid	2.1 g
	H_2O	1000 ml
	pH is adjusted to 6.0	
Radioimmunoprecipitation buffer (RIPA)	Tris HCl	20 mM
	NaCl	150 mM
	EDTA	1 mM
	EGTA	1 mM
	NP-40	1 %
	$Na_4P_2O_7$	2.5 mM
	Sodiumdeoxycholate	1 %
	pH is adjusted to 7.4	
Tris HCl 1,5 M pH=8.8	Tris	80.9 g

	H_2O	500 ml
	pH is adjusted to 8.8	
Tris HCl 0,5 M pH=6.8	Tris	30.3 g
	H_2O	500 ml
	pH is adjusted to 6.8	
SDS 10%	Sodium Dodecyl Sulfate	10 g
	H_2O	100 ml
TBS 10x pH=7.6	NaCl	80 g
	Tris	24.2 g
	H_2O	1000 ml
TBS 1x	TBS 10x	100 ml
	H_2O	900 ml
	Tween-20	1 ml
Laemmli buffer	Tris 1,5M	1,3 ml
	SDS	0,8 g
	Glycerol 87%	4 ml
	Bromophenol blue	0.002 g
	Dithiotreitol	0.61 g
Running Buffer 1x	Tris 25 mM	3.03 g
	Glycine 200 mM	14,4 g
	SDS 0,1%	1 g
	H_2O	1000 ml
Transfer Buffer 1x	Tris 25 mM	60.6 g
	Glycine	288 mg
	H_2O	2000 ml
Western Blot Stacking gel 5%	H_2O	1.4 ml
	30% Acryl-bisacrylamide mix	0.33 ml
	1,5 M Tris pH=6.8	0.25 ml
	10% SDS	20 µl
	10% Ammonium Persulfate	20 µl
	TEMED	2 µl
Western Blot Resolving gel 10%	H_2O	7.9 ml
	30% Acryl-bisacrylamide mix	6.7 ml
	1,5 M Tris pH=8.8	5.6 ml
	10% SDS	200 µl
	10% Ammonium Persulfate	200 µl
	TEMED	8 µl

4.2 Methods

4.2.1 Animal experiments: bleomycin model

Eight- to ten-week old C57BL/6N mice (Charles River Laboratories, Sulzfeld, DE) were used in this study. Mice were housed under standard conditions and had free access to water and laboratory rodent chow. All animal experiments were approved by the Government of Upper Bavaria and registered under project number 55.2-1-54-2532-88-12. Bleomycin instillations were performed by Sarah Hermann, Nadine Adam and Anastasia van den Berg. For the induction of pulmonary fibrosis, mice were instilled 3 units bleomycin sulfate per kg body weight dissolved in 50 µl sterile phosphate-buffered-saline (PBS). Control mice were instilled 50 µl sterile PBS. Intratracheal instillation was performed using a Micro-Sprayer Aerosolizer, Model IA-1C. At day 3, day 7, day 10 and day 14 after instillation, mice were sacrificed. Lung function analysis was performed on day 14 mice by using a Flexivent lung function machine. Afterwards, lungs were excised, flushed with saline to remove remaining blood, and snap-frozen in liquid nitrogen for further analysis.

4.2.2 Human samples

Whole lung homogenates of IPF or healthy donor patients (lung explants not used for transplantation) were used for RNA and protein isolation. Paraffin-embedded tissue sections were used for immunofluorescent stainings. All lung tissue samples were collected in frame of the European IPF registry (eurIPFreg) and provided by the University of Giessen Lung Center Biobank (member of the DZL Platform Biobanking). The study protocol was approved by the Ethics Committee of the Justus-Liebig-University Giessen (No. 111/08 and 58/15).

4.2.3 Cell culture

4.2.3.1 A549 cells

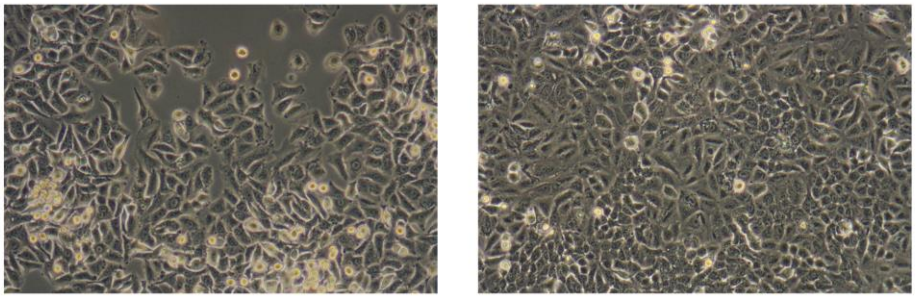

Figure 7: A549 cells in culture.

The human epithelial lung cancer cell line A549 was purchased from the American Type Culture Collection (ATCC) and cultivated in DMEM-F12 media supplemented with 10% FBS and 0,1% P/S.

4.2.3.2 Primary human lung fibroblasts

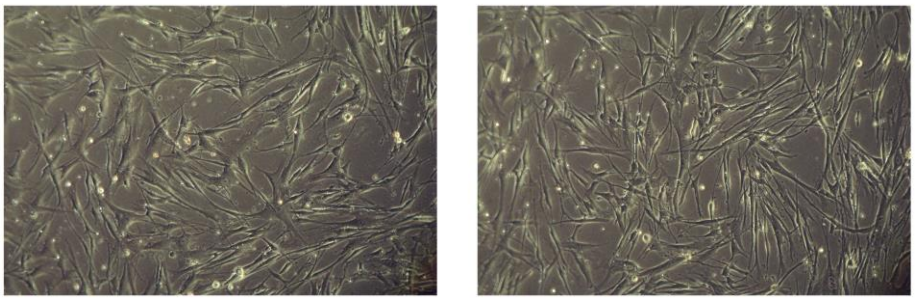

Figure 8: Primary human lung fibroblasts in culture.

Isolation of primary human lung fibroblasts (phLF) was approved by the local ethics committee of the LMU München (333-10). phLF were isolated by Katharina Heinzelmann as published previously (65). In brief, specimen of lung resections were cut in 1-2 cm^2 pieces and digested with collagenase I at 37°C for 2 hours. Digested material was filtered through nylon filters with a pore size of 70 µm. After centrifugation at 400 g and 4°C for 5 minutes, cells were cultured under standard conditions, at 37°C, 5% CO_2 using Dulbecco's Modified Eagle's medium/Nutrient mixture F12 medium (DMEM/F12) supplemented with 20% FBS and 1% penicillin / streptomycin. Medium was changed every 24 – 48 hours and cells were splitted when reaching 80-90% confluency.

4.2.3.3 Primary murine alveolar epithelial type II cells

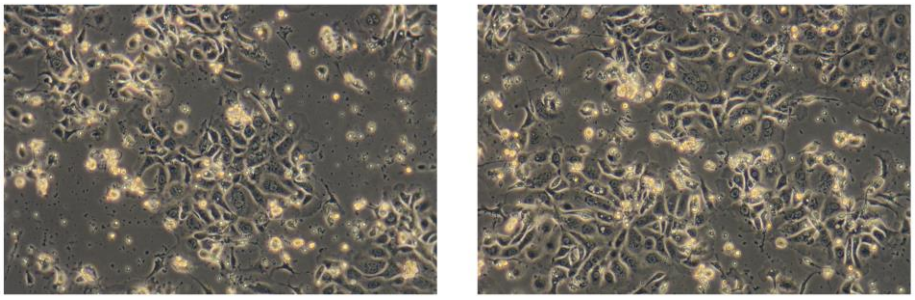

Figure 9: Primary murine alveolar type II cells in culture.

Primary murine alveolar epithelial type II (pmATII) cells were isolated by Kathrin Mutze, Julia Kipp and Anastasia van den Berg as published previously (66, 67). In brief, mice lungs were excised after bronchoalveolar lavage and flushed with 0.9% NaCl solution through the right heart. Lungs were inflated with 1.5 ml dispase and subsequently perfused with 300 µl of 1% low melting point agarose. Agarose filled lungs were incubated for 45 minutes at room temperature. Lungs were then minced and filtered through nylon meshes with pore sizes of 100 µm, 20 µm and 10 µm. Samples were centrifugated at 200 g for 10 minutes. The pellet was resuspended and the resulting cell suspension was incubated on petri dishes coated with antibodies against CD45 and CD16/32 for a negative selection of macrophages and lymphocytes. Negative selection for fibroblasts was performed by adherence on cell culture dishes for 25 minutes. To ensure viability, cells were stained with trypan blue. Afterwards, cells were either snap-frozen in liquid nitrogen for further RNA or protein isolation or seeded in DMEM medium containing 10% FBS, 2 mM L-glutamine, 3.6 mg/ml glucose, 10 mM HEPES and 1% Penicillin/Streptomycin.

4.2.4 Cell treatments

Recombinant human TGF-β1 was used in a concentration of 2 ng/ml, recombinant human WNT3a in a concentration of 100 ng/ml and the glycogen synthase kinase (GSK) 3-β inhibitor CHIR99021 in a concentration of 2 µM. Prior to treatment, cells were incubated with starvation medium containing 0.1% FBS. Cells were washed with warm PBS and subsequently TGF-β1 in starvation medium was added to the respective wells for the indicated period of time.

4.2.4.1 Gene knockdown using siRNA-transfection

siRNA-mediated knockdown was performed in pmATII cells and phLF. pmATII cells were plated in 12-well plates in a density of 1 million cells per well. Transfection was started at day 2 after isolation. Lipofectamine RNAiMAX and 80 nm *Runx2* siRNA or 80 nm scrambled siRNA were each diluted in OptiMEM. After 5 minutes incubation both solutions were mixed and left for 30 minutes. 200 µl of the *Runx2* siRNA mix (siRUNX2) or the scrambled siRNA mix (scr) and 550 µl antibiotic-free ATII medium were added to each well of a 12-well plate. Cells were stopped with ice-cold PBS after 48 hours and stored at -80°C.

phLF were transfected while seeding. *RUNX2* siRNA or scrambled siRNA were used at a concentration of 20 nm. 500 µl of the siRUNX2 transfection mix or scrambled transfection mix were added to each well. Subsequently 250.000 cells in 1500 µl medium were added and incubated for the indicated period of time.

4.2.5 Scratch assay

A549 cells were seeded in 6-well plates at a confluence of 80%, transfected with siRUNX2 or control and starved for 12 hours. Confluent monolayers were wounded by scraping a pipette tip across the monolayer, as previously described (68). After washing with PBS, cells were cultured in starvation medium. Images were captured immediately after the scratch (t = 0h), then observed 24 and 48 hours after the scratch by using a Moticam 1080 BMH camera that was mounted on an inverted microscope with a x4 objective. Each condition was conducted in triplicates, and 3 areas were observed for each well. Images were blindly analysed for the wound area by using ImageJ, and data were expressed as the percentage of wound closure normalized to t = 0h.

4.2.6 RNA analysis

4.2.6.1 RNA isolation from tissue

Snap-frozen murine lungs were homogenized using a Mikrodismembrator S shaking device. Lungs were put into a cryotube together with a small metal grinding ball and shaken at a frequency of 3000 shakes per minute for 30 seconds. 1 ml of Roti-Quick Kit solution 1 was added to the powder and incubated on ice for 20 minutes. 1 ml of Roti-Quick Kit solution 2 was added to lysate. The solution was vortexed and

again incubated on ice for 10 minutes. After centrifugation with 16000 g on 4°C for 15 minutes, the supernatant was transferred to another tube. Subsequently total RNA was isolated using the Peqlab Gold total RNA kit according to the manufacturer's instructions. DNase incubation was performed to increase the purity of the yield. Columns were incubated for 5 minutes with 40 µl RNase free water and RNA was eluted at 5000 g for 5 minutes. The eluted RNA was then diluted 1:5. Finally, samples were stored at -80°C.

4.2.6.2 RNA isolation from cells

Total RNA was isolated using the Peqlab Gold total RNA kit according to the manufacturer's instructions. DNase incubation was performed to increase the purity of the yield. 25 µl to 40 µl RNase free water were added onto the column, depending on the expected amount of RNA. After 2 minutes of incubation RNA was eluted at 5000 g for 1 minute. Subsequently, RNA samples were stored at -80°C.

4.2.6.3 RNA concentration and quality measurement

Using the Nanodrop ND-1000, RNA concentration and quality was measured. Samples were determined to be DNA-free, when A260/280 ratio was higher than 1.8.

4.2.6.4 cDNA Synthesis

1000 ng of total RNA were diluted in 20 µl RNase-free water. Firstly, RNA was denatured at 70°C for 10 minutes in an Eppendorf Mastercycler. Thereafter, 20 µl of RT-PCR Mastermix (Table 16) were added per sample. Reverse transcription of RNA to cDNA was then performed in an Eppendorf Mastercycler, in three cycles: 10 minutes on 20°C, 75 minutes on 43°C, 5 minutes on 99°C. Samples were cooled down to 4°C, diluted 1:5 with RNase-free water and stored at -20°C.

Table 16: Mastermix for RT-PCR

Reagent	Stock conc.	Mastermix conc.	Units	Volume
10x Buffer II	100	20	mM	4 µl
$MgCl_2$	25	10	mM	8 µl
dNTPs	10	1	mM	2 µl
Random Hexamers	50	5	mM	2 µl
RNase-Inhibitor	10	0.5	U	1 µl
Reverse Transcriptase	50	5	U	2 µl

H_2O	1 µl

4.2.6.5 Quantitative Polymerase-Chain-Reaction (qPCR)

qPCR was performed using a Roche Light Cycler 480 II and the compatible SYBR Green Mastermix. Each gene was run in duplicates and data was normalized to Hypoxanthine-guanine phosphoribosyltransferase (*HPRT*). Data were analysed using the Roche Lightcycler Software and are depicted as ΔCt = Ct (*HPRT*) – Ct (target) or as fold change, calculated according to the $2^{-\Delta\Delta Ct}$ method.

Table 17: Mastermix for qPCR

Substance	Concentration	Amount
Light Cycler Roche 480 II SYBR Green Master	2x	5 µl
Primer forward	10 µM	0.25 µl
Primer reverse	10 µM	0.25 µl
H_2O		2 µl
cDNA-Template		2.5 µl

Table 18: Lightcycler program for qPCR

Step	Substep	Temperature	Time	Repetitions
Initial denaturation		95°C	5 min	1x
Run Method	Denaturation	95°C	1 sec	45x
	Annealing	59°C	5 sec	
	Elongation	72°C	10 sec	
Melting Curve		95°C	5 sec	1x
		65°C	1 min	
		97°C		
Cooling		40°C	30 sec	1x

4.2.6.6 Primer design

Murine and human primers were designed with Primer-BLAST (69) . They were designed to cover all transcript variants and to create a PCR product with a size of 70 to 120 base pairs (bp) as well as a melting temperature optimum of 59°C. Other selection criteria were an exon-exon junction-span, a guanine/cytosine content close to 50% and low self-complementary rates. Primers were synthesized at Eurofins Genomics.

4.2.6.7 Primer testing

Primers were tested for working efficiency and dimerization with cDNA-dilutions of 1/8, 1/64 and 1/512. Furthermore, primertests included a no template control. Primer with an efficiency from 1.8 to 2.2 and melting curves with a single peak were further used for qPCR analyses.

4.2.7 Protein analysis

4.2.7.1 Protein isolation from tissue

Lungs were pulverized as described in “RNA isolation from tissue”. Protein lysis buffer was prepared by adding 1 tablet of the proteinase inhibitor complete Mini and 1 tablet of phosphatase inhibitor PhosStop to 10 ml of RIPA buffer. 300 µl of this mixture were added to the powder and incubated on ice for 30 minutes. Lysates were centrifuged for 30 minutes on 4°C and full speed. Supernatant was collected and stored on -80°C.

4.2.7.2 Protein isolation from cells

Cells in 6-well or 12-well plates were lysed with 100 µl to 300 µl of RIPA, depending on the expected amount of protein. The lysate was collected, snap frozen in liquid nitrogen and incubated on ice for 30-60 minutes. After centrifugation for 20 minutes on 4°C and 13000 g, supernatant was collected and stored on -80°C.

4.2.7.3 Protein concentration measurement

Total protein content was measured using a Bicinchoninic acid assay (BCA) kit. Buffer A and Buffer B were mixed in a proportion of 50:1. 100 µl of the mix was added to each well of a 96-well plate. Serial dilutions of BSA served as standard curve. Tissue lysates were further diluted whereas cell lysates were used undiluted. 5 µl of protein lysate were added and the plate was incubated for 30 minutes at 37°C. Subsequently the absorption at 562 nm was determined in a plate reader. The standard curve was calculated and the protein concentration determined accordingly.

4.2.7.4 Western Blotting

Gels were casted according to “Buffers and Recipes“ (Table 15). 4x Laemmli buffer was added to 15 µg protein lysate and RIPA buffer was added for equal volumes. Protein lysates were denatured at 95°C for 5 minutes and chilled on ice. Gels were loaded and run at 80 V for 10 minutes until the lysates fully entered the stacking gel. Subsequently, gels were run at increased voltage of 100 V for 80 minutes. Blotting on Nitrocellulose membranes was performed at 300 mA for 90 minutes. The blots were then blocked in 5% milk for 1 hour and incubated in a solution of primary antibody and Roti-Block overnight on 4°C. At the next day, blots were washed 3 times in TBS-T and incubated in a solution of the respective secondary antibody and 5% milk for 1 hour on room temperature. Blots were again washed 3 times and imaged in the BioRad Chemidoc using ECL, Supersignal West Dura or Supersignal West Femto as substrate. Image analysis was done with the software ImageLab.

4.2.8 Immunofluorescence stainings

Paraffin slides of murine and human lung tissue were incubated overnight at 60°C and subsequently deparaffinized in Xylol two times for 5 minutes, 100% alcohol two times for 2 minutes, 90% alcohol for 1 minute, 80% alcohol for 1 minute, 70% alcohol for 1 minute and rehydrated in distilled water for 30 seconds. Antigen retrieval was performed in a pressure cooker. The slides were covered in citrate buffer and heated at 125°C for 30 seconds. Afterwards, slides were washed three times with 1x Tris buffer and incubated with Triton-X 0.1% for 15 minutes. Slides were again washed three times with 1x Tris buffer and afterwards blocked with 5% BSA Tris for one hour to prevent unspecific binding of the antibody. After removal of the 5% BSA solution, the antibody of interest was diluted in antibody diluent in the respective concentration. The slides were incubated with the antibody solution overnight in a humidified dark chamber on 4°C. Next day, slides were washed three times with 1x Tris buffer and incubated with the respective fluorophore-labeled secondary antibody for 1 hour on room temperature. Slides were washed again and incubated for five minutes in 0.5 µg / ml DAPI solution for visualization of nuclei. After washing, slides were mounted using Dako fluorescence mounting medium and glass covers. Decalcified murine bone was used as positive control of RUNX2 staining. Negative control stainings with only secondary antibody were included. Slides were imaged using a Zeiss Axioimager Microscope. Semi-quantitative analysis was performed using the software ImageJ on at least 3 images per sample. All images presented in one panel were captured by using identical detector settings.

4.2.9 Microarray analysis

4.2.9.1 Gene expression of whole lung homogenates from IPF or donor patients: GSE 47460

A microarray dataset published in the Gene Expression Omnibus (GEO) with the accession number GSE47460 – GPL14550 was used to compare gene expression of IPF and donor patients. Gene expression data of 122 IPF and 91 donor patients was extracted.

4.2.9.2 Gene expression of lung fibroblasts isolated from IPF or donor patients: GSE 17978

A microarray dataset published in the Gene Expression Omnibus (GEO) with the accession number GSE17978 (70) was used to compare gene expression of uncultured primary human lung fibroblasts, isolated from IPF or donor patients. A mean value for gene expression of each gene and patient was calculated by calculating the mean value of gene expression of phLF isolated from two to four different lung regions of one patient.

4.2.10 Statistical analysis

GraphPad Prism 5 was used for statistical analysis of all data. Statistics were performed as indicated in the figure legends.

5. RESULTS

5.1 Characterization of the bleomycin model of pulmonary fibrosis

IPF patients exhibit characteristic lung function changes: decreased diffusing capacity for carbon monoxide (DLCO), reduced forced vital capacity (FVC) as well as decreased compliance and increased resistance (71, 72). Murine lung fibrosis at day 14 after intratracheal bleomycin instillation was confirmed by a reduction of compliance (PBS: 0.042 ± 0.0053 mL / cm H_2O vs. BLEO: 0.017 ± 0.0025 mL / cm H_2O; p = 0.0056) and an increase in resistance (PBS: 0.54 ± 0.054 cm H_2O s / mL vs. BLEO: 1.1 ± 0.015 cm H_2O s / mL; p = 0.012) as measured by lung function analysis (Figure 10). Altered lung function parameters correspond to fibrotic changes in lung architecture with increased lung stiffness similar to IPF lungs.

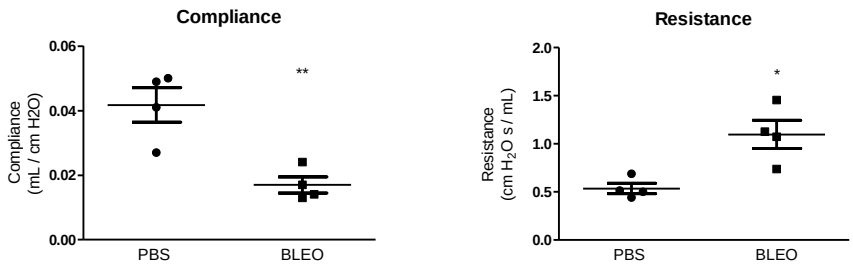

Figure 10: Bleomycin deteriorates lung function in mice 14 days after intratracheal instillation. Lung function analysis was performed on mice 14 days after instillation of PBS or bleomycin, using a FlexiVent machine. n=4 for each group. Statistics: unpaired Student's t-test, * p<0.05, ** p<0.01.

Experimental bleomycin-induced lung fibrosis does not fully recapitulate the histopathological pattern of IPF lungs (73). However, lung histology revealed distorted tissue architecture, increased cell count and increased cell density in hematoxylin & eosin (HE) stainings of BLEO treated lungs (Figure 11).

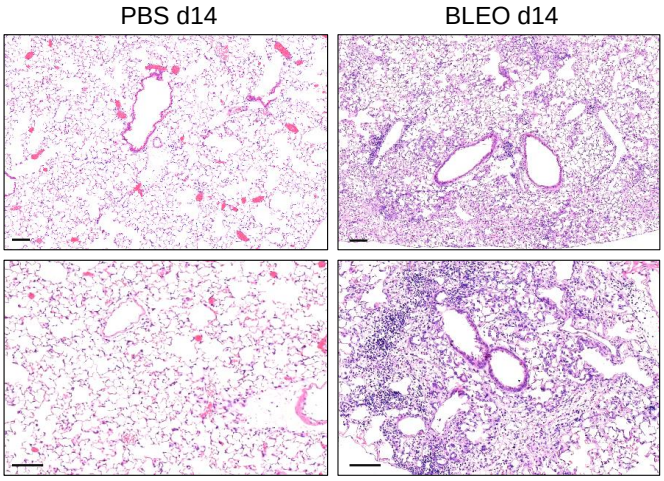

Figure 11: Bleomycin induces changes in lung tissue architecture in mice 14 days after intratracheal instillation. Hematoxylin & eosin stainings were performed on paraffine sections of mice lungs 14 days after instillation of PBS or bleomycin. Representative images of three PBS and three BLEO lungs are shown. Scale bars represent 100 µm.

Gene expression of extracellular matrix (ECM) components was analysed in whole lung tissue lysates over a time course from day 3 to day 14 after bleomycin instillation. Highly significant upregulation of mRNA levels was found for alpha-1 type I collagen *(Col1a1)* (day14: PBS: ΔCt 2.2 ± 0.37 vs. BLEO: ΔCt 4.6 ± 0.18; $p < 0.001$), tenascin-c *(Tnc)* (day14: PBS: ΔCt -3.3 ± 0.78 vs. BLEO: ΔCt 1.5 ± 0.19; $p < 0.001$) and fibronectin *(Fn1)* (day14: PBS: ΔCt 2.5 ± 0.24 vs. BLEO: ΔCt 5.2 ± 0.20; $p < 0.001$) (Figure 12). It is important to notice that upregulation of ECM markers already starts early after lung injury (at day 3-7) and persists after day 10 when the transition towards the fibrotic phase takes place. Upregulation at day 14 corresponds to the increased ECM production and deposition in IPF (74, 75). In contrast, alpha smooth muscle actin *(Acta2)* which is known to be upregulated in human IPF, was unchanged in the bleomycin-model at day 14.

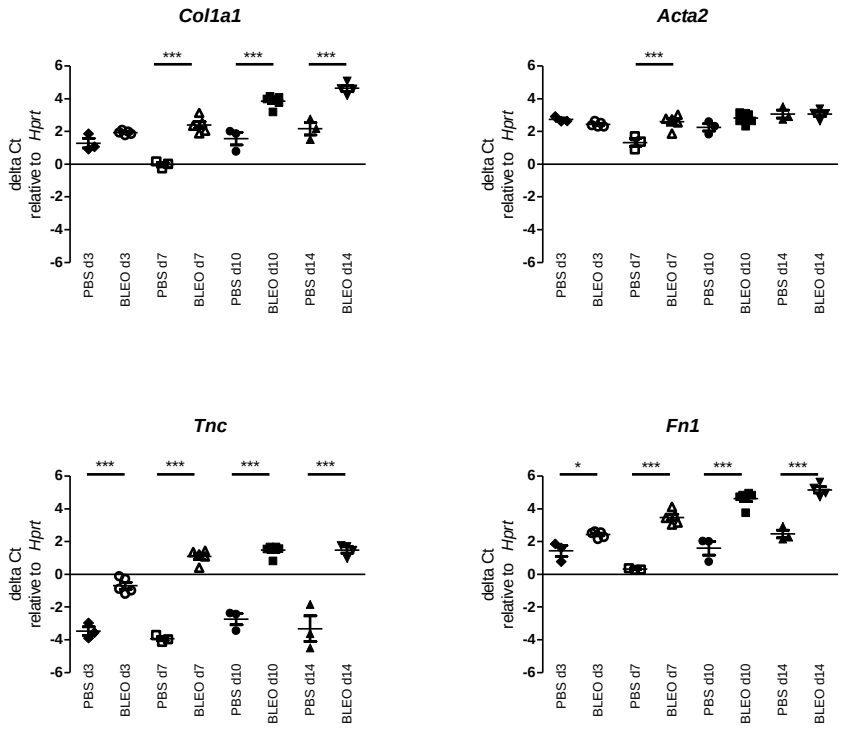

Figure 12: Bleomycin increases mRNA expression of extracellular matrix genes in mice 14 days after intratracheal instillation. Total mRNA was isolated from murine lungs on day 3, day 7, day 10 and day 14 after PBS- or bleomycin instillation. Gene expression of fibrotic marker genes *Col1a1, Acta2, Tnc* and *Fn1* was assessed by qPCR. Data was normalized to *Hprt* and is shown as ΔCt, mean ± SEM. n=3 for each PBS timepoint, n=4-5 for each BLEO timepoint. Statistics: ANOVA, post-test: Bonferroni, compared selected columns, * p<0.05, *** p<0.001.

5.2 Expression of RUNX genes in bleomycin-induced fibrosis

mRNA expression of RUNT-related transcription factors (*Runx1, Runx2, Runx3*) and their main binding-partner core-binding factor beta (*Cbfb*) was determined over a timecourse from day 3 to day 14 after bleomycin instillation. *Runx1* mRNA levels were not significantly altered on any of the four timepoints. *Runx2* as well as *Cbfb* mRNA levels were exclusively increased at day 14, possibly indicating a fibrosis-specific alteration (*Runx2 d14*: PBS: ΔCt -1.7 ± 0.19 vs. BLEO: ΔCt -0.94 ± 0.17; $p < 0.05$) (*Cbfb d14*: PBS: ΔCt -1.3 ± 0.57 vs. BLEO: ΔCt -0.72 ± 0.17; $p < 0.05$). *Runx3*, a known regulator of Wnt-signaling (76), was downregulated on mRNA level on day 7 and day 10, but unchanged on day 14 (Figure 13). Furthermore, the RUNX2 target gene osteopontin (*Spp1)* (77) was confirmed to be highly upregulated in bleomycin-induced fibrosis on all timepoints (*Spp1 d14:* PBS: ΔCt 0.72 ± 0.31 vs. BLEO: 4.8 ± 0.23; $p < 0.001$, data not shown).

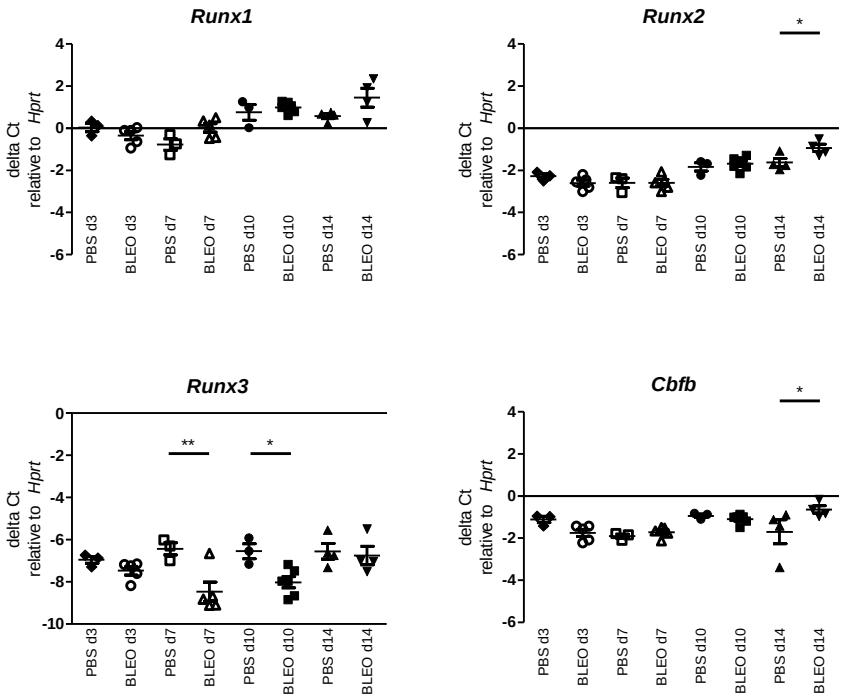

Figure 13: *Runx2* and *Cbfb* mRNA levels are increased on day 14, whereas Runx3 is decreased at day 7 and 10 in bleomycin-induced pulmonary fibrosis. Total mRNA was isolated from murine lungs on day 3, day 7, day 10 and day 14 after PBS- or bleomycin instillation. Gene expression of *Runx1, Runx2, Runx3* and *Cbfb* was assessed by qPCR. Data was normalized to *Hprt* and is shown as ΔCt, mean ± SEM. n=3-4 for each PBS timepoint, n=4-5 for each BLEO timepoint. Statistics: ANOVA, post-test: Bonferroni, compared selected columns, * p<0.05, ** p<0.01, *** p<0.001.

RUNX2 protein expression was assessed by Western Blot analysis. Whole lung protein lysates of bleomycin-treated mice demonstrated increased RUNX2 protein level compared to PBS-treated mice (PBS: 1.0 ± 0.16 vs. BLEO: 3.3 ± 0.46; p = 0.0034) (Figure 14). To ensure this data, increased RUNX2 protein in bleomycin-induced fibrosis was confirmed with a different primary RUNX2 antibody (data not shown).

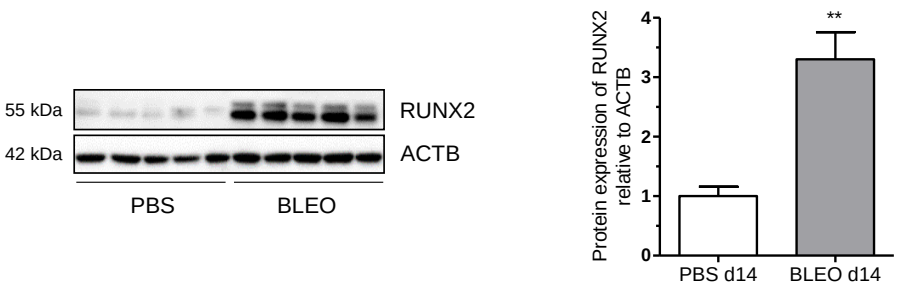

Figure 14: RUNX2 protein level is increased in experimental pulmonary fibrosis. Protein expression of RUNX2 in whole lung homogenates on day 14 after instillation of PBS or bleomycin. Densitometric analysis was performed using β-actin (ACTB) as loading control. n=5 for PBS, n=9 for BLEO. Statistics: unpaired Student's t-test, ** p<0.01.

5.3 Localization of RUNX2 in bleomycin-induced fibrosis

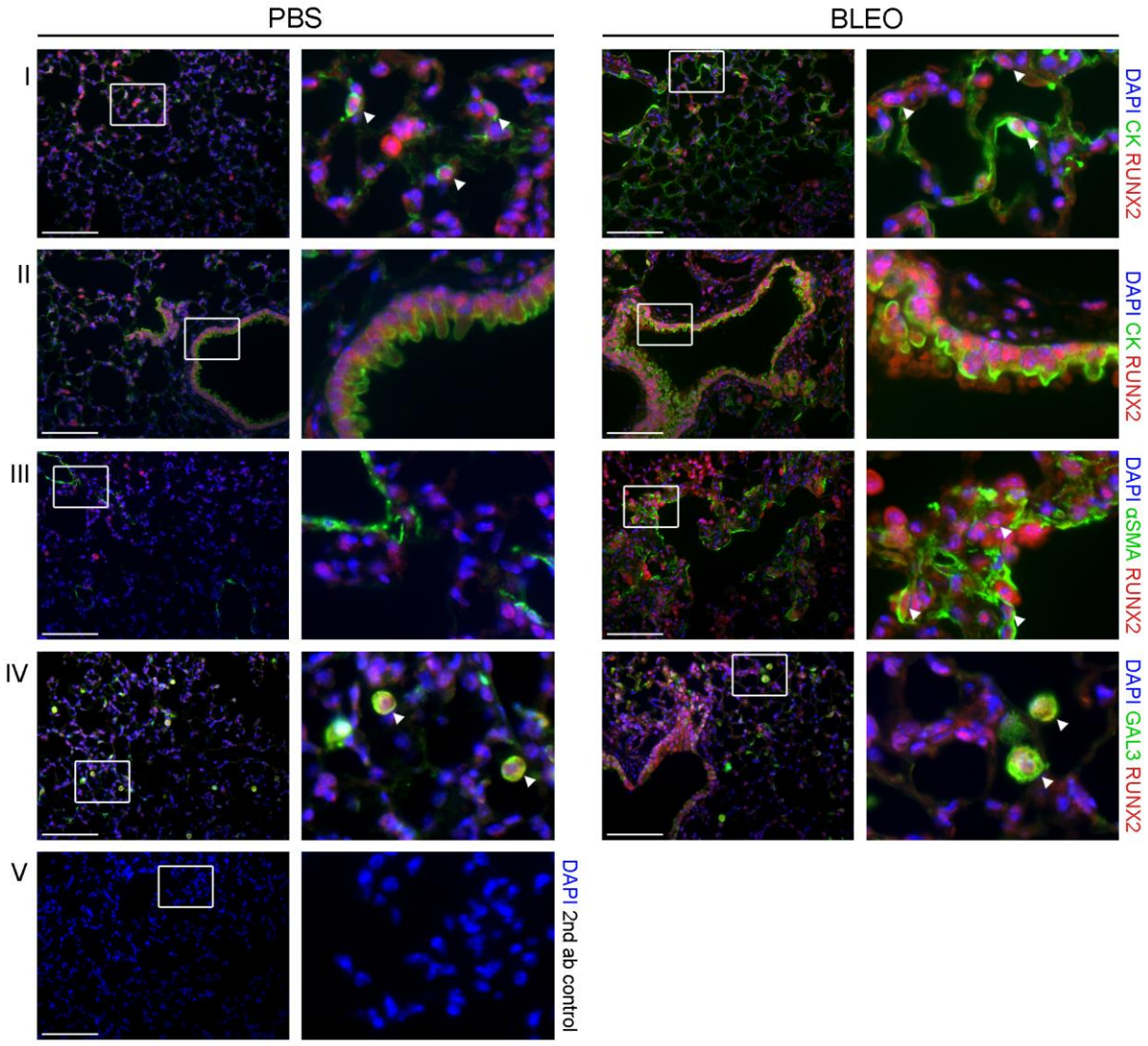

Figure 15: RUNX2 is expressed in alveolar and bronchial epithelium as well as in fibroblasts and alveolar macrophages in bleomycin-induced fibrosis.

Representative immunofluorescence stainings of lung sections of bleomycin- or PBS-treated mice. RUNX2 staining is shown in red, co-staining with cytokeratin (CK, panel I and II), alpha smooth muscle actin (αSMA, panel III) and galectin-3 (GAL3, panel IV) in green. 4′,6-Diamidin-2-phenylindol (DAPI) was used to visualize cell nuclei and is shown in blue. Control staining with only secondary antibody and DAPI is shown in panel V. Higher magnifications of white squares are shown to the right. Scale bars represent 100 µm. n=3 mice for each group.

To determine which cells in murine lung fibrosis express RUNX2 protein, co-stainings of murine lung sections were performed with markers for epithelial cells, myofibroblasts and macrophages. Nuclear staining of RUNX2 was found in alveolar epithelium as well as in bronchial epithelium of fibrotic lungs as evident from co-staining with CK (Figure 15, panel I and II). Furthermore, some αSMA-expressing fibroblasts were found to be RUNX2-positive in PBS and BLEO (Figure 15, panel III). Gal3-expressing

macrophages (Figure 15, panel IV) also expressed RUNX2 protein, but showed a different staining pattern which was rather cytosolic than nuclear (Figure 15, panel IV).

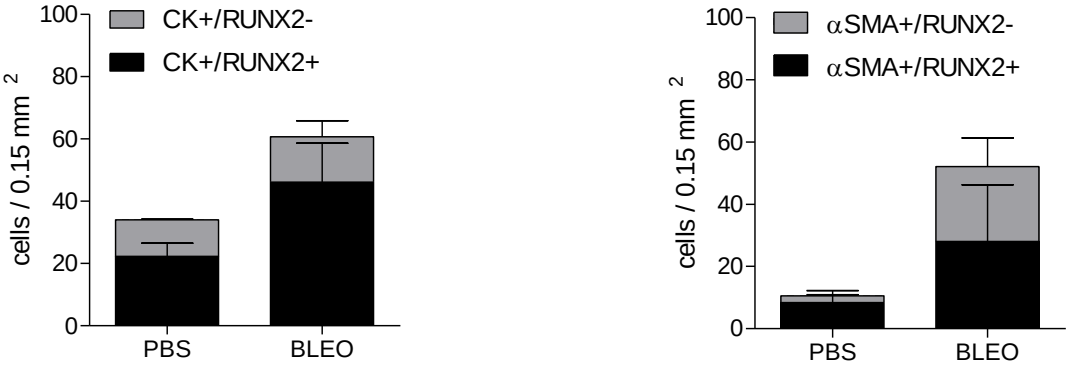

Figure 16: Bleomycin injury leads to an increase in a CK+/RUNX2+ epithelial subpopulation, while the increase in fibroblasts is mainly due to an expansion of an αSMA+/RUNX2- subpopulation. Semiquantitative analysis of IF stainings of Figure 15 was performed with ImageJ software using 3 representative 20x images per mouse and condition. Data shown as mean ± SEM. Statistics are given in Table 19.

Semiquantitative analysis of IF stainings was performed for epithelial (CK+) and mesenchymal (αSMA+) cell populations. Fibrotic lungs demonstrated an increase in epithelial cells determined by CK staining (CK+ total: PBS: 34 ± 2.4 vs BLEO: 61 ± 10 cells / 0.15mm^2, p = 0.064). The increased total number of epithelial cells in bleomycin-induced pulmonary fibrosis was most likely due to an expansion of a RUNX2-positive epithelial subpopulation (CK+/RUNX2+: PBS: 22 ± 2.4 vs BLEO: 46 ± 7.3 cells / 0.15mm^2, p = 0.035). Secondly, a strong increase in (myo-)fibroblasts was determined by αSMA stainings (αSMA+ total: PBS: 11 ± 1.2 vs BLEO: 52 ± 16 cells / 0.15mm^2, p = 0.059). In the αSMA-positive cell population in the non-fibrotic lungs (PBS), only a very small proportion of cells were RUNX2 negative. Interestingly, within the expanded αSMA-positive population in the BLEO lungs, the increase in cells was largely due to a greater RUNX2-negative population (αSMA+/RUNX2-: PBS: 2.1 ± 0.95 vs BLEO: 24 ± 5.3 cells / 0.15mm^2, p = 0.015). A smaller increase could also be noticed in the RUNX2-positive population (Figure 16, Table 19).

Table 19: Bleomycin injury leads to an increase in a CK+/RUNX2+ epithelial subpopulation, while the increase in fibroblasts is mainly due to an expansion of an αSMA+/RUNX2- subpopulation. Semiquantitative analysis of IF stainings of Figure 15 was performed with ImageJ software using 3 representative 20x images per mouse and condition. Data shown as mean ± SEM. Statistics: unpaired Student's t-test.

	PBS (cells / 0.15mm^2)	BLEO (cells / 0.15mm^2)	P value
CK+/RUNX2+	22.22 ± 2.42	46.11 ± 7.25	0.0354
CK+/RUNX2-	11.78 ± 0.11	14.56 ± 2.99	0.4053
αSMA+/RUNX2+	8.44 ± 1.44	28.00 ± 10.55	0.1402
αSMA+/RUNX2-	2.11 ± 0.95	24.11 ± 5.28	0.0148

5.4 Expression of RUNX genes in idiopathic pulmonary fibrosis

Next, *RUNX2* mRNA levels were assessed in whole lung tissue lysates of IPF or donor patients. Here, *RUNX2* mRNA was found to be significantly upregulated in patients with IPF (Donor: ΔCt -0.58 ± 0.18 vs. IPF ΔCt 0.79 ± 0.15, $p < 0.001$). We further detected the upregulation of osteopontin *(SPP1)* mRNA (Donor: ΔCt 1.6 ± 0.68 vs. IPF: ΔCt 4.7 ± 0.31, $p < 0.001$) as well as of matrix metalloproteinase 7 *(MMP7)* mRNA, a protease that cleaves ECM products (Donor: ΔCt -0.18 ± 0.39 vs. IPF: ΔCt 4.2 ± 0.31, $p < 0.001$). These genes have been shown to correlate with the disease course of IPF and were discussed as potential IPF biomarkers (78, 79). Furthermore, we found higher mRNA levels of *ACTA2* (Donor: ΔCt 3.3 ± 0.27 vs. IPF ΔCt 4.7 ± 0.24, $p < 0.001$) and *TNC* (Donor: ΔCt 0.61 ± 0.41 vs. IPF: ΔCt 2.5 ± 0.18, $p < 0.001$) in lungs from IPF patients. (Figure 17).

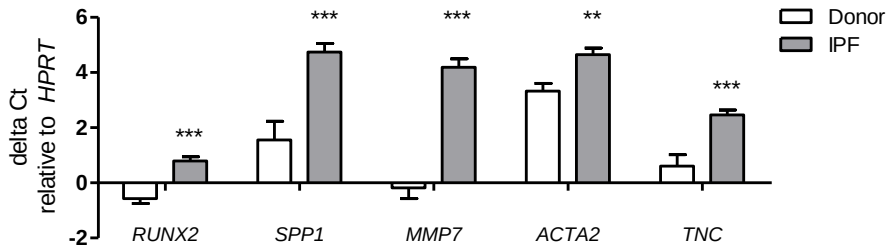

Figure 17: *RUNX2* mRNA levels are increased in IPF patients.

mRNA levels of *RUNX2, SPP1, MMP7, ACTA2, TNC* were assessed by qPCR in whole lung homogenates of IPF and donor patients. Data was normalized to *HPRT* and is shown as ΔCt, mean ± SEM. n=8-16 for donor, n=14-37 for IPF patients. Statistics: unpaired Student's t-test, ** p<0.01, *** p<0.001.

To validate these findings in a larger cohort, gene expression data of IPF and donor patients was extracted from a dataset published by the Lung Tissue Research Consortium (LTRC) with the GSE accession number 47460. Here, an increase of *RUNX1* (Donor: 7.3 ± 0.097 vs. 7.8 ± 0.072, $p < 0.001$) and *RUNX2* (Donor: 7.4 ± 0.051 vs. IPF 8.1 ± 0.047, $p < 0.001$) mRNA was found, as well as a decrease in *RUNX3* mRNA (Donor: 9.7 ± 0.059 vs. IPF: 9.5 ± 0.043, $p < 0.05$). Additionally, the main binding partner of RUNT-related genes, *CBFB* was found to be increased in human pulmonary fibrosis (Donor: 10.6 ± 0.0321 vs. IPF: 10.8 ± 0.0149, $p < 0.001$). *RUNX1* and *RUNX2* levels were negatively correlated to the diffusing capacity of the lung for carbon monoxide (DLCO) (*RUNX1* to DLCO: Pearson r = -0.49, $p < 0.001$) (*RUNX2* to DLCO: Pearson r = -0.49, $p < 0.001$). DLCO is a clinical measurement of gas exchange through the alveolar-capillary membrane, which decreases with the progression of IPF (71). Furthermore, *RUNX1* and *RUNX2* levels were positively correlated with *MMP7* (*RUNX1* to *MMP7*: Pearson r = 0.42, $p < 0.001$) (*RUNX2* to *MMP7*: Pearson r = 0.70, $p < 0.001$) and *SPP1* (*RUNX1* to *SPP1*: Pearson r = 0.46, $p < 0.001$) (*RUNX2* to *SPP1*: Pearson r = 0.67, $p < 0.001$). To a lesser extent, negative correlation with DLCO and positive correlation with IPF biomarkers was also found for *CBFB (CBFB* to DLCO: Pearson r = -0.26, $p < 0.001$; *CBFB* to *MMP7*: 0.37, $p < 0.0001$; *CBFB* to *SPP1*: 0.38, $p < 0.001$). *RUNX3* showed a slightly positive correlation with DLCO (*RUNX3* to DLCO: Pearson r = 0.15, $p = 0.04$) but no correlation with IPF biomarkers (Figure 18).

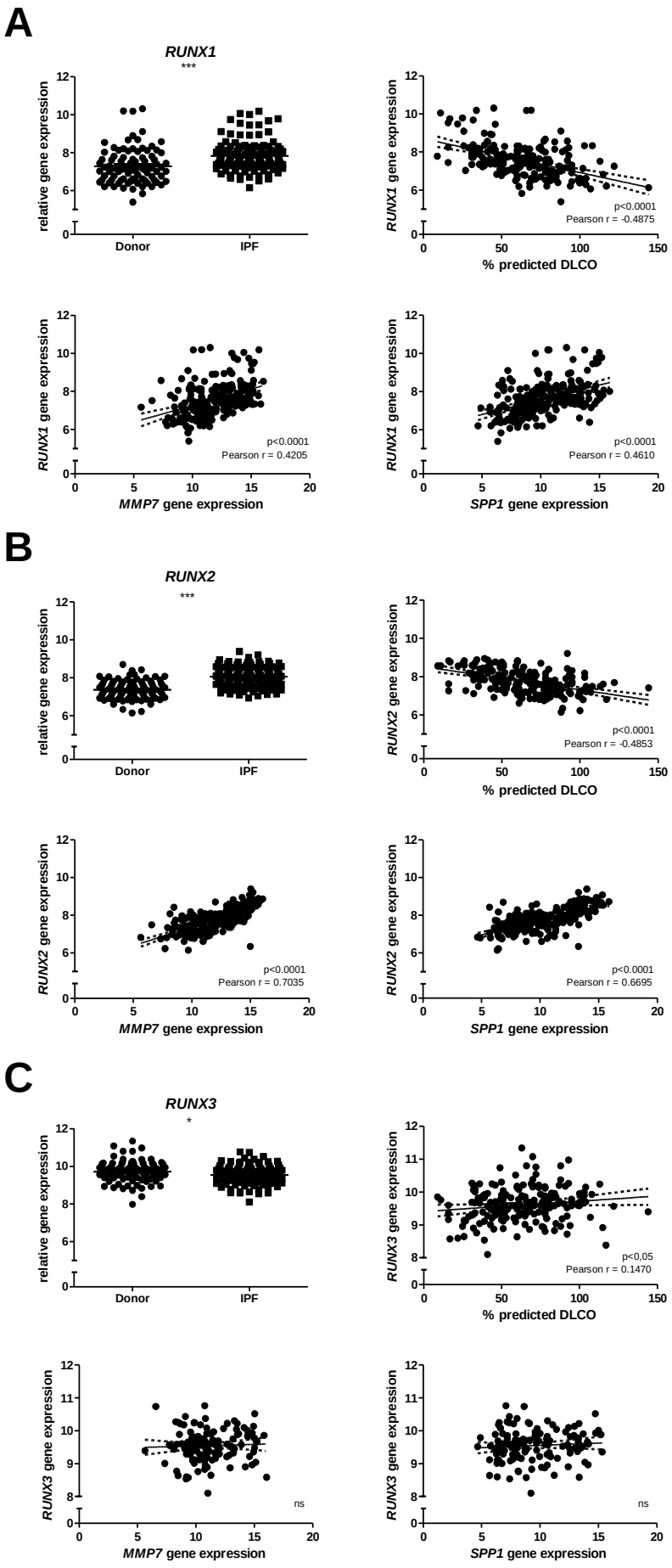
A
RUNX1
***
relative gene expression
Donor
IPF
RUNX1 gene expression
% predicted DLCO
p<0.0001
Pearson r = -0.4875
MMP7 gene expression
p<0.0001
Pearson r = 0.4205
SPP1 gene expression
p<0.0001
Pearson r = 0.4610
B
RUNX2
***
RUNX2 gene expression
p<0.0001
Pearson r = -0.4853
p<0.0001
Pearson r = 0.7035
p<0.0001
Pearson r = 0.6695
C
RUNX3
*
RUNX3 gene expression
p<0,05
Pearson r = 0.1470
ns
ns

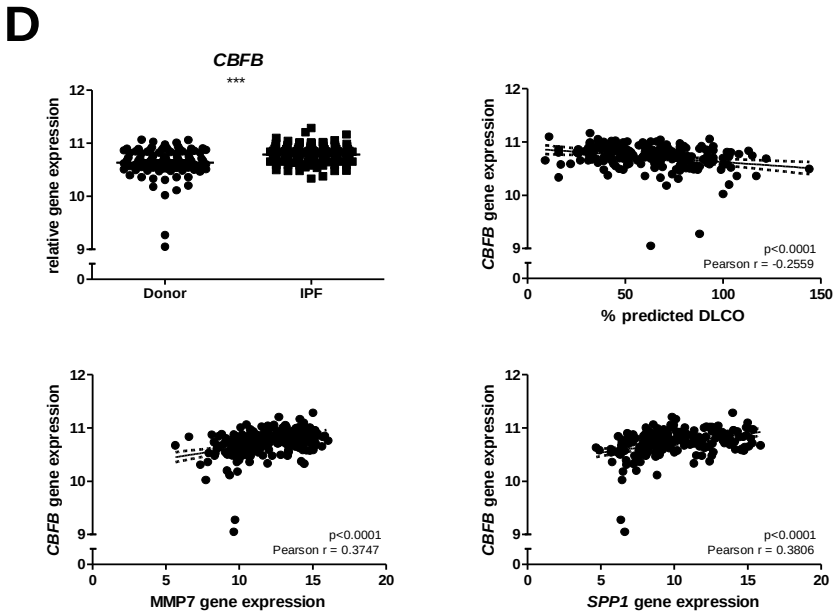

Figure 18: *RUNX* genes are differentially regulated in IPF and *RUNX1, RUNX2* as well as *CBFB* correlate with parameters of disease progression. Analysis of microarray data published with the accession number GSE47460 by the Lung Genomics Research Consortium. Gene expression levels of *RUNX1* (A)*, RUNX2* (B)*, RUNX3* (C) and *CBFB* (D) were assessed in IPF and donor patients. Gene expression was correlated with % predicted diffusing capacity for carbon monoxide (DLCO) or expression levels of matrix metalloproteinase-7 (*MMP7*) and osteopontin (*SPP1*). n=91 for donor, n=122 for IPF patients. Statistics: unpaired Student's t-test, * p<0.05, *** p<0.001; Pearson r was used for correlation analysis.

Protein levels of RUNX2 and αSMA were assessed by Western Blotting. RUNX2 protein expression was significantly increased in whole lung homogenates of IPF patients (Donor: 1.0 ± 0.17 vs. IPF: 1.5 ± 0.11, $p < 0.05$) and seemed to correspond to levels of αSMA (Figure 19).

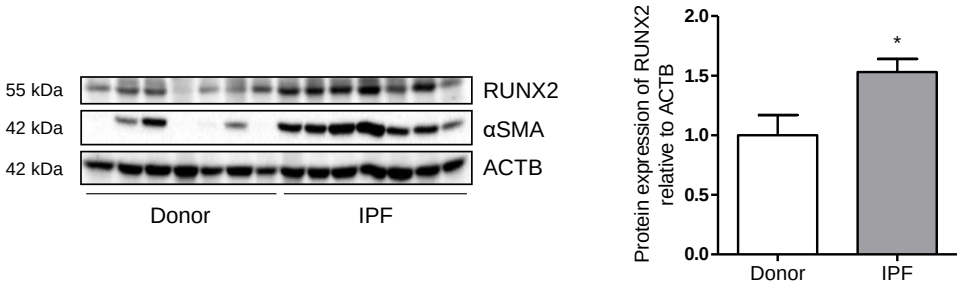

Figure 19: RUNX2 protein level is increased in IPF patients.
Protein expression of RUNX2 and αSMA was determined in whole lung homogenates of IPF and donor patients. Densitometric analysis was performed using β-actin (ACTB) as loading control. n=7 donor, n=7 IPF patients. Statistics: unpaired Student's t-test, * p<0.05.

5.5 Localization of RUNX2 in idiopathic pulmonary fibrosis

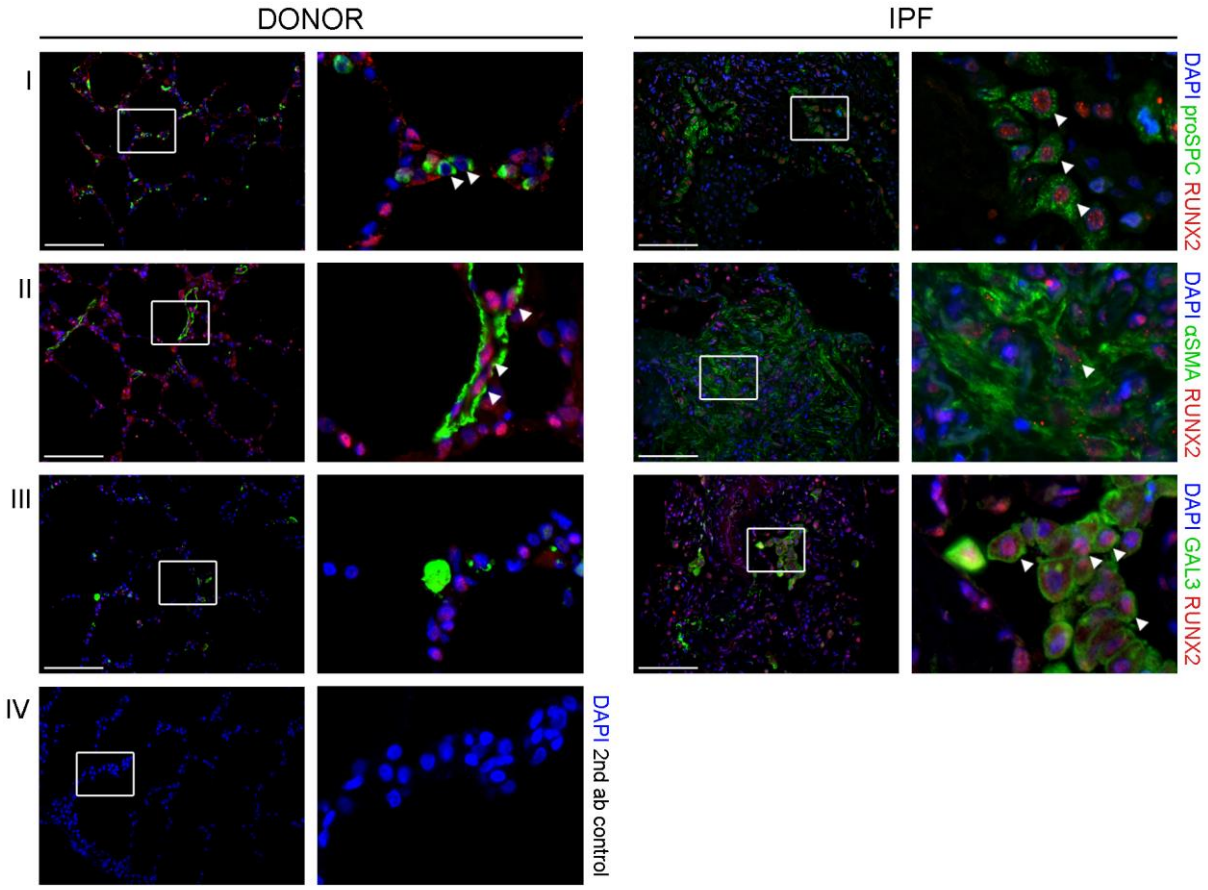

Figure 20: RUNX2 localizes to several cell types and is strongly expressed in proSPC-positive hyperplastic ATII cells. Representative immunofluorescence stainings were performed on paraffine sections of donor and IPF lungs. RUNX2 staining is shown in red, co-staining with pro-surfactant protein C (proSPC, panel I), alpha smooth muscle actin (αSMA, panel II) and galectin-3 (GAL3, panel III) in green. 4′,6-Diamidin-2-phenylindol (DAPI) was used to visualize cell nuclei and is shown in blue. Control staining with only secondary antibody and DAPI is shown in panel IV. Higher magnifications of white squares are shown to the right. Scale bars represent 100 µm. n=3 patients for each group.

Localization of RUNX2 protein in tissue sections of IPF and donor patients was performed by co-staining with pro-surfactant protein C (proSPC) as an ATII cell marker, alpha smooth muscle actin (αSMA) as a myofibroblast / smooth muscle cell marker and galectin-3 (Gal3) as a marker for alveolar macrophages. Nuclear RUNX2 staining was partly found in αSMA-positive myofibroblasts as well as in Gal3-positive alveolar macrophages. Myofibroblast foci seemed to display only few RUNX2 positive fibroblasts. Hyperplastic ATII cells, sometimes completely lining the altered alveoli of IPF lungs, showed the strongest signal with the majority of cells being positive for RUNX2, whereas less RUNX2-nuclear positive ATII cells were detected in donor lungs (Figure 20).

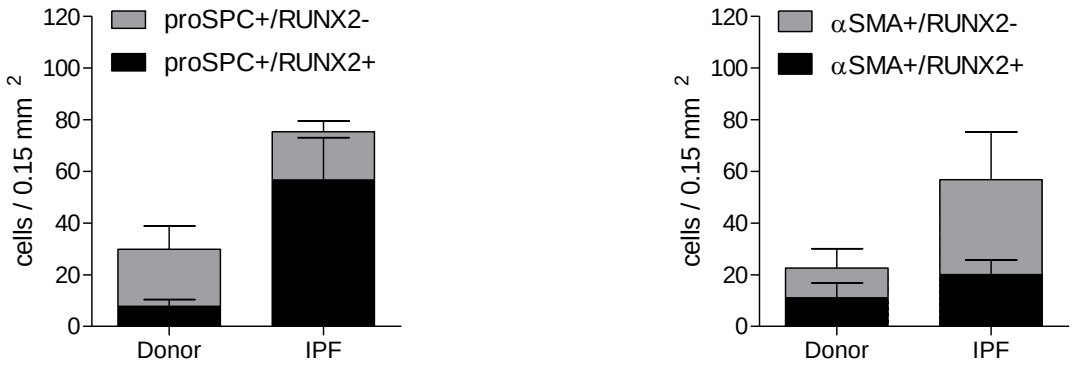

Figure 21: IPF lungs exhibit an expanded proSPC+/RUNX2+ epithelial cell population while the increase in fibroblasts is markedly due to an expansion of RUNX2- fibroblasts. Semiquantitative analysis of IF stainings of Figure 20 was performed with ImageJ software using 3 representative 20x images per patient and condition. Data shown as mean ± SEM. Statistics are given in Table 20.

Semiquantitative analysis of IF stainings revealed similar to the bleomycin-induced model of pulmonary fibrosis a total increase in ATII cells as well as (myo-)fibroblasts in fibrotic lung sections. The increase in proSPC-positive ATII cells in IPF lung sections (proSPC+ total: Donor: 30 ± 6.6 vs IPF: 75 ± 12 cells / 0.15mm^2, p = 0.028) was further characterized by an expansion of a RUNX2-positive subpopulation (proSPC+/RUNX2+: Donor: 7.9 ± 1.5 vs IPF: 57 ± 9.5 cells / 0.15mm^2, p = 0.007). Additionally, the number of αSMA-positive (myo-) fibroblasts was increased in pulmonary fibrosis (αSMA+ total: Donor: 23 ± 7.1 vs IPF: 57 ± 14 cells / 0.15mm^2, p = 0.092). Here, it was mainly the αSMA-positive/RUNX2-negative subpopulation that was expanded in IPF lungs (aSMA+/RUNX2-: Donor: 12 ± 4.3 vs IPF: 37 ± 11 cells / 0.15mm^2, p = 0.092).

Table 20: IPF lungs exhibit an expanded proSPC+/RUNX2+ epithelial cell population while the increase in fibroblasts is markedly due to an expansion of RUNX2- fibroblasts. Semiquantitative analysis of IF stainings of Figure 20 was performed with ImageJ software using 3 representative 20x images per patient and condition. Data shown as mean ± SEM. Statistics: unpaired Student's t-test.

	Donor (cells / 0.15mm^2)	IPF (cells / 0.15mm^2)	P value
proSPC+/RUNX2+	7.89 ± 1.46	56.67 ± 9.45	0.0070
proSPC+/RUNX2-	22.00 ± 5.21	18.67 ± 2.34	0.5903
αSMA+/RUNX2+	11.17 ± 3.34	20.11 ± 3.23	0.1261
αSMA+/RUNX2-	11.45 ± 4.33	36.78 ± 10.62	0.0917

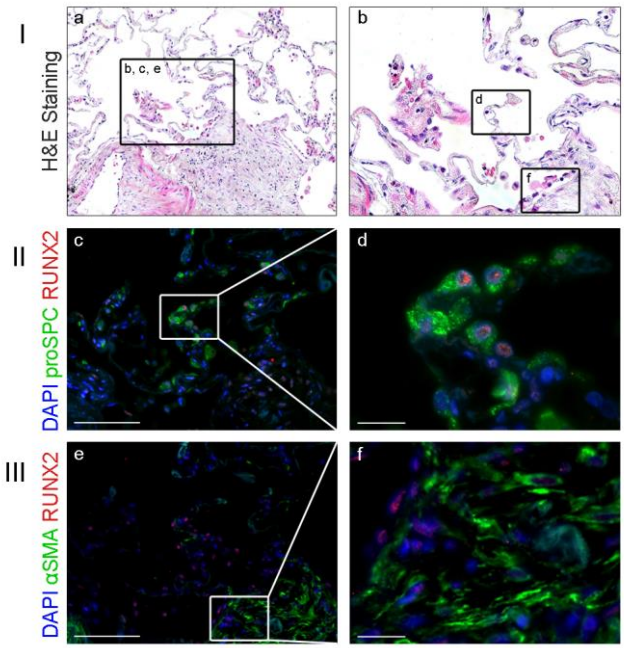

Figure 22: RUNX2 protein is expressed in the nucleus of hyperplastic ATII cells adjacent to a fibroblastic focus. Representative images from H&E stainings (a, b) and immunofluorescence co-stainings for proSPC (green) plus RUNX2 (red; c, d) or co-stainings for αSMA (green) plus RUNX2 (red; e, f). H&E staining is shown for better visualization of the underlying tissue architecture. Higher magnification of white squares in c, e is shown in d, f, respectively. Scale bars represent 100µm (c, e) and 20µm (d, f).

Serial section stainings showed that hyperplastic RUNX2-positive ATII cells were often in close proximity to αSMA-positive myofibroblast foci, suggesting an epithelial-mesenchymal interaction (Figure 22).

5.6 Influence of signaling pathways on RUNX2 gene expression

5.6.1 TGF-β signaling

TGF-β is one of the most important drivers of fibrotic diseases and plays a crucial role in the progression of idiopathic pulmonary fibrosis (60). Interplay between TGF-β signaling and RUNX genes has been shown in various cell types and is relevant for fundamental biological processes such as cell proliferation and differentiation (80, 81). To identify the relation of RUNX factors and TGF-β in lung cells, primary human lung fibroblasts and the human alveolar epithelial cell line A549 were stimulated with recombinant human TGF-β1.

RUNX1 and *RUNX3* mRNA levels were significantly increased by TGF-β1 in phLF (*RUNX1:* ctrl: ΔCt 2.2 ± 0.27 vs. TGF-β1: ΔCt 4.8 ± 0.15; p = 0.0019) (*RUNX3:* ctrl: ΔCt -2.8 ± 0.51 vs. TGF-β1: ΔCt -1.5 ± 0.49, p = 0.0005) (Figure 23). *RUNX2* levels were increased, but this result did not reach statistical significance (*RUNX2:* ctrl: ΔCt -1.4 ± 0.38 vs. TGF-β1: ΔCt -0.45 ± 0.16; p = 0.078). ECM genes *COL1A1, TNC, FN1* and the myofibroblast marker *ACTA2* were increased upon TGF-β1 treatment.

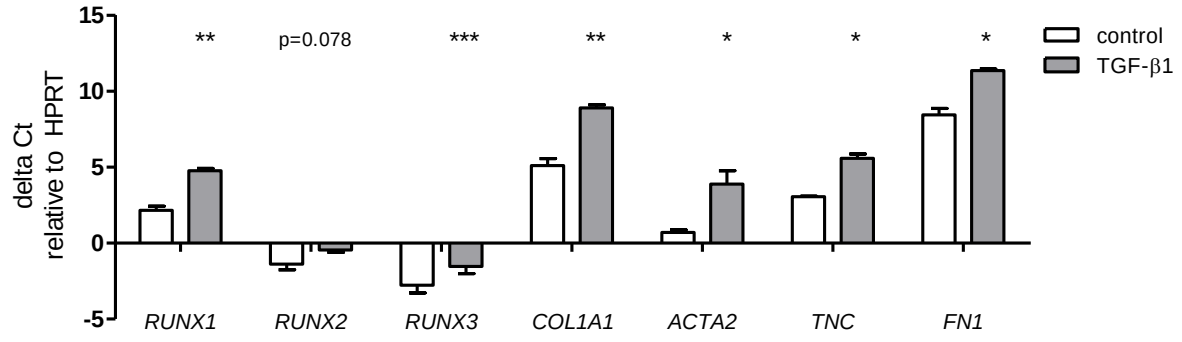

Figure 23: RUNX1 and RUNX3 mRNA levels are increased by TGF-β1 stimulation in phLF. Cells were treated with human recombinant TGF-β1 (2 ng/ml) for 12 hours. Gene expression was analysed by qPCR, normalized to *HPRT* and displayed as ΔCt compared to untreated cells, mean ± SEM. n=3 for control, n=3 for TGF-β1. Statistics: paired Student's t-test, * p<0.05, ** p<0.01, *** p<0.001.

Treatment of A549 cells with TGF-β1 revealed a significant induction of *RUNX1* and *RUNX2* mRNA levels (*RUNX1:* ctrl: ΔCt -2.4 ± 0.029 vs. TGF-β1: ΔCt -0.018 ± 0.065, p = 0.0003) (*RUNX2:* ctrl: ΔCt -8.2 ± 0.34 vs. TGF-β1: ΔCt -5.1 ± 0.10, p = 0.0064). *RUNX3* however, was unchanged. TGF-β1 also induced the expression of fibrotic marker genes *COL1A1, TNC, FN1* whereas *ACTA2* was unchanged (Figure 24).

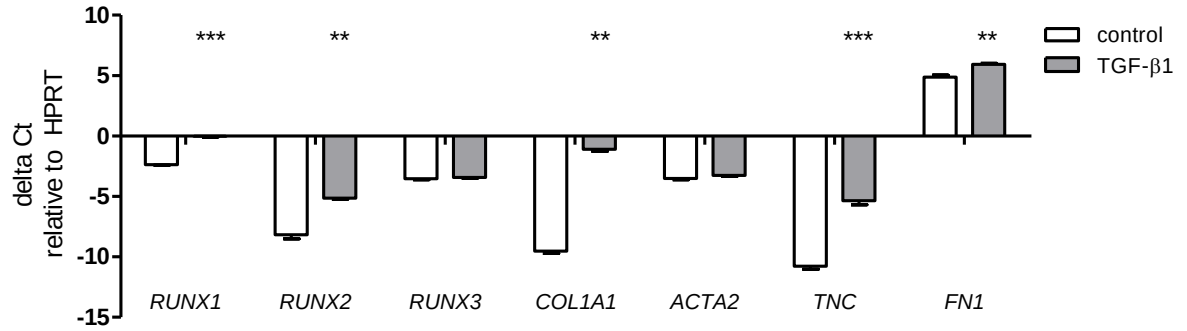

Figure 24: RUNX1 and RUNX2 mRNA levels are increased by TGF-β1 stimulation in A549 cells. Cells were treated with human recombinant TGF-β1 (2 ng/ml) for 12 hours. Gene expression was analysed by qPCR, normalized to *HPRT* and displayed as ΔCt compared to untreated cells, mean ± SEM. n=3 for control, n=3 for TGF-β1. Statistics: paired Student's t-test, ** p<0.01, *** p<0.001.

5.6.2 WNT/β-catenin signaling

Reactivation of the WNT/β-catenin pathway plays a significant role in the development of pulmonary fibrosis and inhibition of WNT/β-catenin signaling was shown to ameliorate pulmonary fibrosis in mice (66, 82-84). Importantly, RUNX2 was found to be a target gene of WNT/β-catenin signaling in osteoblast precursor cells (61). To elucidate a potential effect of WNT/β-catenin signaling on RUNX2 expression, A549 cells, pmATII cells and phLF were treated with recombinant WNT3a protein or CHIR99021, a GSK3β-specific inhibitor that leads to WNT/β-catenin pathway activation.

RUNX2 mRNA levels were strongly increased in A549 cells after a 24h treatment with CHIR99021 (fold change: CHIR99021: 17 ± 3.3, p = 0.0011) (Figure 25 A). An 8h treatment of A549 cells with recombinant WNT3a also led to the induction of RUNX2 mRNA (fold change: WNT3a: 3.8 ± 0.56, p = 0.016) (Figure 25 B). WNT3a treatment of pmATII cells caused a minor increase in RUNX2 mRNA but did not reach statistical significance (Figure 25 C). An induction of RUNX2 mRNA was also seen in phLF upon treatment with CHIR99021 (fold change: CHIR99021: 5.3 ± 1.3, p = 0.035) (Figure 25 D).

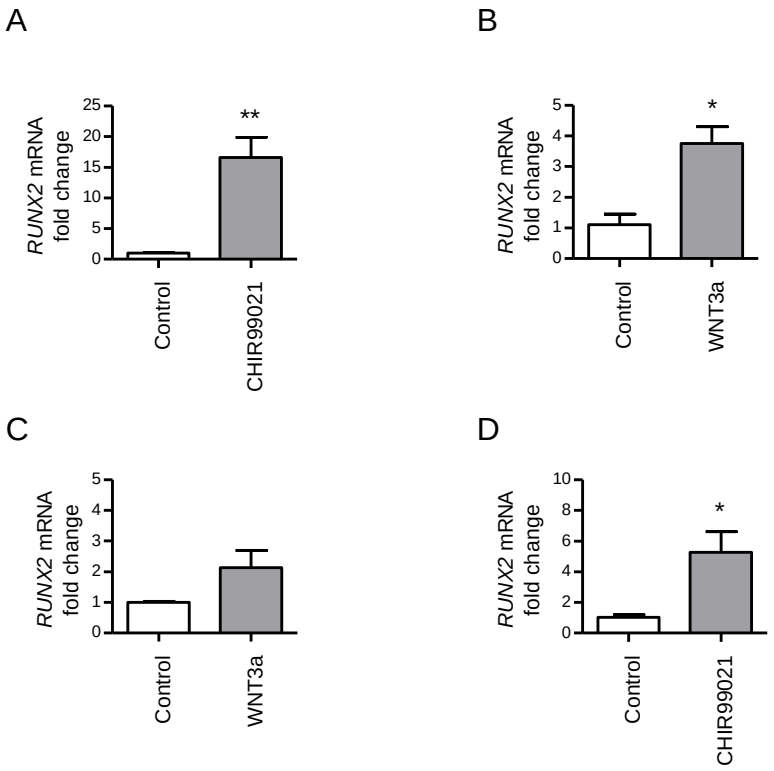

Figure 25: RUNX2 mRNA expression is increased by WNT/β-catenin activation in A549 cells and primary human lung fibroblasts. A) A549 cells were treated with the WNT/β-catenin activating compound CHIR99021 (2 µM) or vehicle control for 24h. n=5 for control, n=4 for CHIR99021. B) A549 cells were treated with recombinant human WNT3a (100 ng/ml) or vehicle control for 8h. n=3 for each group. C) pmATII cells were treated with recombinant human WNT3a (100 ng/ml) or vehicle control for 12h. n=3 for each group. D) phLF were treated with the WNT/β-catenin activating compound CHIR99021 (2 µM) or vehicle control for 24h. n=3 for each group. In all experiments, gene expression was analysed by qPCR, normalized to *HPRT* and displayed as fold change to vehicle control, mean ± SEM. Statistics: unpaired Student's t-test, * $p<0.05$, ** $p<0.01$.

5.7 Expression and function of RUNX2 in ATII cells

Alveolar epithelial cell damage is a key feature of IPF (79). ATII cells are regarded as lung stem cells, giving rise to ATI cells and thereby initiating repair processes (85-87). However, in IPF ATII cells are often altered, displaying hyperplasia and exhibiting either apoptosis or hyperproliferation (88). RUNX2 was localized to hyperplastic ATII cells by immunofluorescence stainings (Figure 20), therefore the function of RUNX2 was further studied in healthy and injured alveolar epithelial cells.

5.7.1 Expression of RUNX2 in primary murine ATII cells

To evaluate if RUNX2 expression is differentially regulated in pmATII cells in bleomycin-induced fibrosis, pmATII cells were isolated on day 14 after intratracheal PBS- or bleomycin-instillation and total mRNA was extracted. qPCR analysis revealed a significant upregulation of *Runx2* (PBS: ΔCt -3.4 ± 0.18 vs. BLEO: ΔCt -2.0 ± 0.22, $p < 0.001$), the pro-migratory gene S100 Calcium Binding Protein A4 (*S100a4)* (PBS: ΔCt -3.2 ± 0.16 vs. BLEO: ΔCt -0.53 ± 0.31, $p < 0.001$) and the pro-proliferatory gene cyclin D1 *(Ccnd1)* (PBS: ΔCt 3.8 ± 0.18 vs. BLEO: ΔCt 4.4 ± 0.14, $p < 0.05$) in fibrotic lungs. Furthermore, the fibrotic marker genes *Tnc* and *Fn1* were found to be increased (Figure 26). *Runx1* and *Cbfb* mRNA levels were not altered in ATII cells isolated from fibrotic lungs compared to non-fibrotic lungs.

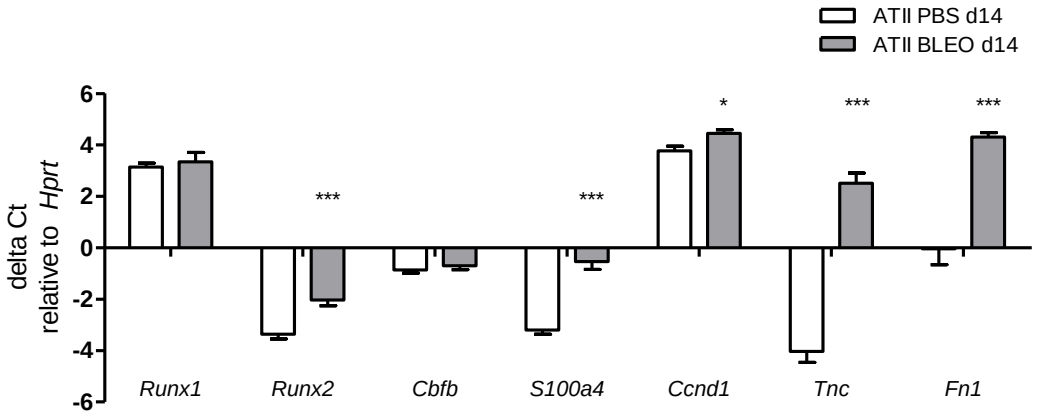

Figure 26: RUNX2 is upregulated in primary murine ATII cells isolated from fibrotic mouse lungs. On day 14 after instillation of PBS or bleomycin, mice were sacrificed and ATII cells were isolated. Gene expression was analysed by qPCR, data was normalized to *Hprt* and is shown as ΔCt, mean ± SEM. n=4-8 for PBS, n=4-9 for BLEO. Statistics: paired Student's t-test, ** $p<0.01$, *** $p<0.001$.

To evaluate RUNX2 protein expression and localization, ATII cells were isolated at day 14 after intratracheal instillation of PBS or bleomycin. After isolation, cells were seeded on coverslips and subjected to immunofluorescence staining. A clear increase in RUNX2 protein in ATII cells from fibrotic mice lungs compared to non-fibrotic lungs was noticed. RUNX2 was strongly expressed in the nucleus of fibrotic ATII cells and prominent staining was also seen in proliferating fibrotic ATII cells (Panel III). In comparison, RUNX2 staining in non-fibrotic ATII cells was less intense and RUNX2 mainly localized to the cytosol (Figure 27). Interestingly, RUNX2 staining was not homogenously distributed throughout the nucleus, but localized to certain nuclear areas, whereas other nuclear areas were spared out.

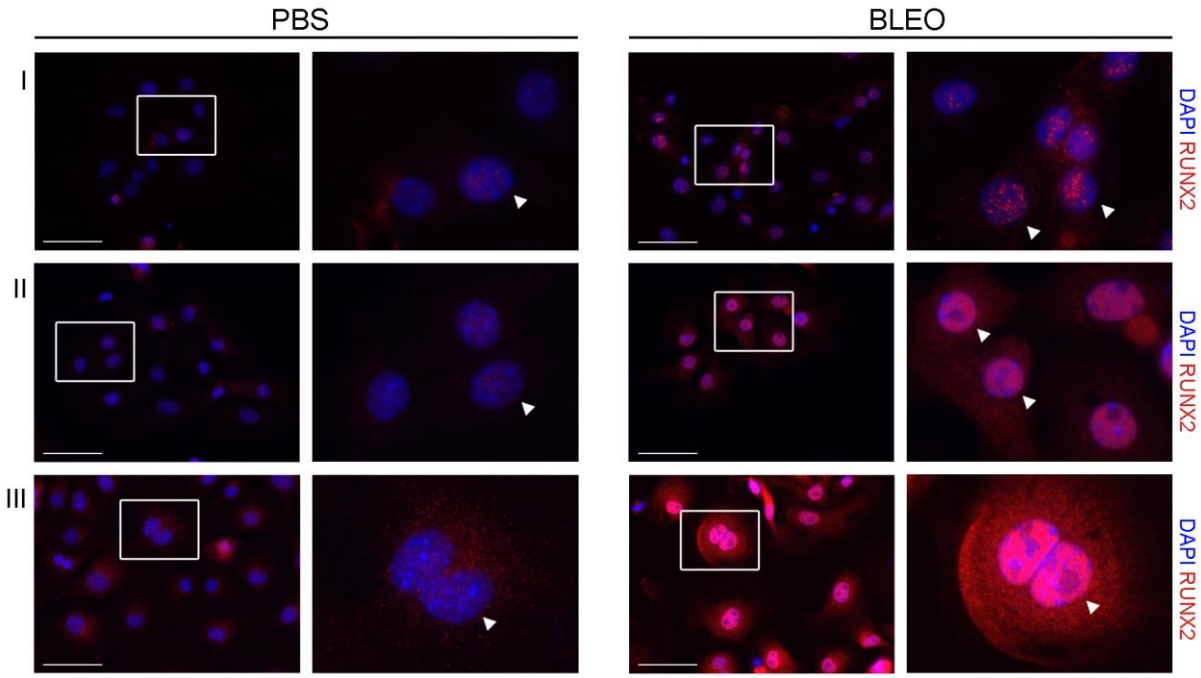

Figure 27: RUNX2 protein expression is upregulated in fibrotic pmATII cells and localizes to the cell nucleus. Representative immunofluorescence stainings of isolated ATII cells from non-fibrotic and fibrotic mouse lungs. RUNX2 staining is shown in red. DAPI was used to visualize cell nuclei and is shown in blue. Scale bars represent 50µm. n = 3 mice for each group.

5.7.2 Knockdown of RUNX2 in primary murine ATII cells

To delineate RUNX2 function in healthy and injured alveolar epithelium, RUNX2 knockdown experiments were performed in primary murine ATII cells isolated on day 14 after bleomycin or PBS instillation. RUNX2 knockdown was confirmed by qPCR in the PBS group (fold change to PBS scr: siRUNX2: 0.31 ± 0.057; p = 0.001) and in the BLEO group (fold change to BLEO scr: siRUNX2: 0.42 ± 0.057; p = 0.0006). Loss of RUNX2 led to a decrease of *S100a4* mRNA levels (fold change to PBS scr: 0.48 ± 0.068; p = 0.0024) as well as to a reduction of *Ccnd1* (fold change to PBS scr: 0.75 ± 0.074; p = 0.021) in uninjured ATII cells. In ATII cells from bleomycin-treated mice only the reduction of *Ccnd1* mRNA (fold change to BLEO scr: 0.74 ± 0.075, p = 0.041) reached statistical significance upon loss of RUNX2. However, *S100a4* expression seemed to go in similar direction with the knockdown as observed in the PBS ATIIs (Figure 28). Surprisingly, *Spp1* was unaltered in the PBS- as well as in the BLEO-group. Previous studies suggested a role of RUNX2 in epithelial-mesenchymal transition in A549 cells (89). Therefore, several epithelial (*Spc, Zo-1, Cdh1, Ocln*) and mesenchymal markers (*S100a4, Acta2, Twist*) as well as the EMT transcription factor *Snai2* were evaluated by qPCR analysis. Except

for the described changes in *S100a4* mRNA, no clear evidence for RUNX2 regulating EMT in primary ATII cells was found (data not shown).

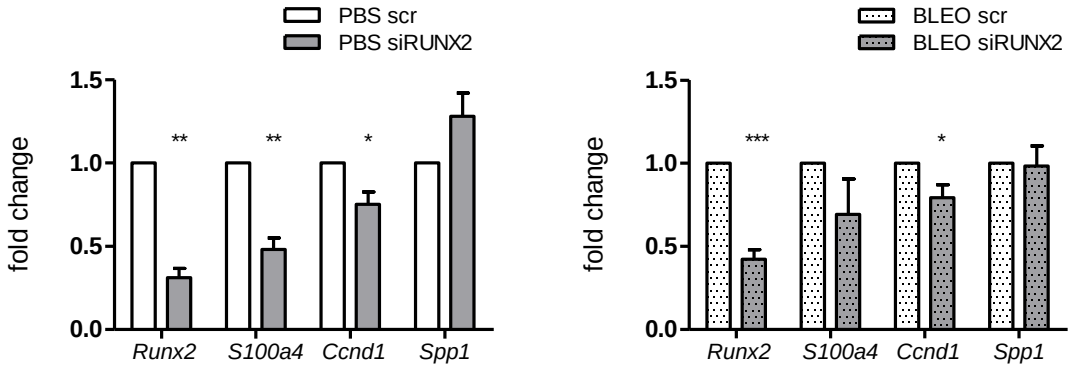

Figure 28: Loss of RUNX2 in pmATII cells decreases *Ccnd1* and *S100a4* mRNA levels. Primary murine ATII cells isolated on day 14 after instillation of PBS or bleomycin were cultured and transfected with RUNX2-specific siRNA (siRUNX2) or scrambled siRNA (scr). Knockdown was performed for 48 hours. Gene expression was analysed by qPCR, normalized to HPRT and displayed as fold change compared to scrambled siRNA control, mean ± SEM. n=6 for PBS scr, n=6 for PBS siRUNX2, n=4-5 for BLEO scr, n=4-5 for BLEO siRUNX2. Statistics: paired Student's t-test * p<0.05, ** p<0.01, *** p<0.001.

The downregulation of CCND1 on mRNA level was confirmed on protein level by Western blotting of cell lysates of transfected pmATII cells (fold change to scr: siRUNX2: 0.72 ± 0.12 SEM) (Figure 29).

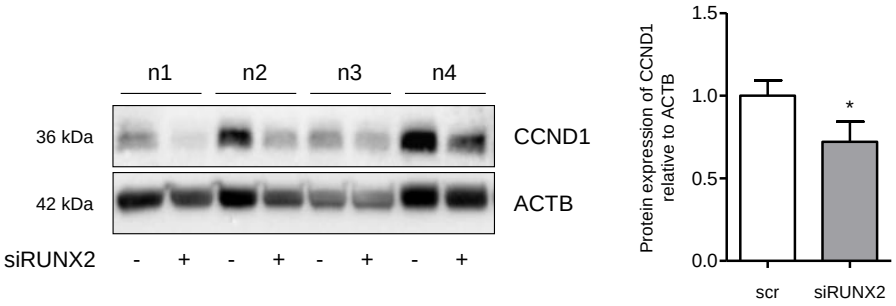

Figure 29: Loss of RUNX2 in pmATII cells decreases CCND1 protein levels. Protein expression of CCND1 was determined in cell lysates of scr- or siRUNX2-transfected primary murine ATII cells isolated 14 days after instillation of bleomycin. Densitometric analysis was performed using β-actin (ACTB) as loading control.

To investigate a potential effect of RUNX2 on cell migration, siRNA-mediated knockdown of RUNX2 was performed in A549 cells and a pipet tip scratch was made in an almost confluent cell layer. Cell migration into the scratch was captured for 48h. Already 24h after the scratch a significant reduction in cell migration could be observed in the siRUNX2-transfected cells compared to scr-transfected cells (scr:

21% ± 1.2% vs siRUNX2: 7.3% ± 1.3% wound closure, p < 0.01). This effect was even more prominent after 48h (scr: 34% ± 1.7% vs siRUNX2: 10% ± 1.4% wound closure, p < 0.001).

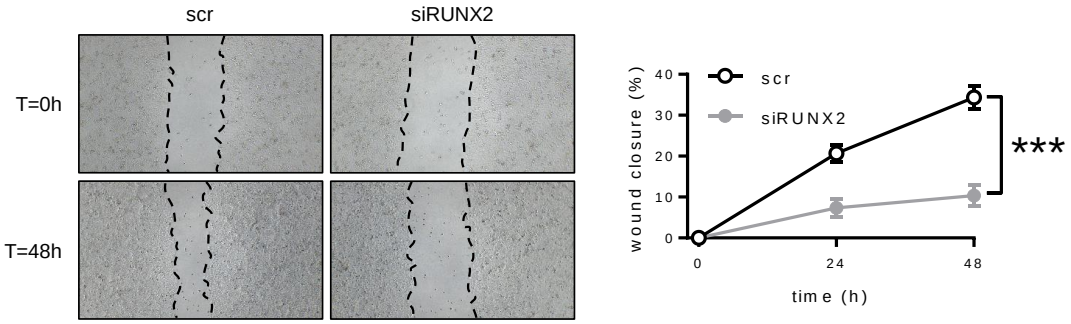

Figure 30: Knockdown of RUNX2 reduces cell migration. A pipet-tip scratch was made in a cell layer of A549 cells transfected with RUNX2-specific siRNA (siRUNX2) or scrambled siRNA (scr). Representative images (n = 3) at 0 and 48h are shown (left). Original magnification, 4x. Data are expressed as percentage of wound closure normalized to wound area at t = 0h, mean ± SEM; n = 3 for each group. Statistics: unpaired Student's t test, *** p<0.001.

5.8 Expression and function of RUNX2 in lung fibroblasts

Myofibroblasts are thought to be the main cell type responsible for extracellular matrix (ECM) deposition and are known for the expression of fibrotic marker genes COL1A1, ACTA2, TNC and FN1 (90). Since immunofluorescent stainings suggested decreased RUNX2 in myofibroblasts, expression levels of RUNX2 and its function were studied in isolated primary human lung fibroblasts (phLF).

5.8.1 Gene expression of cultured IPF and donor fibroblasts

To determine if RUNX genes were differentially expressed in phLF in IPF, fibroblasts were isolated from IPF and donor lungs. Fibroblasts were cultured until passage 3, harvested and total mRNA and protein were extracted. No differences in RUNX2 mRNA and protein expression (data not shown), nor in the expression of fibrotic marker mRNA (*COL1A1, ACTA2, TNC, FN1*) or protein (FN1, αSMA) was observed (Figure 31).

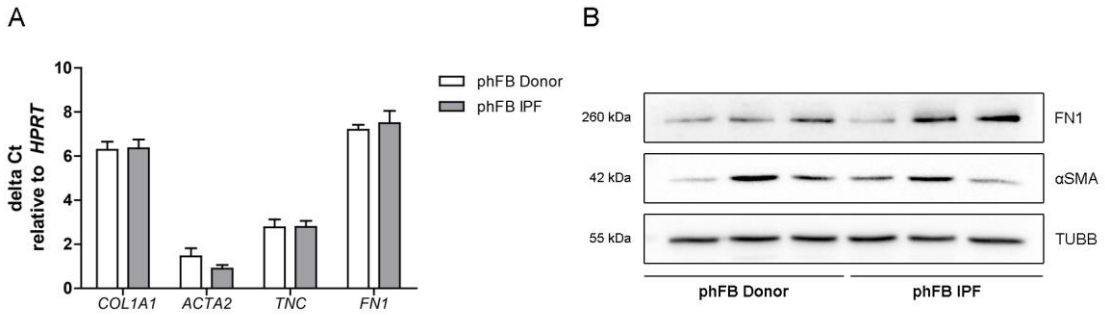

Figure 31: Cultured IPF and donor fibroblasts do not show differential expression of fibrotic marker genes. Primary human lung fibroblasts were isolated from IPF and donor lungs and cultured until passage 3. (A) Gene expression was analysed by qPCR, normalized to *HPRT* and displayed as ΔCt, mean ± SEM. n=3 for each group. (B) Protein expression of FN1 and αSMA was determined by Western Blot analysis. β-tubulin (TUBB) was used as loading control. Statistics: unpaired Student's t-test.

5.8.2 Gene expression of non-cultured IPF and donor fibroblasts

Recently, it has been demonstrated that gene expression of IPF fibroblasts is strongly dependent on the ECM the fibroblasts are cultured on (91). To rule out that gene expression patterns were altered due to cell culture on plastic dishes, we analysed a publicly available microarray dataset (GSE17978) where total mRNA was processed right after the isolation of fibroblasts (70). Here, we found significant downregulation of *RUNX2* (Donor: 0.87 ± 0.049 vs. IPF 0.55 ± 0.061; p = 0.0031) but not of *RUNX1* or *RUNX3* in IPF fibroblasts and identified a significant negative correlation between mRNA levels of *RUNX2* and the fibrotic markers *COL1A1* (*RUNX2* to *COL1A1*: Pearson r = -0.52; p = 0.028) and *ACTA2 (RUNX2* to *ACTA2:* Pearson r = -0.51; p = 0.029) (Figure 32).

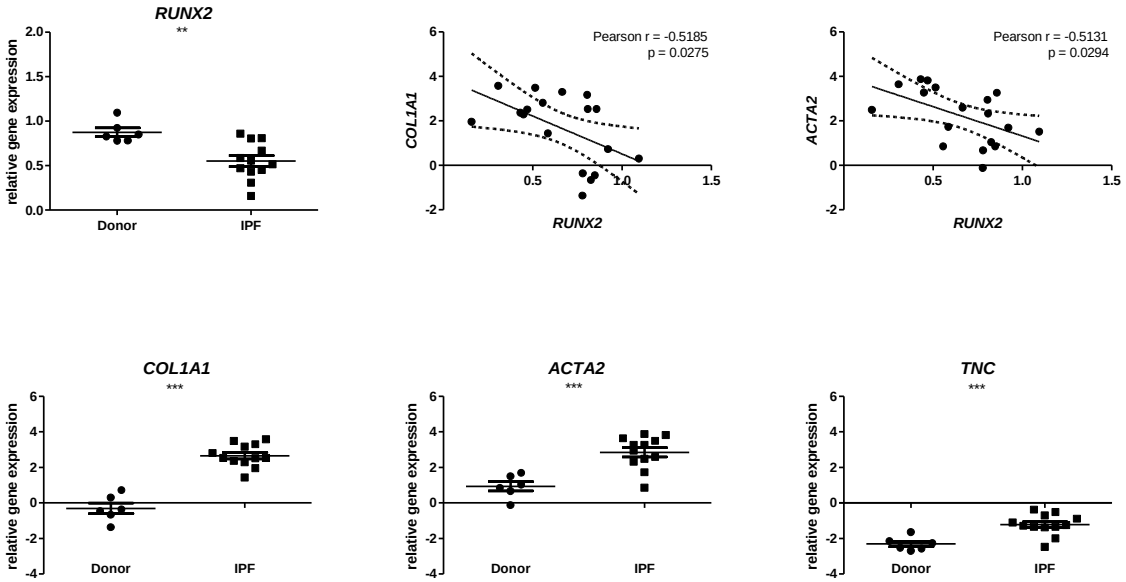

Figure 32: *RUNX2* mRNA levels are decreased in non-cultured fibroblasts isolated from IPF lungs and negatively correlate with *COL1A1* and *ACTA2* mRNA levels.

Analysis of microarray data published with the accession number GSE17978. Gene expression levels of *RUNX2* were assessed in non-cultured fibroblasts, isolated from IPF and donor lungs and correlated to expression levels of *COL1A1* and *ACTA2*. Fibrotic marker genes *COL1A1, ACTA2* and *TNC* were evaluated in this dataset. Statistics: unpaired Student's t-test, ** p<0.01, *** p<0.001. Pearson r was used for correlation analysis.

5.8.3 Knockdown of RUNX2 in primary human lung fibroblasts

siRNA-mediated knockdown of RUNX2 decreased RUNX2 mRNA levels (fold change to scr: 0.056 ± 0.0072; p = 0.0001). Notably, similar gene expression alterations as in the siRNA treated pmATII cells could be observed: *S100A4* (fold change to scr: 0.47 ± 0.054; p = 0.0093) and *CCND1* mRNA levels (fold change to scr: 0.57 ± 0.039; p = 0.0039) were reduced. Interestingly, ECM marker genes *COL1A1* (fold change to scr: 2.4 ± 0.13; p = 0.0005), *ACTA2* (fold change to scr: 2.5 ± 0.30; p = 0.0054) and *TNC* (fold change to scr: 2.2 ± 0.43; p = 0.041) were upregulated upon knockdown of RUNX2 (Figure 33 A). We furthermore assured that *RUNX1* levels were unaffected (data not shown). Western blotting of whole cell lysates followed by densitometry to β-actin confirmed RUNX2 knockdown (fold change to scr: 0.57 ± 0.049; p = 0.012) and COL1 upregulation (fold change to scr: 2.5 ± 0.078; p = 0.0029) on protein level (Figure 33 B).

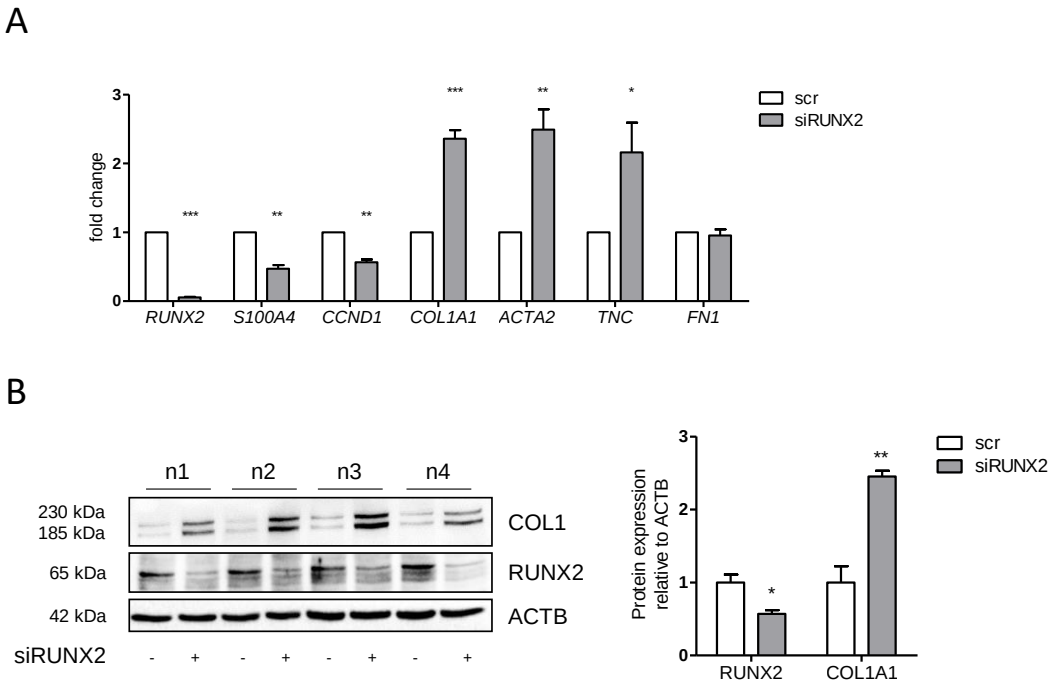

Figure 33: Loss of RUNX2 increases expression of ECM genes and decreases *S100A4, CCND1* mRNA in phLF. Cells were transfected with RUNX2-specific siRNA (siRUNX2) or scrambled siRNA (scr). Knockdown was performed for 72 hours. (A) Gene expression was analysed by qPCR, normalized to *HPRT* and displayed as fold change compared to scrambled control, mean ± SEM. n=4 for scr, n=4 for siRUNX2. (B) Protein expression of RUNX2 and type I collagen (COL1) was determined in cell lysates of scr- or siRUNX2-transfected primary human lung fibroblasts. Densitometric analysis was performed using β-actin (ACTB) as loading control. n=4 for scr, n=4 for siRUNX2. Statistics: paired Student's t-test, * p<0.05, ** p<0.01, *** p<0.001.

5.8.4 Knockdown of RUNX2 in primary human lung fibroblasts combined with TGF-β treatment

Given the importance of TGF-β signaling in pulmonary fibrosis and myofibroblast differentiation, a combination of RUNX2 knockdown and TGF-β1 treatment was performed. Interestingly, RUNX2 knockdown seemed to potentiate the TGF-β1 stimulation, as mRNA levels of *COL1A1, TNC* and *FN1* were significantly increased in phLF in the siRUNX2 + TGF-β1 group compared to phLF in the scr + TGF-β1 group (*COL1A1:* scr + TGF-β1: 3.2 ± 0.39 vs. siRUNX2 + TGF-β1: 4.9 ± 0.40; $p < 0.01$) (*TNC:* scr + TGF-β1: 3.6 ± 0.62 vs. siRUNX2 + TGF-β1: 7.8 ± 1.5; $p < 0.01$) (*FN1:* scr + TGF-β1: 2.6 ± 0.096 vs. siRUNX2 + TGF-β1: 4.1 ± 0.46; $p < 0.001$) (Figure 34).

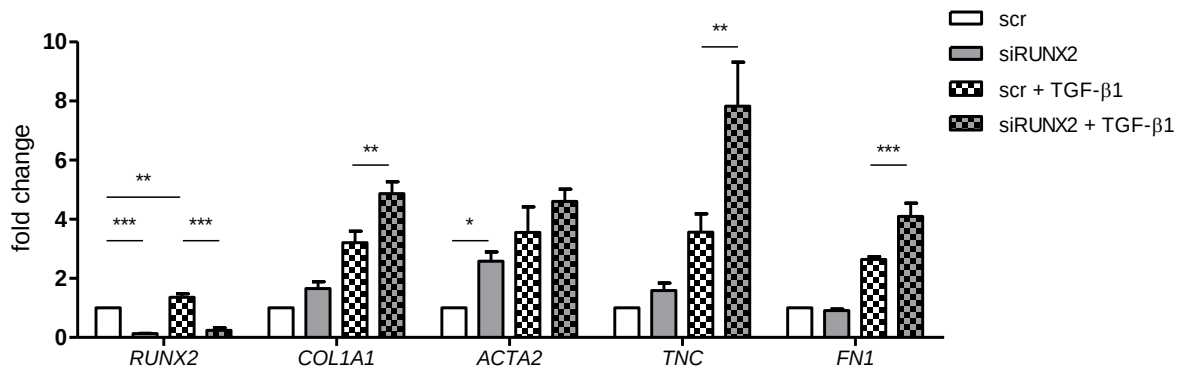

Figure 34: Loss of RUNX2 enhances TGF-β1 induced ECM gene expression. siRNA-mediated knockdown of RUNX2 was performed for 24 hours. Subsequently, cells were starved and afterwards stimulated with 2 ng/ml TGF-β1 for 12 hours respectively. Gene expression was analysed by qPCR, normalized to HPRT and displayed as fold change compared to scrambled control, mean ± SEM. n=6 for scr, n=6 for siRUNX2. Statistics: One-way ANOVA, Bonferroni's Multiple Comparison Test, * $p<0.05$, ** $p<0.01$, *** $p<0.001$.

6. DISCUSSION

Idiopathic pulmonary fibrosis is a chronic lung disease characterized by excessive scar formation in the lungs. Patients, predominantly aged males, suffer from progressive dyspnea that finally leads to respiratory failure. The prognosis of IPF is poor and to date, therapeutic options remain limited (92). Numerous biological processes have been implicated in IPF, amongst them the reactivation of developmental pathways like WNT/β-catenin or SHH as well as the secretion of growth factors like TGF-β or PDGF that stimulate myofibroblast differentiation and lead to excessive deposition of extracellular matrix (92, 93). The Runt-related transcription factors are a family of three genes essential for cell differentiation, proliferation, apoptosis and lineage specification (28, 30) that have a close interconnection with TGF-β and WNT/β-catenin pathways (64, 80, 81). RUNT genes have been shown to play major roles in development and disease of multiple organs and RUNX2 as well as RUNX3 have previously been demonstrated to play roles in alveolar epithelial cells (30, 33, 89, 94). RUNX2 has further been found in lungs with pulmonary ossification, a rare disease linked to pulmonary fibrosis (53). Interestingly, RUNX2 was also found to have beneficial effects in murine kidney fibrosis (47). While recent studies have reported that RUNX2 might be involved in the pathogenesis of pulmonary hypertension and asthma (95, 96), RUNX2 has not been studied in the context of pulmonary fibrosis and only little is known about RUNX2 function in organ fibrosis in general.

6.1 Characterization of the bleomycin model of pulmonary fibrosis

This study was partially based on a mouse model of pulmonary fibrosis induced by single intratracheal instillation of bleomycin. This model is commonly used for IPF research and captures several pathological characteristics of IPF: First, deterioration of lung function parameters (Figure 10) with fibrotic lungs displaying reduced compliance and increased resistance. This corresponds well to lung function alterations in IPF patients, who usually exhibit decreased DLCO, decreased forced vital capacity (FVC) and increased resistance (71, 72). Second, bleomycin injury led to changes in lung architecture with patchy fibrosis patterns (Figure 11). Fundamental changes in whole lung and cell-specific gene expression patterns mimicked the situation in IPF lungs, e.g. the upregulation of ECM genes like COL1A1, TNC and FN1 (Figure 12, Figure 26). In contrast to human IPF however, ACTA2 mRNA, which encodes the protein alpha smooth muscle actin, was not increased on day 14 in our

experiments. Few ATII cells were found to be hyperplastic, as typically seen in IPF. This feature of pulmonary fibrosis can more prominently be observed in models with repetitive intratracheal bleomycin instillations (23). Confirmation of the bleomycin-induced pulmonary fibrosis model is additionally provided by data that the newly approved IPF drugs nintedanib and pirfenidone were effective in reducing fibrosis severity (73, 97). It is important to mention that bleomycin-induced fibrosis in mice does not recapitulate all characteristics of human IPF. In the murine model, fibrosis develops subsequent to an inflammatory phase, whereas inflammation only plays a minor role in IPF. Pulmonary fibrosis in the single bleomycin model resolves by itself after a variable time, which is in sharp contrast to the progressive nature of IPF. Furthermore, the histopathological pattern of bleomycin-induced fibrosis does not display fibroblastic foci as in the human disease (23, 73).

Consequently, our experiments did not only involve samples derived from bleomycin-induced pulmonary fibrosis but included numerous IPF patient samples, from lung tissue specimen to primary human fibroblasts to large, publicly available datasets generated by other researchers.

6.2 RUNX genes are differentially expressed in pulmonary fibrosis

Initially, the expression of all three runt-related transcription factors, together with their cofactor CBFB, was studied in experimental and human pulmonary fibrosis. RUNX1 was not significantly altered on any of the timepoints from day 3 to day 14 in bleomycin-induced fibrosis but was upregulated in human IPF and correlated with IPF biomarkers SPP1 and MMP7 as well as with reduced lung function, measured by DLCO. TGF-β1 induced the expression of RUNX1 in both primary human lung fibroblasts and the human lung epithelial cell line A549. RUNX1 is a key factor in hematopoiesis and the induction of leukemia (98). It functions as a tumor suppressor gene as determined by loss-of function mutations in leukemia and breast cancer or reduced expression in aggressive lung adenocarcinoma (99-101). However, several studies also demonstrated an oncogenic role for RUNX1 with an increased expression in a variety of tumor cell types and associated increased cell proliferation and survival (102, 103). RUNX1 has not been studied in human or experimental fibrosis yet. Kim et al. found a role for RUNX1 in mesenchymal stem cell renewal, while the subsequent downregulation of RUNX1 in these cells induced myofibroblast differentiation, an essential feature of fibrotic diseases (38). Interestingly, interdependent regulation of S100A4 and RUNX1 has been demonstrated in lung adenocarcinoma

(104). This is of particular interest, since we demonstrated that S100A4 is upregulated in fibrotic pmATII cells and because RUNX2 mediated S100A4 expression in pmATII cells and phLF. In the human IPF dataset we analysed, the nearly similar expression pattern of RUNX1 and RUNX2 as well as the similar correlation with DLCO stood out. Together, this might point towards an overlapping function of RUNX1 and RUNX2 in IPF, as it has been suggested in leukemia cells (103, 105). Further studies have to elucidate cell-specific localization of RUNX1 and its function on target genes and biological mechanisms in pulmonary fibrosis.

RUNX3 mRNA was significantly downregulated on day 7 and day 10 in bleomycin-induced fibrosis. This is of interest, since day 10 represents a transition between the inflammatory and the fibrotic phase of this model (22). RUNX3 was also downregulated in IPF patients but only correlated to a minor extent to DLCO and did not correlate at all with MMP7 or SPP1. RUNX3 has previously been shown to decrease the activity of WNT/β-catenin-signaling by interaction with the β-catenin/TCF4 complex (76). WNT-signaling has been implicated in the pathophysiology of IPF as a driver of exaggerated healing processes, leading to scar formation in the lung (106). Therefore, downregulation of RUNX3 might contribute to the development of fibrosis by sustaining aberrant repair by reduced inhibition of WNT signaling. RUNX3 has further been described to be both tumor suppressor and oncogene and is dysregulated in a variety of cancer types (30). Interestingly, loss of RUNX3 led to spontaneous EMT in gastric epithelial cells while reduced RUNX3 expression in ATII cells was associated with EMT in bronchopulmonary dysplasia (94, 107). As EMT has been suggested to contribute to the pathophysiology of IPF, further studies are needed to clarify the role of RUNX3 in alveolar epithelial cells in IPF.

RUNX2, as well as the main binding partner of RUNX proteins, CBFB, were exclusively upregulated on day 14, when fibrosis starts to peak in the bleomycin model and not significantly changed on the inflammation-dominated timepoints. This might indicate a fibrosis specific mechanism for the regulation of these two genes. We discovered that mRNA level of RUNX2 was significantly increased in two cohorts of IPF patients. RUNX2 was not only upregulated on transcriptional level, strong upregulation of RUNX2 protein in experimental fibrosis and human IPF could also be seen by Western Blot analysis. We showed that high expression levels of RUNX2 were correlated to decreased lung function and increased injury biomarkers. Correlation analysis stated similar correlation of both RUNX1 and RUNX2 to decreased lung function, however, the correlation to SPP1 and MMP7 was closer for RUNX2. It is not clearly

possible to state if high RUNX2 levels were causal to decreased lung function. It is also conceivable that progression of the disease led to increased RUNX2 expression. Parallel to this observation, it was reported that RUNX2 is upregulated in different epithelial tumors including lung cancer and frequently correlates with poor prognosis (45, 46, 108, 109). It has been shown that IPF patients have higher incidence of lung cancer and several similarities in signaling pathways involved in fibrosis and tumorigenesis have been highlighted (110, 111). Therefore, we propose that future studies should evaluate RUNX2 as a prognostic marker in IPF and dissect the common roles of RUNX2 in lung cancer and fibrosis. Further experiments localized changes in RUNX2 expression to alveolar epithelial cells and lung fibroblasts and its functional role in these cells was studied. The results will be discussed in the following, respective paragraphs.

6.3 RUNX2 does not regulate SPP1 expression in ATII cells or phLF

Osteopontin (SPP1) has previously been demonstrated to be one of the most upregulated genes in murine and human pulmonary fibrosis (91). We confirmed its upregulation on mRNA level in our model and found significant increases on all observed timepoints. It is known that SPP1 is not specific for (pulmonary) fibrosis but plays a general role in a variety of processes and diseases that involve inflammation, tissue regeneration and repair (92-94). Osteopontin also has a significant role in lung development as seen in a study of SPP1 knockout mice (112). In the context of bone, SPP1 is a classical target of RUNX2, therefore it was assumed to be an indicator of RUNX2 activity (75). However, in the following siRNA experiments, SPP1 could not be proven to be regulated by RUNX2 in pmATII cells or phLF. This might be due to a distinct set of RUNX coactivators or repressors in these cells. However, it is still possible that SPP1 might be regulated by RUNX2 in bronchial epithelium or macrophages in IPF.

6.4 Increased RUNX2 in ATII cells stimulates CCND1 and proliferation

ATII cells are cuboidal shaped cells that have been shown to be stem cells in the lung during steady-state conditions and following lung injury (87). Rock et al. demonstrated that ATII cells are responsible for the regeneration of ATI cells after bleomycin-induced lung injury (86). Underlining the central role of ATII cell injury in the pathophysiology of IPF, disturbed ATII cell homeostasis e.g. in patients with surfactant protein mutations causes familial pulmonary fibrosis whereas targeted ATII cell injury directly

leads to pulmonary fibrosis (113-115). Colocalization studies in lung tissue of experimental fibrosis and human IPF demonstrated an increased RUNX2-positive epithelial cell population in fibrosis. Interestingly, increased nuclear RUNX2 protein was specifically found in hyperplastic alveolar epithelial type II cells in IPF, often closely located to fibroblastic foci. Confirmatory, a prominent increase in nuclear RUNX2 was found in fibrotic ATII cells isolated from bleomycin-treated mice. Intranuclear localization of RUNX2 indicates RUNX2 activity, due to its function as transcriptional activator or repressor (116). Previous reports showed that ATII cells in pulmonary fibrosis undergo apoptosis and necrosis (88, 117, 118). Controversially, ATII cells isolated from fibrotic murine lungs exhibited increased proliferative capacity (66) and IPF patient lungs displayed higher levels of the proliferation marker and WNT-target gene CCND1 (83). This might be due to different subpopulations of ATII cells, one undergoing apoptosis after injury whereas another population becomes hyperproliferative to reconstitute the damaged epithelium. In our experiments, loss of RUNX2 in ATII cells led to decreased expression of CCND1, suggesting that higher RUNX2 levels enhance epithelial proliferation. In line with these findings, depletion of RUNX2 is associated with reduced regenerative potential in mammary epithelium and interferes with mammary organoid formation (119). Of note, RUNX2 expression in the mammary gland was localized to mammary basal cells, a compartment where mammary stem cells are thought to reside (120). Murine RUNX2-negative breast cancers showed reduced levels of CCND1 and KI-67 expression compared to RUNX2-positive breast cancers (121). Furthermore, in a study with 137 human breast cancer specimen a significant correlation between high RUNX2 levels and elevated levels of the proliferation marker KI-67 was demonstrated (109). It is therefore proposed that overexpression of RUNX2 in ATII cells is an essential element in an attempt of regeneration and/or stem cell self-renewal following lung injury.

6.5 Increased RUNX2 in ATII cells stimulates S100A4 and migration

In addition to cell proliferation, several other cellular functions and phenotypes have been associated with alveolar cell alterations and reprogramming in IPF (122). It has been reported that ATII cells isolated from fibrotic lungs are able to partly acquire fibroblast properties, e.g. the enhanced expression of mesenchymal genes like COL1 and αSMA (123-125). RUNX2 has been demonstrated to play a significant role in epithelial-to-mesenchymal transition (EMT) in the lung epithelial cell line A549, as well as in breast cancer and thyroid carcinoma cells (41, 44, 89). While we did not observe differences in

epithelial marker gene expression (such as Snai2, E-Cadherin, or tight junction protein 1) upon RUNX2 knockdown (data not shown), we discovered that S100A4, a mesenchymal marker and migratory gene, was positively regulated by RUNX2 in ATII cells. S100A4 was initially described as a fibroblast marker upregulated in experimental and human lung fibrosis (126). We found increased S100A4 expression in fibrotic ATII cells, which might indicate reprogramming of these cells. Other groups demonstrated increased S100A4 staining in TTF1-positive epithelial cells in experimental lung fibrosis (127). Further studies highlighted that S100A4-positive fibroblasts were partly derived from lung epithelium after bleomycin injury, however they rarely showed a myofibroblast phenotype (128). RUNX2-dependent regulation of S100A4 has been linked to a migratory profile associated with metastasis in breast and prostate cancer (39, 41). Additionally, high RUNX2 expression was significantly correlated to higher incidence of metastasis in breast and lung cancer (45, 46). Confirmatory, RUNX2 silencing reduced migration of A549 cells in a wound healing assay. Altogether, the data indicate that RUNX2 initiates a process of reprogramming in alveolar epithelial cells and exerts a migratory effect through the induction of S100A4 in injured alveolar epithelium. This concept is in line with a recent study demonstrating that S100A4-positive cells, surrounding fibroblastic foci in IPF, are highly proliferative and constitute an active fibrotic front (129).

6.6 Decreased RUNX2 in phLF enhances myofibroblast differentiation

Another hallmark of IPF is the accumulation of activated αSMA-positive myofibroblasts in fibroblastic foci, producing excessive amounts of extracellular matrix. There are several hypotheses regarding the origin of these activated myofibroblasts. Potential sources include bone-marrow derived mesenchymal progenitor cells, fibrocytes, proliferating residential lung fibroblasts or alveolar epithelial cells that become fibroblast-like through EMT (17, 130). A recent study proved that targeted apoptosis of myofibroblasts was able to partially reverse dermal fibrosis and thus might also represent a promising therapeutic strategy for pulmonary fibrosis (131). In this work we found decreased expression of RUNX2 protein in fibrotic foci, decreased mRNA expression of RUNX2 in isolated fibrotic fibroblasts and observed an increase in a RUNX2-negative αSMA-positive cell population in IPF. Our data revealed that RUNX2 silencing in fibroblasts enhanced myofibroblast differentiation through the induction of COL1A1, ACTA2 and TNC genes. Notably, we analysed a publicly available microarray data set comparing IPF and donor fibroblasts, in which we found that loss of RUNX2 correlated with increased COL1A1 and

ACTA2 expression. Similar to our findings, it has been reported that downregulation of RUNX1 is necessary for the differentiation of mesenchymal stem cells towards myofibroblasts. The authors reported that knockdown of RUNX1 led to upregulation of myofibroblast markers TNC and ACTA2 (38). Since we excluded alterations in RUNX1 expression in our studies, this goes in line with the partially overlapping function of RUNX genes. Furthermore, RUNX2 has been shown to suppress the expression of type 1 collagen in non-osseous mesenchymal cells (132). Importantly, upregulation of αSMA, COL1 and COL3 have been reported in a RUNX2 heterozygous knockout mice subjected to a ureteral obstruction model of kidney fibrosis (47). We further demonstrated that RUNX2 regulated the expression of S100A4 and CCND1 in lung fibroblasts, similar to the regulation in epithelial cells. Recently Xia et al. showed that fibroblastic foci consist of an αSMA-positive/Procollagen-positive/KI-67-negative core, with an active fibrotic surface, that is S100A4-positive/KI-67-positive (129). This is in agreement with our data, suggesting that fibroblastic foci are primarily RUNX2 negative, and that downregulation of RUNX2 in these fibroblasts leads to increased ECM production and decreased proliferative capacity. It will be necessary to elucidate the cell-specific contribution of RUNX2 by studying pulmonary fibrosis in fibroblast-specific RUNX2 knockout mice in the future.

6.7 RUNX2 is a target of TGF-β and WNT/β-catenin signaling

Chronic epithelial injury and subsequent hyperplasia of ATII cells with the release of growth factors and cytokines are key features of IPF that contribute to distorted epithelial-mesenchymal crosstalk and myofibroblast function (133). Several signaling pathways have been demonstrated to be involved in fibrogenesis, among them are the TGF-β and WNT/β-catenin pathways (17). Our findings of differential RUNX2 expression in experimental and human IPF raise the question which mechanisms are involved in either up- or downregulating RUNX2 in different cell types. We observed that WNT/β-catenin activation induces a robust increase of RUNX2 in epithelial cells and lung fibroblasts. This is in agreement with previous reports that demonstrated RUNX2 to be a WNT/β-catenin target gene in osteoblastic cells and mammary epithelium (61, 119). We further showed that RUNX2 was upregulated upon treatment with TGF-β1 in A549 cells, but not in lung fibroblasts. Interestingly, excessive interplay between RUNX genes and TGF-β signaling has been described. RUNX2 can modulate the expression of TGF-βRI and/or downstream targets of TGF-β signaling such as SMAD3 (39, 47, 64). Enhanced TGF-β signaling can in turn upregulate RUNX2 on transcriptional level, as observed in this study, and further

at the posttranscriptional level through the phosphorylation of RUNX2 by ERK1/2 (28, 134). WNT-induced RUNX2 expression and the subsequent modulation of TGF-βRI by RUNX2 might represent a regulatory crosstalk of both signaling pathways and might further serve as a feedback loop enhancing RUNX2 overexpression (64). However, our results raise the question how RUNX2 is downregulated in myofibroblasts. This might be explained by the distinct availability of secreted profibrotic mediators within the local microenvironment between alveolar epithelial cells and fibroblasts. With respect to WNT signaling, which can be divided into two main pathways (a canonical WNT/β-catenin signaling and a non-canonical β-catenin independent pathway) (135), we and others have provided evidence of a differential WNT ligand signature, with an increase of non-canonical WNT ligand (such as WNT5A and WNT5B) expression by fibroblasts (136, 137). This altered signaling pattern might act differentially on several cell types depending on the expression of specific WNT surface receptors. The transcription factor TWIST1 represents another potential regulator of RUNX2 expression in fibroblasts. TWIST1 has been demonstrated to downregulate RUNX2 expression in zebrafish embryos (138) as well as in human mesenchymal stem cells by directly binding to the RUNX2 promotor (139). Interestingly, several groups have shown that TWIST1 is expressed in human IPF as well as in murine models of pulmonary fibrosis. Two studies demonstrated TWIST1 staining in alveolar epithelial cells and fibroblasts, whereas another study exclusively located TWIST1 to fibrotic fibroblasts (140-142). Therefore, increased TWIST1 expression in fibrotic fibroblasts might be responsible of downregulating RUNX2, leading to myofibroblast differentiation and increased ECM deposition.

6.8 Future perspective

Emerging evidence points towards a significant role for RUNX genes mediating p53-dependent apoptosis after DNA-damage (143, 144). Ozaki et al. demonstrated that a complex of RUNX2 and p53 binds to p53-target promotors and inhibits pro-apoptotic activity of p53 in response to adriamycin treatment (144). Kaminski et al. discovered that the administration of aerosolized thyroid hormone ameliorates pulmonary fibrosis in mice by reducing apoptosis in alveolar epithelial cells (145). Interestingly, RUNX2 can be regulated through activation of the thyroid hormone receptor (146). Thus, it is imaginable that RUNX2 upregulation in alveolar epithelial cells contributes to reducing epithelial cell death after bleomycin-exposure in experimental pulmonary fibrosis as well as in IPF. Further studies

might elucidate the contribution of RUNX2 to IPF pathophysiology in regard to the interaction with apoptosis and thyroid hormone pathways.

One limitation of this study resides in the lack of *in vivo* evidence concerning the cell-specific contribution of RUNX2 to the development and progression of lung fibrosis. In future studies, this should be addressed using transgenic mice with conditional and cell-specific deletion of RUNX2 and would also help to identify cell-specific RUNX2 activators/repressors that could be investigated as therapeutic targets for IPF.

6.9 Conclusions

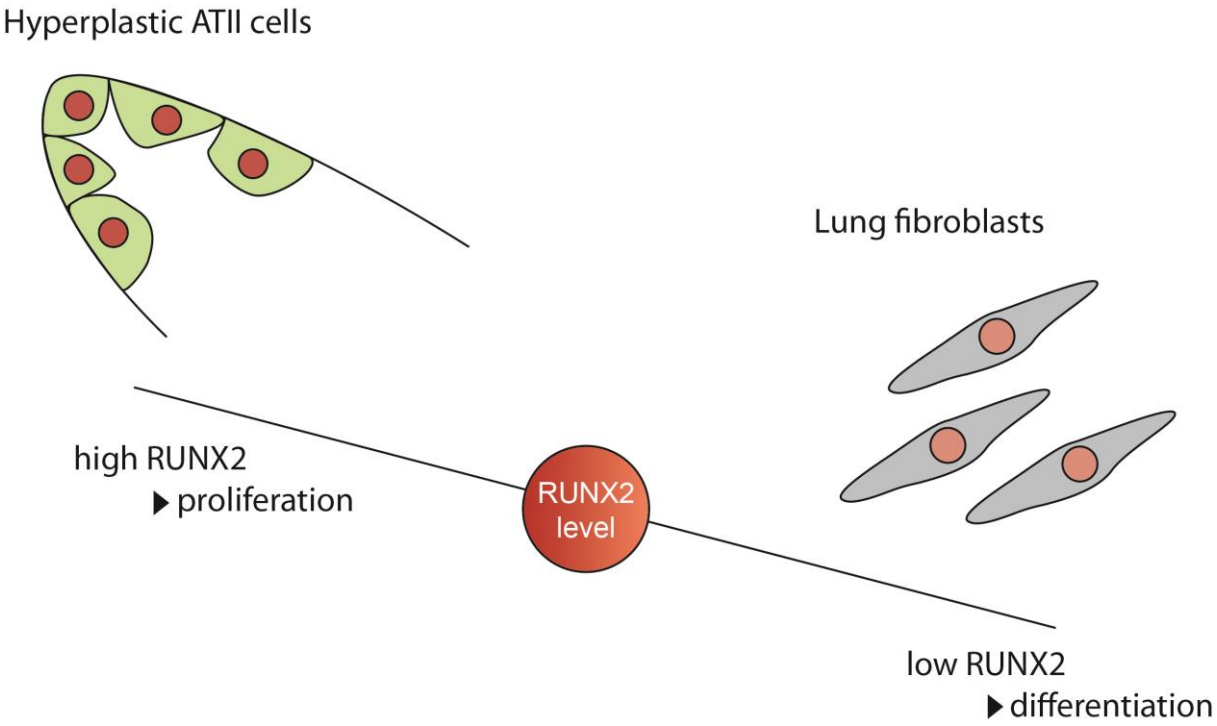

Figure 35: Model of RUNX2 function in pulmonary fibrosis.

A simplified model of our findings is shown in Figure 35. In summary, we found upregulation of RUNX2 in whole tissue of fibrotic lungs, correlating with disease progression. At the cellular level, we found altered RUNX2 expression in ATII cells and lung fibroblasts. Increased expression of RUNX2 in epithelial cells might represent an attempt of regeneration, preserving cells in a proliferating and undifferentiated state. Importantly and in contrast to the alveolar epithelial cell compartment, our data suggest that the αSMA-positive myofibroblast population, which is increased in pulmonary fibrosis, is primarily RUNX2-negative. Knockdown experiments depicted that reduced RUNX2 expression in lung fibroblasts

correlated with the upregulation of fibrotic marker genes, thereby contributing to myofibroblast differentiation and ECM deposition. The results of this study indicate that RUNX2 levels might serve as a novel surrogate marker of IPF progression and that cell-specific modulation of RUNX2 could be a therapeutic approach for treating IPF patients in the future.

7. REFERENCES

7.1 Bibliography

1. Raghu G, Collard HR, Egan JJ, Martinez FJ, Behr J, Brown KK, et al. An official ATS/ERS/JRS/ALAT statement: idiopathic pulmonary fibrosis: evidence-based guidelines for diagnosis and management. Am J Respir Crit Care Med. 2011;183(6):788-824.

2. Travis WD, Costabel U, Hansell DM, King TE, Jr., Lynch DA, Nicholson AG, et al. An official American Thoracic Society/European Respiratory Society statement: Update of the international multidisciplinary classification of the idiopathic interstitial pneumonias. Am J Respir Crit Care Med. 2013;188(6):733-48.

3. Hutchinson J, Fogarty A, Hubbard R, McKeever T. Global incidence and mortality of idiopathic pulmonary fibrosis: a systematic review. Eur Respir J. 2015;46(3):795-806.

4. King TE, Pardo A, Selman M. Idiopathic pulmonary fibrosis. The Lancet. 2011;378(9807):1949-61.

5. Sverzellati N. Highlights of HRCT imaging in IPF. Respir Res. 2013;14 Suppl 1:S3.

6. Funke M, Geiser T. Idiopathic pulmonary fibrosis: the turning point is now! Swiss medical weekly. 2015;145:w14139.

7. Raghu G, Amatto VC, Behr J, Stowasser S. Comorbidities in idiopathic pulmonary fibrosis patients: a systematic literature review. Eur Respir J. 2015;46(4):1113-30.

8. Richeldi L, Kreuter M, Selman M, Crestani B, Kirsten AM, Wuyts WA, et al. Long-term treatment of patients with idiopathic pulmonary fibrosis with nintedanib: results from the TOMORROW trial and its openlabel extension. Thorax. 2017.

9. Richeldi L, du Bois RM, Raghu G, Azuma A, Brown KK, Costabel U, et al. Efficacy and safety of nintedanib in idiopathic pulmonary fibrosis. N Engl J Med. 2014;370(22):2071-82.

10. Iyer SN, Gurujeyalakshmi, G. and Giri S. N. . Effects of Pirfenidone on Procollagen Gene Expression at the Transcriptional Level in Bleomycin Hamster Model of Lung Fibrosis. J Pharmacol Exp Ther. 1999;289(1).

11. Iyer SN, Gurujeyalakshmi, G. and Giri S. N. . Effects of Pirfenidone on Transforming Growth Factor Gene Expression at the Transcriptional Level in Bleomycin Hamster Model of Lung Fibrosis. J Pharmacol Exp Ther. 1999;291(1).

12. Iyer SN, Margolin SB, Hyde DM, Giri SN. Lung fibrosis is ameliorated by pirfenidone fed in diet after the second dose in a three-dose bleomycin-hamster model. Exp Lung Res. 1998;24.

13. Kolb M, Bonella F, Wollin L. Therapeutic targets in idiopathic pulmonary fibrosis. Respir Med. 2017;131:49-57.

14. King TE, Jr., Bradford WZ, Castro-Bernardini S, Fagan EA, Glaspole I, Glassberg MK, et al. A phase 3 trial of pirfenidone in patients with idiopathic pulmonary fibrosis. N Engl J Med. 2014;370(22):2083-92.

15. Behr J, Gunther A, Bonella F, Geissler K, Koschel D, Kreuter M, et al. [German Guideline for Idiopathic Pulmonary Fibrosis - Update on Pharmacological Therapies 2017]. Pneumologie. 2017;71(7):460-74.

16. Davies HR, Richeldi L, Walters EH. Immunomodulatory agents for idiopathic pulmonary fibrosis. The Cochrane database of systematic reviews. 2003(3):Cd003134.

17. Fernandez IE, Eickelberg O. New cellular and molecular mechanisms of lung injury and fibrosis in idiopathic pulmonary fibrosis. The Lancet. 2012;380(9842):680-8.

18. Selman M, Pardo A. Role of epithelial cells in idiopathic pulmonary fibrosis: from innocent targets to serial killers. Proc Am Thorac Soc. 2006;3(4):364-72.

19. Selman M, A P. Idiopathic pulmonary fibrosis: an epithelial/fibroblastic cross-talk disorder. Respir Res. 2002.

20. Selman M, Pardo A, Kaminski N. Idiopathic pulmonary fibrosis: aberrant recapitulation of developmental programs? PLoS Med. 2008;5(3):e62.

21. Sleijfer S. Bleomycin-Induced Pneumonitis. Chest. 2001;120:617-24.

22. Camus P, Bonniaud P, Fanton A, Camus C, Baudaun N, Foucher P. Drug-induced and iatrogenic infiltrative lung disease. Clin Chest Med. 2004;25(3):479-519, vi.

23. Moore BB, Lawson WE, Oury TD, Sisson TH, Raghavendran K, Hogaboam CM. Animal models of fibrotic lung disease. Am J Respir Cell Mol Biol. 2013;49(2):167-79.

24. Moeller A, Ask K, Warburton D, Gauldie J, Kolb M. The bleomycin animal model: a useful tool to investigate treatment options for idiopathic pulmonary fibrosis? Int J Biochem Cell Biol. 2008;40:362-82.

25. Peng R, Sridhar S, Tyagi G, Phillips JE, Garrido R, Harris P, et al. Bleomycin induces molecular changes directly relevant to idiopathic pulmonary fibrosis: a model for "active" disease. PLoS One. 2013;8(4):e59348.

26. Tahir H. Tahirov, Taiko Inoue-Bungo, Hisayuki Morii, Atsushi Fujikawa, Motoko Sasaki, Kazumi Kimura, et al. Structural Analyses of DNA Recognition by the AML1/Runx-1 Runt Domain and Its Allosteric Control by CBFb. Cell. 2001;104:755-67.

27. Xuemei Huang JWP, Nancy A. Speck and John H. Bushweller. Solution structure of core binding factor b and map of the CBFa binding site. Nature Structural Biology. 1999;6.

28. Blyth K, Cameron ER, Neil JC. The RUNX genes: gain or loss of function in cancer. Nat Rev Cancer. 2005;5(5):376-87.

29. Levanon D, Groner Y. Structure and regulated expression of mammalian RUNX genes. Oncogene. 2004;23(24):4211-9.

30. Ito Y, Bae SC, Chuang LS. The RUNX family: developmental regulators in cancer. Nat Rev Cancer. 2015;15(2):81-95.

31. Chuang LS, Ito K, Ito Y. RUNX family: Regulation and diversification of roles through interacting proteins. International journal of cancer Journal international du cancer. 2013;132(6):1260-71.

32. Tsukasa Okuda Jv, Scott W. Hiebert, Gerard Grosveld and James R. Downing. AML1, the Target of Multiple Chromosomal Translocations in Human Leukemia, Is Essential for Normal Fetal Liver Hematopoiesis. Cell. 1996;84:321-30.

33. Lee KS, Lee YS, Lee JM, Ito K, Cinghu S, Kim JH, et al. Runx3 is required for the differentiation of lung epithelial cells and suppression of lung cancer. Oncogene. 2010;29(23):3349-61.

34. Florian Otto TC, Anders P. Thornell, Angela Denzel, Kimberly C. Gilmour, Gordon W. H. Stamp, Stefan Mundlos, Paul B. Selby, Ian R. Rosewell, Rosa S. P. Beddington, Bjorn R. Olsen, and Michael J. Owen. Cbfa1, a Candidate Gene for Cleidocranial Dysplasia Syndrome, Is Essential for Osteoblast Differentiation and Bone Development. Cell. 1997;89.

35. Silva FP, Morolli B, Storlazzi CT, Anelli L, Wessels H, Bezrookove V, et al. Identification of RUNX1/AML1 as a classical tumor suppressor gene. Oncogene. 2003;22(4):538-47.

36. Browne G, Taipaleenmaki H, Bishop NM, Madasu SC, Shaw LM, van Wijnen AJ, et al. Runx1 is associated with breast cancer progression in MMTV-PyMT transgenic mice and its depletion in vitro inhibits migration and invasion. J Cell Physiol. 2015;230(10):2522-32.

37. Ferrari N, Mohammed ZMA, Nixon C, Mason SM, Mallon E, McMillan DC, et al. Expression of RUNX1 Correlates with Poor Patient Prognosis in Triple Negative Breast Cancer. PLoS ONE. 2014;9(6):e100759.

38. Kim W, Barron DA, San Martin R, Chan KS, Tran LL, Yang F, et al. RUNX1 is essential for mesenchymal stem cell proliferation and myofibroblast differentiation. Proc Natl Acad Sci U S A. 2014;111(46):16389-94.

39. Baniwal SK, Khalid O, Gabet Y, Shah RR, Purcell DJ, Mav D, et al. Runx2 transcriptome of prostate cancer cells: insights into invasiveness and bone metastasis. Mol Cancer. 2010;9:258.

40. Boregowda RK, Olabisi OO, Abushahba W, Jeong BS, Haenssen KK, Chen W, et al. RUNX2 is overexpressed in melanoma cells and mediates their migration and invasion. Cancer Lett. 2014;348(1-2):61-70.

41. Chimge NO, Baniwal SK, Little GH, Chen YB, Kahn M, Tripathy D, et al. Regulation of breast cancer metastasis by Runx2 and estrogen signaling: the role of SNAI2. Breast Cancer Res. 2011;13(6):R127.

42. Ferrari N, McDonald L, Morris JS, Cameron ER, Blyth K. RUNX2 in mammary gland development and breast cancer. J Cell Physiol. 2013;228(6):1137-42.

43. Kayed H, Jiang X, Keleg S, Jesnowski R, Giese T, Berger MR, et al. Regulation and functional role of the Runt-related transcription factor-2 in pancreatic cancer. Br J Cancer. 2007;97(8):1106-15.

44. Niu DF, Kondo T, Nakazawa T, Oishi N, Kawasaki T, Mochizuki K, et al. Transcription factor Runx2 is a regulator of epithelial-mesenchymal transition and invasion in thyroid carcinomas. Lab Invest. 2012;92(8):1181-90.

45. Li H, Zhou RJ, Zhang GQ, Xu JP. Clinical significance of RUNX2 expression in patients with nonsmall cell lung cancer: a 5-year follow-up study. Tumour Biol. 2013;34(3):1807-12.

46. Yang Z, Zhang B, Liu B, Xie Y, Cao X. Combined Runx2 and Snail overexpression is associated with a poor prognosis in breast cancer. Tumour Biol. 2015.

47. Kim JI, Jang HS, Jeong JH, Noh MR, Choi JY, Park KM. Defect in Runx2 gene accelerates ureteral obstruction-induced kidney fibrosis via increased TGF-beta signaling pathway. Biochimica et biophysica acta. 2013;1832(10):1520-7.

48. Kanne JP, Godwin JD, Takasugi JE, Schmidt RA, Stern EJ. Diffuse pulmonary ossification. Journal of thoracic imaging. 2004;19(2):98-102.

49. Fernandez Crisosto CA, Quercia Arias O, Bustamante N, Moreno H, Uribe Echevarria A. [Diffuse pulmonary ossification associated with idiopathic pulmonary fibrosis]. Archivos de bronconeumologia. 2004;40(12):595-8.

50. Bisceglia M, Chiaramonte A, Panniello G, Tucci A, Orcioni GF, Colby TV. Selected case from the Arkadi M. Rywlin international pathology slide series: diffuse dendriform pulmonary ossification: report of 2 cases with review of the literature. Advances in anatomic pathology. 2015;22(1):59-68.

51. Popelka CG, Kleinerman J. Diffuse pulmonary ossification. Archives of internal medicine. 1977;137(4):523-5.

52. Martinez JB, Ramos SG. Dendriform pulmonary ossification. The Lancet. 2013;382(9904):e22.

53. Kim GY, Kim J, Kim TS, Han J. Pulmonary adenocarcinoma with heterotopic ossification. J Korean Med Sci. 2009;24(3):504-10.

54. Ku JL, Kang SB, Shin YK, Kang HC, Hong SH, Kim IJ, et al. Promoter hypermethylation downregulates RUNX3 gene expression in colorectal cancer cell lines. Oncogene. 2004;23(40):6736-42.

55. Li Q-L, Kim H-R, Kim W-J, Choi J-K, Hee Lee Y, Kim H-M, et al. Transcriptional silencing of the RUNX3 gene by CpG hypermethylation is associated with lung cancer. Biochemical and Biophysical Research Communications. 2004;314(1):223-8.

56. Omar MF, Ito K, Nga ME, Soo R, Peh BK, Ismail TM, et al. RUNX3 downregulation in human lung adenocarcinoma is independent of p53, EGFR or KRAS status. Pathology oncology research : POR. 2012;18(4):783-92.

57. Sakakura C, Hagiwara A, Miyagawa K, Nakashima S, Yoshikawa T, Kin S, et al. Frequent downregulation of the runt domain transcription factors RUNX1, RUNX3 and their cofactor CBFB in gastric cancer. International journal of cancer Journal international du cancer. 2005;113(2):221-8.

58. Kim WJ, Kim EJ, Jeong P, Quan C, Kim J, Li QL, et al. RUNX3 inactivation by point mutations and aberrant DNA methylation in bladder tumors. Cancer Res. 2005;65(20):9347-54.

59. Ito Y, Miyazono K. RUNX transcription factors as key targets of TGF-b superfamily signaling. Curr Opinion in Genetics & Development. 2003;13:43-7.

60. Fernandez IE, Eickelberg O. The impact of TGF-beta on lung fibrosis: from targeting to biomarkers. Proc Am Thorac Soc. 2012;9(3):111-6.

61. Gaur T, Lengner CJ, Hovhannisyan H, Bhat RA, Bodine PV, Komm BS, et al. Canonical WNT signaling promotes osteogenesis by directly stimulating Runx2 gene expression. J Biol Chem. 2005;280(39):33132-40.

62. Lee KS, Hong SH, Bae SC. Both the Smad and p38 MAPK pathways play a crucial role in Runx2 expression following induction by transforming growth factor-b and bone morphogenetic protein. Oncogene. 2002;21:7156-63.

63. Alliston T, Choy L, Ducy P, Karsenty G, Derynck R. TGF-b induced repression of CBFA1 by Smad3 decreases cbfa1 and osteocalcin expression and inhibits osteoblast differentiation. The EMBO journal. 2001;20(9):2254-72.

64. McCarthy TL, Centrella M. Novel links among Wnt and TGF-beta signaling and Runx2. Mol Endocrinol. 2010;24(3):587-97.

65. Staab-Weijnitz CA, Fernandez IE, Knuppel L, Maul J, Heinzelmann K, Juan-Guardela BM, et al. FK506-Binding Protein 10, a Potential Novel Drug Target for Idiopathic Pulmonary Fibrosis. Am J Respir Crit Care Med. 2015;192(4):455-67.

66. Konigshoff M, Kramer M, Balsara N, Wilhelm J, Amarie OV, Jahn A, et al. WNT1-inducible signaling protein-1 mediates pulmonary fibrosis in mice and is upregulated in humans with idiopathic pulmonary fibrosis. J Clin Invest. 2009;119(4):772-87.

67. Mutze K, Vierkotten S, Milosevic J, Eickelberg O, Konigshoff M. Enolase 1 and protein disulfide isomerase associated 3 regulate Wnt/beta-catenin driven alveolar epithelial cell trans-differentiation. Dis Model Mech. 2015.

68. Bellaye PS, Burgy O, Colas J, Fabre A, Marchal-Somme J, Crestani B, et al. Antifibrotic role of alphaB-crystallin inhibition in pleural and subpleural fibrosis. Am J Respir Cell Mol Biol. 2015;52(2):244-52.

69. Primer-Blast Website [Available from: http://www.ncbi.nlm.nih.gov/tools/primer-blast/.

70. Emblom-Callahan MC, Chhina MK, Shlobin OA, Ahmad S, Reese ES, Iyer EP, et al. Genomic phenotype of non-cultured pulmonary fibroblasts in idiopathic pulmonary fibrosis. Genomics. 2010;96(3):134-45.

71. Martinez FJ, Flaherty K. Pulmonary function testing in idiopathic interstitial pneumonias. Proc Am Thorac Soc. 2006;3(4):315-21.

72. H. Bachofen MS. Lung Tissue Resistance in Diffuse Interstitial Pulmonary Fibrosis. J Clin Invest. 1967;Vol. 46(No 1):133-40.

73. Jenkins RG, Moore BB, Chambers RC, Eickelberg O, Konigshoff M, Kolb M, et al. An Official American Thoracic Society Workshop Report: Use of Animal Models for the Preclinical Assessment of Potential Therapies for Pulmonary Fibrosis. Am J Respir Cell Mol Biol. 2017;56(5):667-79.

74. Wynn TA, Ramalingam TR. Mechanisms of fibrosis: therapeutic translation for fibrotic disease. Nat Med. 2012;18(7):1028-40.

75. Thannickal VJ, Henke CA, Horowitz JC, Noble PW, Roman J, Sime PJ, et al. Matrix biology of idiopathic pulmonary fibrosis: a workshop report of the national heart, lung, and blood institute. Am J Pathol. 2014;184(6):1643-51.

76. Ito K, Lim AC, Salto-Tellez M, Motoda L, Osato M, Chuang LS, et al. RUNX3 attenuates beta-catenin/T cell factors in intestinal tumorigenesis. Cancer cell. 2008;14(3):226-37.

77. Patricia Ducy RZ, Valerie Geoffroy, Amy L. Ridall, and Gerard Karsenty. Osf2/Cbfa1: A Transcriptional Activator of Osteoblast Differentiation. Cell. 1997;89.

78. Ivan O. Rosas TJR, Kazuhisa Konishi, Yingze Zhang, Kevin Gibson, Anna E. Lokshin,, Kathleen O. Lindell JC, Sandra D. MacDonald, Annie Pardo, Frank Sciurba, James Dauber,, Moises Selman BRG, Naftali Kaminski. MMP1 and MMP7 as Potential Peripheral Blood Biomarkers in Idiopathic Pulmonary Fibrosis. PLoS MEDICINE. 2008.

79. Borensztajn K, Crestani B, Kolb M. Idiopathic Pulmonary Fibrosis: From Epithelial Injury to Biomarkers - Insights from the Bench Side. Respiration. 2013;86(6):441-52.

80. Ito Y, Miyazono K. RUNX transcription factors as key targets of TGF-β superfamily signaling. Current Opinion in Genetics & Development. 2003;13(1):43-7.

81. Miyazono K, Maeda S, Imamura T. Coordinate regulation of cell growth and differentiation by TGF-beta superfamily and Runx proteins. Oncogene. 2004;23(24):4232-7.

82. Aumiller V, Balsara N, Wilhelm J, Gunther A, Konigshoff M. WNT/beta-catenin signaling induces IL-1beta expression by alveolar epithelial cells in pulmonary fibrosis. Am J Respir Cell Mol Biol. 2013;49(1):96-104.

83. Konigshoff M, Balsara N, Pfaff EM, Kramer M, Chrobak I, Seeger W, et al. Functional Wnt signaling is increased in idiopathic pulmonary fibrosis. PLoS One. 2008;3(5):e2142.

84. Henderson WR, Jr., Chi EY, Ye X, Nguyen C, Tien YT, Zhou B, et al. Inhibition of Wnt/beta-catenin/CREB binding protein (CBP) signaling reverses pulmonary fibrosis. Proc Natl Acad Sci U S A. 2010;107(32):14309-14.

85. Rock J, Konigshoff M. Endogenous lung regeneration: potential and limitations. Am J Respir Crit Care Med. 2012;186(12):1213-9.

86. Rock JR, Barkauskas CE, Cronce MJ, Xue Y, Harris JR, Liang J, et al. Multiple stromal populations contribute to pulmonary fibrosis without evidence for epithelial to mesenchymal transition. Proc Natl Acad Sci U S A. 2011;108(52):E1475-83.

87. Barkauskas CE, Cronce MJ, Rackley CR, Bowie EJ, Keene DR, Stripp BR, et al. Type 2 alveolar cells are stem cells in adult lung. J Clin Invest. 2013;123(7):3025-36.

88. Uhal B, Joshi I, Hughes WF, Ramos C, Pardo A, M S. Alveolar epithelial cell death adjacent to underlying myofibroblasts in advanced fibrotic human lung. Am J Physiol Lung Cell Mol Physiol. 1998;275:L1192-L9.

89. Hsu YL, Huang MS, Yang CJ, Hung JY, Wu LY, Kuo PL. Lung tumor-associated osteoblast-derived bone morphogenetic protein-2 increased epithelial-to-mesenchymal transition of cancer by Runx2/Snail signaling pathway. J Biol Chem. 2011;286(43):37335-46.

90. Klingberg F, Hinz B, White ES. The myofibroblast matrix: implications for tissue repair and fibrosis. J Pathol. 2013;229(2):298-309.

91. Parker MW, Rossi D, Peterson M, Smith K, Sikstrom K, White ES, et al. Fibrotic extracellular matrix activates a profibrotic positive feedback loop. J Clin Invest. 2014;124(4):1622-35.

92. Richeldi L, Collard HR, Jones MG. Idiopathic pulmonary fibrosis. The Lancet. 2017;389(10082):1941-52.

93. Wolters PJ, Collard HR, Jones KD. Pathogenesis of idiopathic pulmonary fibrosis. Annu Rev Pathol. 2014;9:157-79.

94. Yang H, Fu J, Yao L, Hou A, Xue X. Runx3 is a key modulator during the epithelial-mesenchymal transition of alveolar type II cells in animal models of BPD. Int J Mol Med. 2017;40(5):1466-76.

95. Ruffenach G, Chabot S, Tanguay VF, Courboulin A, Boucherat O, Potus F, et al. Role for Runt-related Transcription Factor 2 in Proliferative and Calcified Vascular Lesions in Pulmonary Arterial Hypertension. Am J Respir Crit Care Med. 2016;194(10):1273-85.

96. Shi N, Zhang J, Chen SY. Runx2, a novel regulator for goblet cell differentiation and asthma development. FASEB J. 2017;31(1):412-20.

97. Schaefer CJ, Ruhrmund DW, Pan L, Seiwert SD, Kossen K. Antifibrotic activities of pirfenidone in animal models. Eur Respir Rev. 2011;20(120):85-97.

98. Okuda T, van Deursen J, Hiebert SW, Grosveld G, Downing JR. AML1, the target of multiple chromosomal translocations in human leukemia, is essential for normal fetal liver hematopoiesis. Cell. 1996;84(2):321-30.

99. Mangan JK, Speck NA. RUNX1 mutations in clonal myeloid disorders: from conventional cytogenetics to next generation sequencing, a story 40 years in the making. Crit Rev Oncog. 2011;16(1-2):77-91.

100. Banerji S, Cibulskis K, Rangel-Escareno C, Brown KK, Carter SL, Frederick AM, et al. Sequence analysis of mutations and translocations across breast cancer subtypes. Nature. 2012;486(7403):405-9.

101. Ramsey J, Butnor K, Peng Z, Leclair T, van der Velden J, Stein G, et al. Loss of RUNX1 is associated with aggressive lung adenocarcinomas. J Cell Physiol. 2018;233(4):3487-97.

102. Scheitz CJ, Lee TS, McDermitt DJ, Tumbar T. Defining a tissue stem cell-driven Runx1/Stat3 signalling axis in epithelial cancer. The EMBO journal. 2012;31(21):4124-39.

103. Goyama S, Schibler J, Cunningham L, Zhang Y, Rao Y, Nishimoto N, et al. Transcription factor RUNX1 promotes survival of acute myeloid leukemia cells. J Clin Invest. 2013;123(9):3876-88.

104. Matsubara D, Niki T, Ishikawa S, Goto A, Ohara E, Yokomizo T, et al. Differential expression of S100A2 and S100A4 in lung adenocarcinomas: clinicopathological significance, relationship to p53 and identification of their target genes. Cancer Sci. 2005;96(12):844-57.

105. Morita K, Suzuki K, Maeda S, Matsuo A, Mitsuda Y, Tokushige C, et al. Genetic regulation of the RUNX transcription factor family has antitumor effects. J Clin Invest. 2017;127(7):2815-28.

106. Konigshoff M, Eickelberg O. WNT signaling in lung disease: a failure or a regeneration signal? Am J Respir Cell Mol Biol. 2010;42(1):21-31.

107. Voon DC, Wang H, Koo JK, Nguyen TA, Hor YT, Chu YS, et al. Runx3 protects gastric epithelial cells against epithelial-mesenchymal transition-induced cellular plasticity and tumorigenicity. Stem Cells. 2012;30(10):2088-99.

108. Li W, Xu S, Lin S, Zhao W. Overexpression of runt-related transcription factor-2 is associated with advanced tumor progression and poor prognosis in epithelial ovarian cancer. J Biomed Biotechnol. 2012;2012:456534.

109. Onodera Y, Miki Y, Suzuki T, Takagi K, Akahira J, Sakyu T, et al. Runx2 in human breast carcinoma: its potential roles in cancer progression. Cancer Sci. 2010;101(12):2670-5.

110. Konigshoff M. Lung cancer in pulmonary fibrosis: tales of epithelial cell plasticity. Respiration. 2011;81(5):353-8.

111. Horowitz JC, Osterholzer JJ, Marazioti A, Stathopoulos GT. “Scar-cinoma”: viewing the fibrotic lung mesenchymal cell in the context of cancer biology. European Respiratory Journal. 2016.

112. Ganguly K, Martin TM, Concel VJ, Upadhyay S, Bein K, Brant KA, et al. Secreted phosphoprotein 1 is a determinant of lung function development in mice. Am J Respir Cell Mol Biol. 2014;51(5):637-51.

113. Nogee LM, Dunbar AE, 3rd, Wert SE, Askin F, Hamvas A, Whitsett JA. A mutation in the surfactant protein C gene associated with familial interstitial lung disease. N Engl J Med. 2001;344(8):573-9.

114. Wang Y, Kuan PJ, Xing C, Cronkhite JT, Torres F, Rosenblatt RL, et al. Genetic defects in surfactant protein A2 are associated with pulmonary fibrosis and lung cancer. Am J Hum Genet. 2009;84(1):52-9.

115. Sisson TH, Mendez M, Choi K, Subbotina N, Courey A, Cunningham A, et al. Targeted injury of type II alveolar epithelial cells induces pulmonary fibrosis. Am J Respir Crit Care Med. 2010;181(3):254-63.

116. Zaidi SK, Javed A, Pratap J, Schroeder TM, J JW, Lian JB, et al. Alterations in intranuclear localization of Runx2 affect biological activity. J Cell Physiol. 2006;209(3):935-42.

117. Barbas-Filho JV FM, Sesso A, Kairalla RA, Carvalho CR, Capelozzi VL. Evidence of type II pneumocyte apoptosis in the pathogenesis of idiopathic pulmonary fibrosis (IFP)/usual interstitial pneumonia (UIP). J Clin Pathol. 2001;54:132-8.

118. Waisberg DR, Barbas-Filho JV, Parra ER, Fernezlian S, de Carvalho CR, Kairalla RA, et al. Abnormal expression of telomerase/apoptosis limits type II alveolar epithelial cell replication in the early remodeling of usual interstitial pneumonia/idiopathic pulmonary fibrosis. Human pathology. 2010;41(3):385-91.

119. Ferrari N, Riggio AI, Mason S, McDonald L, King A, Higgins T, et al. Runx2 contributes to the regenerative potential of the mammary epithelium. Sci Rep. 2015;5:15658.

120. McDonald L, Ferrari N, Terry A, Bell M, Mohammed ZM, Orange C, et al. RUNX2 correlates with subtype-specific breast cancer in a human tissue microarray, and ectopic expression of Runx2 perturbs differentiation in the mouse mammary gland. Dis Model Mech. 2014;7(5):525-34.

121. Owens TW, Rogers RL, Best SA, Ledger A, Mooney AM, Ferguson A, et al. Runx2 is a novel regulator of mammary epithelial cell fate in development and breast cancer. Cancer Res. 2014;74(18):5277-86.

122. Blackwell TS, Tager AM, Borok Z, Moore BB, Schwartz DA, Anstrom KJ, et al. Future directions in idiopathic pulmonary fibrosis research. An NHLBI workshop report. American journal of respiratory and critical care medicine. 2014;189(2):214-22.

123. Yang J, Wheeler SE, Velikoff M, Kleaveland KR, LaFemina MJ, Frank JA, et al. Activated alveolar epithelial cells initiate fibrosis through secretion of mesenchymal proteins. Am J Pathol. 2013;183(5):1559-70.

124. Kim KK, Kugler MC, Wolters PJ, Robillard L, Galvez MG, Brumwell AN, et al. Alveolar epithelial cell mesenchymal transition develops in vivo during pulmonary fibrosis and is regulated by the extracellular matrix. Proc Natl Acad Sci U S A. 2006;103(35):13180-5.

125. Marmai C, Sutherland RE, Kim KK, Dolganov GM, Fang X, Kim SS, et al. Alveolar epithelial cells express mesenchymal proteins in patients with idiopathic pulmonary fibrosis. Am J Physiol Lung Cell Mol Physiol. 2011;301(1):L71-8.

126. Lawson WE, Polosukhin VV, Zoia O, Stathopoulos GT, Han W, Plieth D, et al. Characterization of fibroblast-specific protein 1 in pulmonary fibrosis. Am J Respir Crit Care Med. 2005;171(8):899-907.

127. Veronika Pozharskaya ET-G, Mauricio Rojas, Anthony Gal, Minal Amin, Sheila Dollard, Jesse Roman, Arlene A. Stecenko, Ana L. Mora. Twist: A Regulator of Epithelial-Mesenchymal Transition in Lung Fibrosis. PLoS One. 2009.

128. Tanjore H, Xu XC, Polosukhin VV, Degryse AL, Li B, Han W, et al. Contribution of epithelial-derived fibroblasts to bleomycin-induced lung fibrosis. Am J Respir Crit Care Med. 2009;180(7):657-65.

129. Xia H, Gilbertsen A, Herrera J, Racila E, Smith K, Peterson M, et al. Calcium-binding protein S100A4 confers mesenchymal progenitor cell fibrogenicity in idiopathic pulmonary fibrosis. J Clin Invest. 2017;127(7):2586-97.

130. Wynn TA. Cellular and molecular mechanisms of fibrosis. J Pathol. 2008;214(2):199-210.

131. David Lagares, Alba Santos, Paula E. Grasberger, Fei Liu, Clemens K. Probst, Rod A. Rahimi, et al. Targeted apoptosis of myofibroblasts with the BH3 mimetic ABT-263 reverses established fibrosis. Sci Transl Med. 2017.

132. K. Tsuji YI, and M. Noda. Expression of the PEBP2aA/AML3/CBFA1 Gene is regulated by BMP4/7 Heterodimer and Its Overexpression suppresses Type I Collagen and Osteocalcin Gene Expression in Osteoblastic and Nonosteoblastic Mesenchymal Cells. Bone. 1998;22:87-92.

133. Sakai N, Tager AM. Fibrosis of two: Epithelial cell-fibroblast interactions in pulmonary fibrosis. Biochimica et biophysica acta. 2013;1832(7):911-21.

134. Ji C, Casinghino S, Chang DJ, Chen Y, Javed A, Ito Y, et al. CBFa(AML/PEBP2)-related elements in the TGF-β type I receptor promoter and expression with osteoblast differentiation. Journal of Cellular Biochemistry. 1998;69(3):353-63.

135. Baarsma HA, Konigshoff M, Gosens R. The WNT signaling pathway from ligand secretion to gene transcription: molecular mechanisms and pharmacological targets. Pharmacol Ther. 2013;138(1):66-83.

136. Baarsma HA, Skronska-Wasek W, Mutze K, Ciolek F, Wagner DE, John-Schuster G, et al. Noncanonical WNT-5A signaling impairs endogenous lung repair in COPD. J Exp Med. 2017;214(1):143-63.

137. van Dijk EM, Menzen MH, Spanjer AI, Middag LD, Brandsma CA, Gosens R. Noncanonical WNT-5B signaling induces inflammatory responses in human lung fibroblasts. Am J Physiol Lung Cell Mol Physiol. 2016;310(11):L1166-76.

138. Yang DC, Tsai CC, Liao YF, Fu HC, Tsay HJ, Huang TF, et al. Twist controls skeletal development and dorsoventral patterning by regulating runx2 in zebrafish. PLoS One. 2011;6(11):e27324.

139. Yang DC, Yang MH, Tsai CC, Huang TF, Chen YH, Hung SC. Hypoxia inhibits osteogenesis in human mesenchymal stem cells through direct regulation of RUNX2 by TWIST. PLoS One. 2011;6(9):e23965.

140. Bridges RS, Kass D, Loh K, Glackin C, Borczuk AC, Greenberg S. Gene expression profiling of pulmonary fibrosis identifies Twist1 as an antiapoptotic molecular "rectifier" of growth factor signaling. Am J Pathol. 2009;175(6):2351-61.

141. Pozharskaya V, Torres-Gonzalez E, Rojas M, Gal A, Amin M, Dollard S, et al. Twist: a regulator of epithelial-mesenchymal transition in lung fibrosis. PLoS One. 2009;4(10):e7559.

142. Lomas NJ, Watts KL, Akram KM, Forsyth NR, Spiteri MA. Idiopathic pulmonary fibrosis: immunohistochemical analysis provides fresh insights into lung tissue remodelling with implications for novel prognostic markers. Int J Clin Exp Pathol. 2012;5(1):58-71.

143. Yamada C, Ozaki T, Ando K, Suenaga Y, Inoue K, Ito Y, et al. RUNX3 modulates DNA damage-mediated phosphorylation of tumor suppressor p53 at Ser-15 and acts as a co-activator for p53. J Biol Chem. 2010;285(22):16693-703.

144. Ozaki T, Wu D, Sugimoto H, Nagase H, Nakagawara A. Runt-related transcription factor 2 (RUNX2) inhibits p53-dependent apoptosis through the collaboration with HDAC6 in response to DNA damage. Cell Death Dis. 2013;4:e610.

145. Yu G, Tzouvelekis A, Wang R, Herazo-Maya JD, Ibarra GH, Srivastava A, et al. Thyroid hormone inhibits lung fibrosis in mice by improving epithelial mitochondrial function. Nat Med. 2017.

146. Carr FE, Tai PW, Barnum MS, Gillis NE, Evans KG, Taber TH, et al. Thyroid Hormone Receptor-beta (TRbeta) Mediates Runt-Related Transcription Factor 2 (Runx2) Expression in Thyroid Cancer Cells: A Novel Signaling Pathway in Thyroid Cancer. Endocrinology. 2016;157(8):3278-92.

7.2 List of figures

7.3 List of tables

8. ACKNOWLEDGEMENTS

Bei Melanie Königshoff bedanke ich mich für die Möglichkeit in einer aktiven, internationalen Arbeitsgruppe meine ersten Schritte in der experimentellen Forschung machen zu können. Ich habe ihre konstruktive Kritik, Motivation und Anerkennung immer sehr geschätzt.

Sarah Hermann und Hoeke Baarsma halfen mit konstruktiver Kritik, neuen Ideen und zahlreichen nützlichen Ratschlägen.

Maria Magdalena Stein danke ich für ihre hervorragende Einweisung in die grundlegenden Techniken der Molekularbiologie und ihre unermüdliche Hilfestellung bei Problemen. Bedanken möchte ich mich auch bei Ana van den Berg und Julia Kipp für die ATII Zell-Isolationen und bei Nadine Adam für technische Unterstützung.

Sarah Hermann, Hoeke Baarsma, Kathrin Mutze, John-Poul Ng-Blichfeldt, und Mareike Lehmann halfen beim Korrekturlesen und waren stets hilfsbereit bei Fragen und Schwierigkeiten. Danke auch an Philipp Leippe für das Korrekturlesen meiner Arbeit.

Bei allen, bisher noch nicht genannten Mitarbeitern des MK-Labs, Stephan Klee, Wiola Skronska-Wasek, Aina Martin Medina, Rita Costa, Florian Ciolek, Henrik Ulke, Lara Buhl, Chiharu Ota, Darcy Wagner, Cedric Thiel, Hani Alsafadi, Noor Christiaens und Rabea Imker bedanke ich mich für die gute und gemeinschaftliche Atmosphäre im Lab.

Meinen großartigen Mitbewohnern Christian, Robin, Manu und Pius danke ich für unsere gute Zeit und unseren Zusammenhalt in der WG.

Zu guter Letzt gebührt mein größter Dank meiner Familie. Ohne euch hätte ich das alles nie geschafft!

9. APPENDIX

9.1 Publications and Presentations

9.1.1 Publications

Mümmler C, Burgy O, Hermann S, Mutze K, Günther A, Königshoff M; Cell-specific expression of runt-related transcription factor 2 contributes to pulmonary fibrosis; *FASEB J*, 2018, 32(2): 703-716 (IF: 5.498)

9.1.2 Oral presentations

Nov. 2015: „*RUNX2 is upregulated in idiopathic pulmonary fibrosis",* Herbsttagung der Sektion Zellbiologie, Pathophysiologie/Aerosolmedizin sowie Infektiologie und Tuberkulose in der Deutschen Gesellschaft für Pneumologie und Beatmungsmedizin e.V., Munich, Germany

Feb. 2015: *"The role of ossification-related proteins in the progression of IPF",* Advances in IPF Research (AIR) Symposium, Potsdam, Germany

9.1.3 Poster presentations

May 2016: *"RUNX2 regulates mesenchymal cell differentiation and extracellular matrix production in pulmonary fibrosis"*, American Thoracic Society (ATS) congress, San Francisco, USA

Oct. 2015: *"The role of RUNX2 in idiopathic pulmonary fibrosis",* Munich Pittsburgh Lung Conference, Munich, Germany

Mar. 2015: *"The role of ossification-related proteins in the progression of IPF",* German-French Retreat Helmholtz Research School "Lung Biology and Disease", Tegernsee, Germany

Jan. 2015: *"The role of ossification-related proteins in the progression of IPF",* Deutsches Zentrum für Lungenforschung (DZL) annual meeting, Hamburg, Germany

9.2 Eidesstattliche Erklärung

Hiermit erkläre ich, ***Carlo Mümmler***, an Eides statt,

dass ich die vorliegende Dissertation mit dem Titel

„Runt-related transcription factor 2 in pulmonary fibrosis"

selbständig verfasst, mich außer der angegebenen keiner weiteren Hilfsmittel bedient und alle Erkenntnisse, die aus dem Schrifttum ganz oder annähernd übernommen sind, als solche kenntlich gemacht und nach ihrer Herkunft unter Bezeichnung der Fundstelle einzeln nachgewiesen habe.

Ich erkläre des Weiteren, dass die hier vorgelegte Dissertation nicht in gleicher oder in ähnlicher Form bei einer anderen Stelle zur Erlangung eines akademischen Grades eingereicht wurde.

München, den 13.06.2018 Carlo Mümmler